

**Rational Synthesis and Electron Transfer Behaviors of
Heterometallic Multinuclear Complexes**

Hitoshi IZU

The Graduate University for Advanced Studies, SOKENDAI

**School of Physical Sciences
Department of Structural Molecular Science**

Contents

General Introduction	3
Chapter 1 On-demand Installation of Metal Ions into Pentanuclear Metal Complexes	17
Chapter 2 Electron Juggling in Clustered Five Redox Sites	45
Chapter 3 Rational Synthetic Strategy for Heterometallic Tetranuclear Complexes	71
General Conclusion	97
Acknowledgements	99
List of Publications	101

General Introduction

1-1. Multinuclear Metal Complex

Multinuclear metal complexes are an attractive class of materials because the strong electronic interactions between composed metal ions can provide unique electronic structures, which cannot be achieved in mononuclear metal complexes. Owing to their characteristic electronic structures, thus far, there have been a number of reports on artificial multinuclear metal complexes that exhibit excellent redox, photochemical and magnetic properties, and reactivity in addition to some examples in natural enzymes. Due to their nice properties and reactivity, multinuclear metal complexes have been investigated well and are expected to be functional materials for future practical applications.

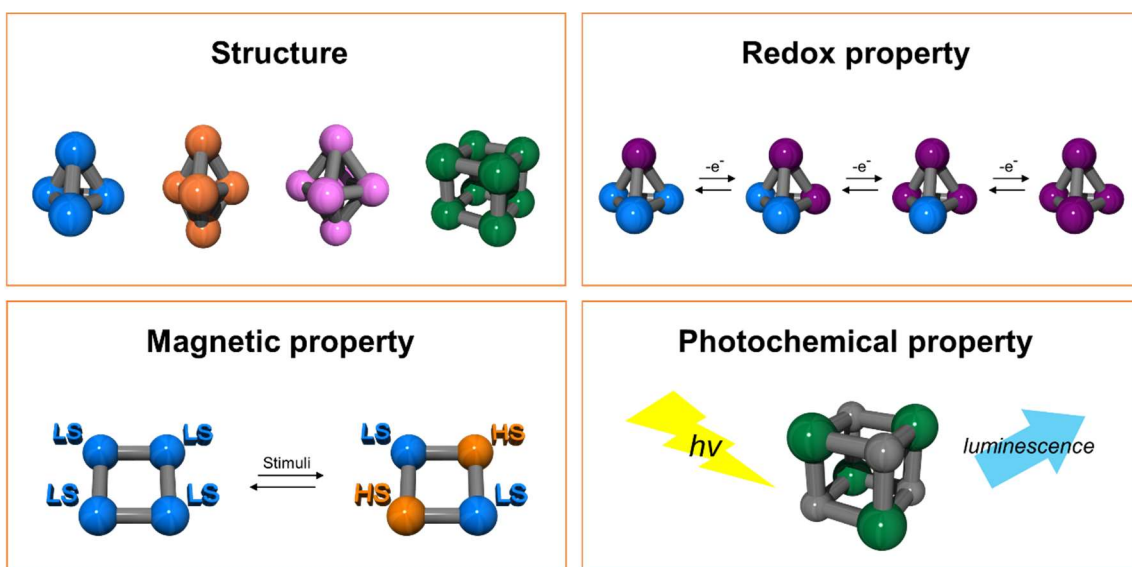


Figure I-1 | Characteristics of multinuclear metal complexes.

1-2. Characteristics of Multinuclear Metal Complex

1-2-1. Structure

Multinuclear metal complexes are constructed by multiple metal ions and bridging ligands. The structures of multinuclear metal complexes are determined by the nature of metal ions and ligands and also combinations of metal ions and ligands. Therefore, various kinds of multinuclear metal complexes with unique structures are observed by changing these factors.¹⁻¹²

For instance, M. Fujita and co-workers reported a molecular square containing 4 palladium ions.¹³ It is the first report of molecular square and the complex is constructed by 90° cis-protected palladium(II) ions and 4,4'-bipyridine as a linker. In addition, P. J. Stang and co-workers reported various molecular squares constructed by diphosphine-blocked cis-blocked palladium(II) ions and platinum(II) ions, and established a large library of molecular squares of various sizes and functions.¹⁴

Furthermore, M. Fujita and co-workers reported a molecular ball composed of 12 palladium(II) ions (Figure I-2, a).^{15,16} In this complex, 12 palladium(II) ions in square-planar geometry are assembled with 24 units of rigid bent dipyrindine linker. Interestingly, when dipyrindylthiophene was used as a bent linker, it resulted in the formation of a giant molecular ball constructed by 24 palladium(II) ions in square-planar geometry and 48 curved bridging ligands (Figure I-2, b).¹⁷

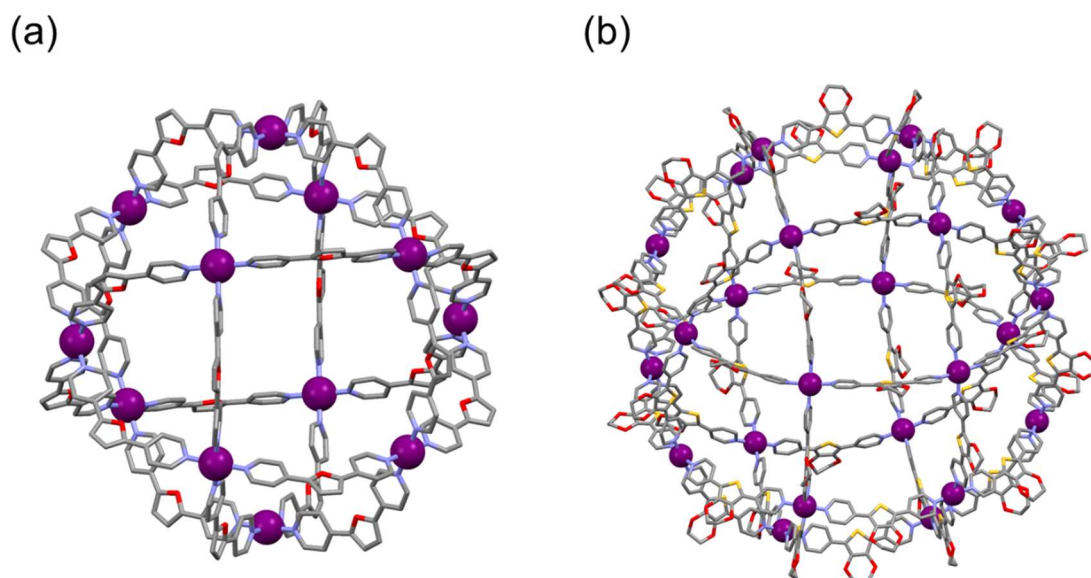


Figure I-2 | Structures of molecular balls constructed by (a) 12 Pd²⁺ ions^{15,16} and (b) 24 Pd²⁺ ions¹⁷.

1-2-2. Redox Property

Multinuclear metal complexes enable to construct multi electron transfer systems.¹⁸⁻²³ The multi electron transfer reactions can be achieved by reflecting the number of redox-active metal ions even if the changes of the oxidation state in each metal center is just one. For instance, trinuclear ruthenium complex reported by T. J. Meyer and co-workers can exhibit multistep one electron transfer reactions (Figure I-3). These electron transfer reactions are originated from the redox of ruthenium centers.²⁴

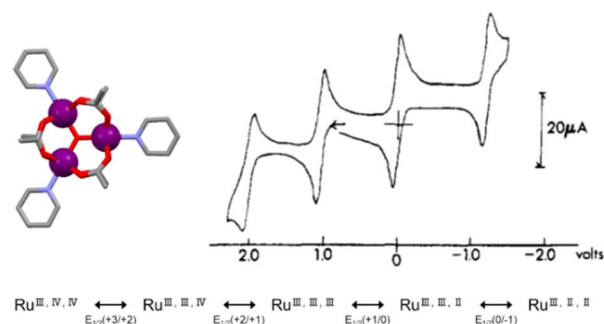


Figure I-3 | Core structure and a cyclic voltammogram of the trinuclear ruthenium complex.²⁴ (© 1975 American Chemical Society)

The features of electron transfer reaction are determined both by the nature of metal ions and the coordination environment of metal ions. In addition, multinuclear metal complexes can show intramolecular electron transfer reactions between metal ions by their strong electronic interactions. The intramolecular electron transfer reactions afford the generation of various charge isomers. For instance, C. P. Kubiak and co-workers reported unique redox behaviors in a hexanuclear ruthenium complex.²⁵⁻²⁶ The ruthenium complex has two trinuclear ruthenium cores bridged by a pyrazine and exhibits flexible oxidation/reduction reactions. Interestingly, one electron reduced state of the complex showed intramolecular electron transfer reaction via the pyrazine bridge (Figure I-4). In other oxidation states, the complex did not show intramolecular electron transfer reaction. These phenomena are originated from the strong electronic interactions between metal centers.

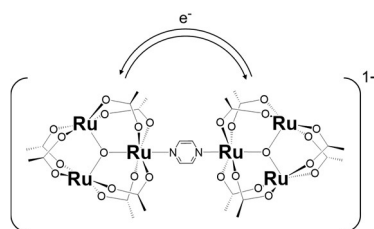


Figure I-4 | Intramolecular electron transfer reaction in the hexanuclear ruthenium complex reported by C. P. Kubiak and co-workers.

1-2-3. Magnetic Property

The magnetic interaction between paramagnetic centers has been investigated in detail. Especially, multinuclear metal complexes which have paramagnetic metal ions have attracted much attentions because they can exhibit unique magnetic properties and their magnetic properties can be changed by reflecting the kinds of metal ions and/or the number of metal ions.

The acetate bridged multinuclear metal complex composed of 12 manganese ions is an interesting material as a single molecule magnet (Figure I-5, left).²⁷ The complex has a cubane type core constructed by 4 Mn^{IV} ions at the center of the structure. In addition, the core is surrounded by other 8 Mn^{III} ions bridged by acetate ligands and oxo ligands. The complex has ferromagnetic interaction between 4 Mn^{IV} ions in the cubane core and antiferromagnetic interaction between other 8 Mn^{III} ions. (Figure I-5, right) Due to these two magnetic interactions, the complex can exhibit ferrimagnetism and work as a magnet.²⁸⁻³¹

In addition, multinuclear structures can also effect on a spin crossover effect. The multinuclear structure can emphasize a cooperative effect compared with the mononuclear structure, then the multinuclear metal complexes can exhibit drastic spin conversion with temperature hysteresis.³²⁻³⁶

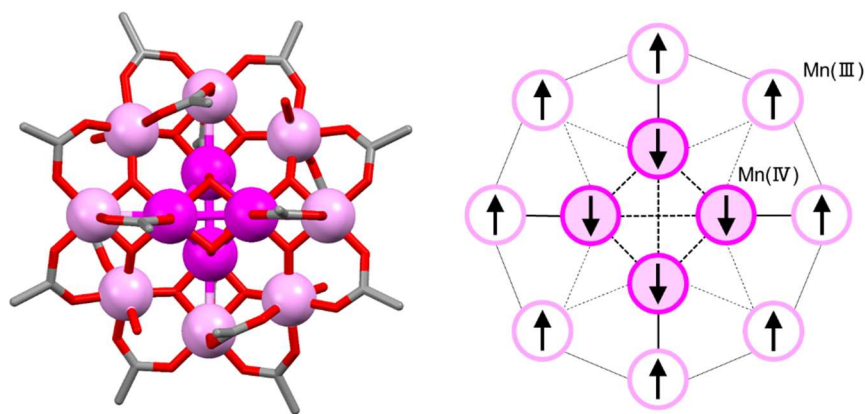


Figure I-5 | Molecular structure (left) and spin structure (right) of the dodecanuclear manganese complex.²⁷⁻³¹

1-2-4. Photochemical Property

Some multinuclear metal complexes can also exhibit photochemical properties.³⁷⁻⁴¹ These photochemical properties are originated from the distinct electronic structures determined by the interaction between metal ions as well as the interaction between metal ion and ligand.

The tetranuclear copper complexes which have the distorted cubane structure, $\text{Cu}_4\text{X}_4\text{L}_4$, exhibit luminescence (Figure I-6, a).⁴² The complexes are constructed by 4 copper ions, 4 halides (X) and 4 monodentate ligands (L). The distance between copper ions are functions of both the halide and the ligand. For example, respective tetranuclear complexes of $\text{Cu}_4\text{Cl}_4\text{L}_4$ and $\text{Cu}_4\text{I}_4\text{L}_4$ demonstrate cubane configurations, the Cu-Cu distances are different between $\text{Cu}_4\text{Cl}_4\text{L}_4$ and $\text{Cu}_4\text{I}_4\text{L}_4$ due to the effect of halides.^{43,44} Notably, $\text{Cu}_4\text{I}_4\text{L}_4$ is strongly luminescent at ambient temperature as a solid and in solution, while $\text{Cu}_4\text{Cl}_4\text{L}_4$ shows no luminescence in solution and only weak room temperature emission as a solid.⁴⁵

In addition, the photochemical properties of multinuclear metal complexes can be tuned by changing their structures. This is because the electronic structure is also determined by not only the interactions between components but also the structure. Therefore, various kinds of multinuclear metal complexes with unique photochemical properties have been reported (Figure I-6, b).⁴⁶⁻⁴⁹

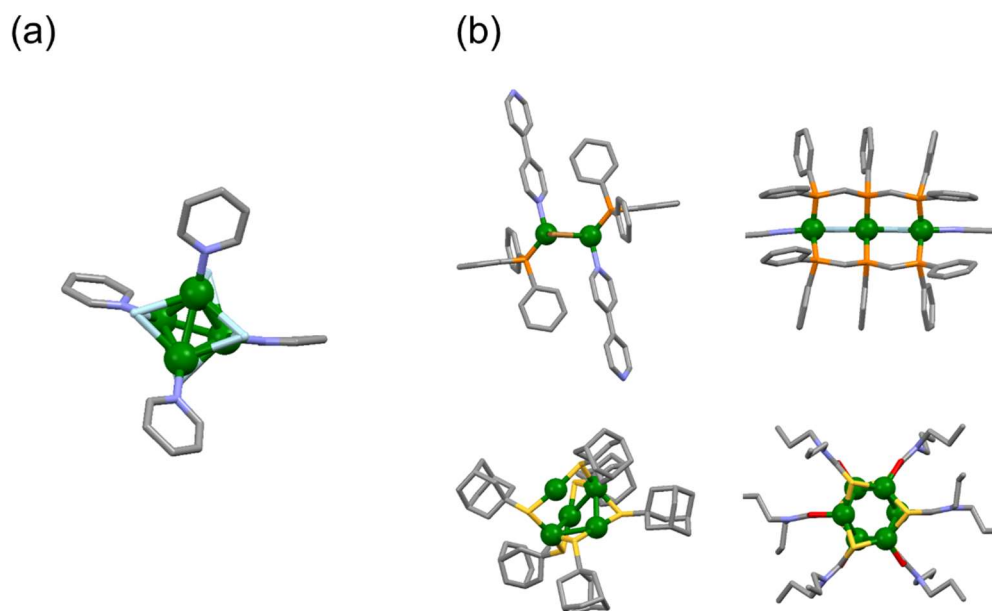


Figure I-6 | (a) the structure of $\text{Cu}_4\text{X}_4\text{L}_4$ and (b) the structures of various multinuclear copper complexes which exhibit photochemical properties.

1-2-5. Reactivity

Multinuclear metal complexes can work as useful catalyst by taking advantage of their multinuclear structures. The metal centers can work as not only the active centers but also the redox mediators. In addition, multinuclear metal complexes can exhibit flexible redox behaviors reflecting the number of redox-active metal ions. Therefore, multinuclear metal complexes are suitable to store and transfer multi electrons.⁵⁰⁻⁵⁵

S. Masaoka and co-workers revealed that pentanuclear iron complex, **Fe₅**, can catalyze water oxidation reaction with extremely high turnover frequency.⁵⁶ **Fe₅** is composed of 5 iron ions and 6 ligands. **Fe₅** can exhibit flexible one-electron transfer reactions involving in the redox of Fe^{III}/Fe^{II} due to the strong electronic interactions between iron ions. Interestingly, two iron ions at the apical position can work as the charge storage sites. Actually, the redox storage sites contribute to the flexible electron transfer reactions in **Fe₅**. In addition, other three iron ions in the triangle core work as the adjacent active sites to promote O-O bond formation.

Two features of multinuclear structure, (1) the flexible redox behaviors attributed to the strong electronic interaction and charge storage sites and (2) the adjacent active sites, greatly contribute to the high catalytic activity of **Fe₅**.

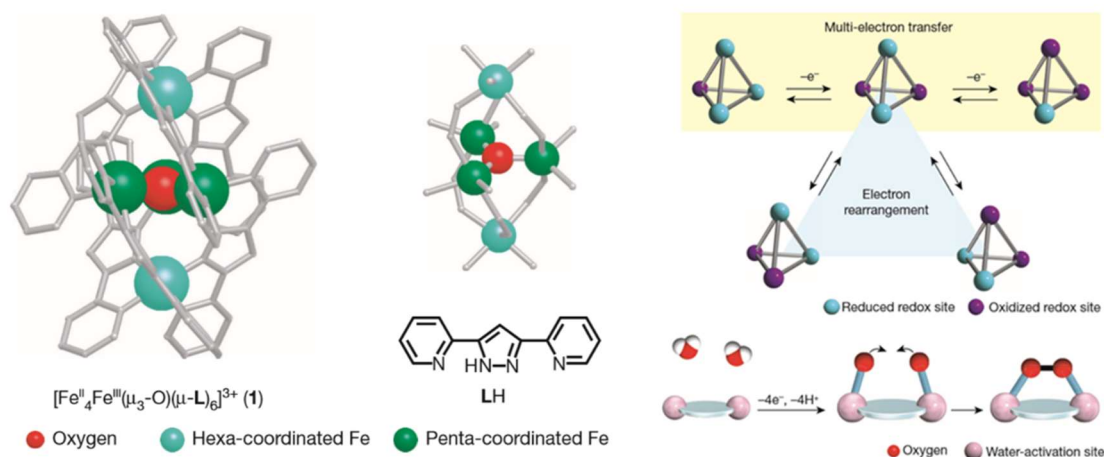


Figure I-7 | Design of the pentanuclear iron complex for water oxidation reaction.⁵⁶
(© 2016 Springer Nature)

1-3. Multinuclear Metal Complexes in Nature

Multinuclear metal complexes play important roles in nature system because some metalloenzymes have multinuclear structure in their active center (Figure I-8).⁵⁷⁻⁶¹

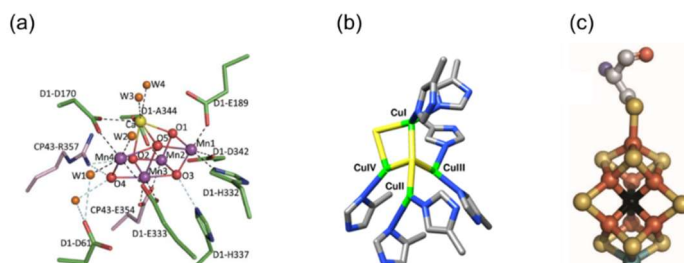


Figure I-8 | Structures of (a) OEC, (b) active site of nitrous oxide reductase and (c) FeMoco of nitrogenase. (© 2011 Springer Nature, © 2014 American Chemical Society and © 2011 American Association for the Advancement of Science)

For instance, the Oxygen Evolving Complex (OEC) in photosystem II which has cubane structure composed of Mn_4CaO_5 can catalyze water oxidation reaction and its redox intermediates are known as S_i states ($i = 0-4$). The flexible electron transfer reactions of the OEC can generate each S_i state and oxidizing equivalents can be stored in each state. Then the fully oxidized OEC can oxidize H_2O to O_2 efficiently.⁶²⁻⁶⁴ In the turn of catalytic cycle, it should be noted that intramolecular electron transfer occurs at S_2 state. The intramolecular electron transfer suppresses back electron transfer reaction (Figure I-9). The features of multinuclear metal complexes greatly contribute to the catalytic cycle of OEC.

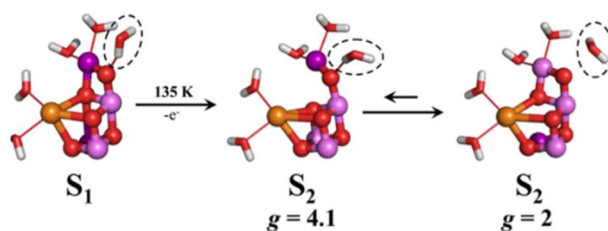


Figure I-9 | Structures of OEC at S_1 state and S_2 states. OEC has spin isomer at S_2 state. Mn^{3+} ions are shown in purple, Mn^{4+} ions are shown in lavender. (© 2017 American Chemical Society)

Furthermore, the function of nitrous oxide reductase is also supported by multinuclear metal complex constructed by four copper ions. The intramolecular electron transfer between copper ions promotes the coordination of the substrate to copper ion, and the transformation to the product from the substrate.^{60,65} So multinuclear metal complexes are fundamental materials not only in artificial system but also in natural system.

1-4. Purpose of This Thesis

Multinuclear metal complexes potentially generate various electronic states, between which the number and/or the position of the oxidized metal centers are different, and the difference in the distribution of oxidation states, largely affects the electronic structure and the physical property of the species. In other words, the control over the distribution of the oxidation states in the multinuclear metal complexes can be an important strategy for obtaining the material with the target functionality.

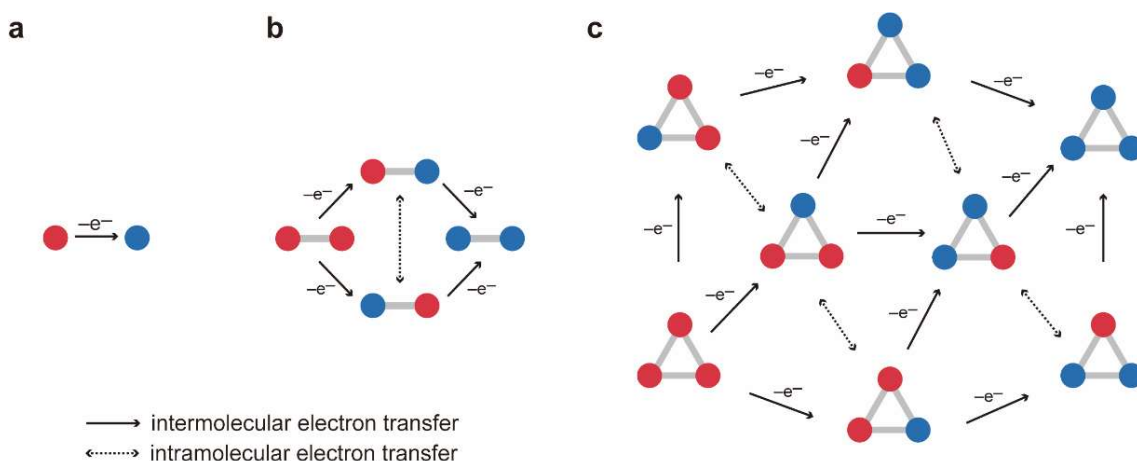
In principle, the distribution of the oxidation states alters via the following two electron transfer reactions; (i) the oxidation/reduction of composed metal ions and (ii) the intramolecular electron transfer between composed metal ions (Scheme I-1). These two reactions allow multinuclear metal complexes to have various electronic structures and promote their excellent functions. Given that the electron transfer reactions in multinuclear metal complexes are predominantly determined both by the nature of each composed metal ion and the electronic interaction between the composed metal ions, the systematic investigation of the redox behaviors on a series of multinuclear metal complexes, in which composed metal ions are controllable with keeping the same molecular framework, is of great significance. This is because the distribution of the oxidation states can be controlled by installing the desired metal ions into the specific position of the multinuclear metal complex and such systematic investigation would provide a comprehensive guideline to understand the redox behavior of multinuclear metal complex.

However, although studies on the multinuclear metal complexes are abundant, such replacement of the composed metal ions had been achieved mostly relying on the fruit serendipity, and on-demand installation of the metal ions into multinuclear metal complex with desired molecular framework is still challenging. Because of such lack in the rational synthetic route, the construction of definitive strategy to manipulate the distribution of oxidation states in multinuclear metal complex had not been achieved.

In order to achieve it, a rational synthetic strategy to enable the on-demand installation of desired metal ions into specific position in multinuclear metal complex has to be established. Therefore, the rational synthetic strategy can afford a series of multinuclear metal complexes that have different arrangement of metal ions with keeping the same molecular framework. In addition, the rational synthetic strategy also leads the systematic investigation of the redox behavior in the obtained complexes. The systematic investigation should provide new insight for the deeper understanding to control over the redox behavior of multinuclear metal complex, which would lead to the construction of the guideline to determine the manner of the electron transfer reaction in multinuclear

metal complex as well as novel strategy to develop a new class of the functional materials.

Therefore, in this thesis, the author focused on the development of the rational synthetic strategy for obtaining the series of heterometallic multinuclear complexes and the systematic investigation of redox behavior in the obtained complexes.



Scheme I-1 | Schematic representation of the electron transfer reactions in the multinuclear metal complexes. Red and blue circles denote the reduced and oxidized cores, respectively. As the number of redox cores increases, the redox behaviour becomes more complicated, which makes predicting/controlling the electron transfers increasingly difficult.

1-5. Survey in This Thesis

Chapter 1 describes the rational synthetic strategy for heterometallic pentanuclear complexes. In this chapter, pentanuclear structure which constructed by five metal ions and 3,5-bis(2-pyridyl)pyrazole (Hbpp) is chosen as a molecular scaffold due to the nice redox flexibility. The synthesis of heterometallic pentanuclear complex was achieved by stepwise synthetic method using a mononuclear metal complex as a precursor. In this synthetic strategy, a relatively substitution inert ruthenium ion was reacted with three equivalent of Hbpp ligands under harsh condition to afford a ruthenium mononuclear complex. The obtained complex was subsequently reacted with different kinds of metal ion that is substitution labile under milder condition, and the desired pentanuclear structure formed without scrambling of metal ions. The obtained complex was well characterized by ESI TOF-MS, elemental analysis and single-crystal X-ray diffraction. By adopting the strategy, a series of heterometallic pentanuclear complexes were successfully constructed with keeping the same molecular framework.

Chapter 2 describes the redox behaviors of the heterometallic pentanuclear complexes synthesized in chapter 1. The systematic investigation for homometallic pentanuclear complexes as well as heterometallic pentanuclear complexes was performed to clarify the effect on the difference of composed metal ions. Their redox behaviors were investigated by electrochemical measurement, UV-vis absorption spectroscopy and UV-SEC measurement. The electrochemical measurement of these complexes revealed that they can exhibit some redox waves reflecting the number of redox active metal centers in their structures and the potentials depended on the nature of composed metal ions. In addition, UV-vis absorption spectroscopy and UV-SEC measurement revealed the unique redox process, the reduction-upon-oxidation reaction, proceeded in Ru_2Fe_3 complex, Fe_5 complex and Ru_2Mn_3 complex. In the case of Fe based complexes, it was indicated that the substitution of iron ion to ruthenium ion can change the step corresponding to the reduction-upon-oxidation reaction. On the other hands, it was also indicated that the unique electron transfer process can be induced by the installation of ruthenium ion in the case of manganese based complex. Furthermore, the systematic investigation in this chapter allow us to know the two factors that impact the redox behavior of the pentanuclear metal complex.

Chapter 3 describes the synthetic strategy of heterometallic tetranuclear complex which has new kinds of structure. The heterometallic tetranuclear complex was also synthesized by stepwise complexation like heterometallic pentanuclear complex described in chapter 1. In the case of synthesis of heterometallic tetranuclear complex, a meridional isomer of the ruthenium mononuclear complex was used as a precursor, while

a facial isomer was used for the synthesis of heterometallic pentanuclear complex. By using the meridional isomer, a series of heterometallic tetranuclear complexes was successfully synthesized. The structures of the obtained complexes preserved the feature of the structure of the precursor. The tetranuclear complexes have relatively large vacant site around the hydroxo-bridged metal centers due to the different orientation of the ligands. As the summary of chapters 1 and 3, two different series of heterometallic multinuclear complexes can rationally and selectively be synthesized by using the geometrical isomer of the ruthenium mononuclear complex in the stepwise synthetic strategy.

References

1. R. Chakrabarty, P. S. Mukherjee, P. J. Stang, *Chem. Rev.*, **2011**, *111*, 6810.
2. S. R. Seidel, P. J. Stang, *Acc. Chem. Res.*, **2002**, *35*, 972.
3. S. Leininger, B. Olenyuk, P. J. Stang, *Chem. Rev.*, **2000**, *100*, 853.
4. M. Fujita, M. Tominaga, A. Hori, B. Therrien, *Acc. Chem. Res.*, **2005**, *38*, 371.
5. M. Fujita, *Chem. Soc. Rev.*, **1998**, *27*, 417.
6. C. J. Brown, F. D. Toste, R. G. Bergman, K. N. Raymond, *Chem. Rev.*, **2015**, *115*, 3012.
7. D. L. Caulder, K. N. Raymond, *Acc. Chem. Res.*, **1999**, *32*, 975.
8. J.-M. Lehn, *Chem. Soc. Rev.*, **2007**, *36*, 151.
9. J.-M. Lehn, *Science*, **2002**, *295*, 2400.
10. F. A. Cotton, C. Lin, C. A. Murillo, *Acc. Chem. Res.*, **2001**, *34*, 759.
11. L.-J. Chen, H.-B. Yang, M. Shionoya, *Chem. Soc. Rev.*, **2017**, *46*, 2555.
12. P. V. Rao, R. H. Holm, *Chem. Rev.*, **2004**, *104*, 527.
13. M. Fujita, J. Yazaki, K. Ogura, *J. Am. Chem. Soc.*, **1990**, *112*, 5645.
14. P. J. Stang, B. Olenyuk, *Acc. Chem. Res.*, **1997**, *30*, 502.
15. M. Tominaga, K. Suzuki, M. Kawano, T. Kusakawa, T. Ozaki, S. Sakamoto, K. Yamaguchi, M. Fujita, *Angew. Chem. Int. Ed.*, **2004**, *43*, 5621.
16. D. Fujita, A. Takahashi, S. Sato, M. Fujita, *J. Am. Chem. Soc.*, **2011**, *133*, 13317.
17. Q.-F. Sun, J. Iwasa, D. Ogawa, Y. Ishido, S. Sato, T. Ozeki, Y. Sei, K. Yamaguchi, M. Fujita, *Science*, **2010**, *328*, 1144.
18. S. Romain, J. Rich, C. Sens, T. Stoll, J. Benet-Buchholz, A. Llobet, M. Rodriguez, I. Romero, R. Clérac, C. Mathonière, C. Duboc, A. Deronzier, M.-N. Collomb, *Inorg. Chem.*, **2011**, *50*, 8427.
19. M. Nihei, T. Nankawa, M. Kurihara, H. Nishihara, *Angew. Chem. Int. Ed.*, **1999**, *38*, 1098.
20. M. Murata, S. Habe, S. Araki, K. Namiki, T. Yamada, N. Nakagawa, T. Nankawa, M. Nihei, J. Mizutani, M. Kurihara, H. Nishihara, *Inorg. Chem.*, **2009**, *131*, 1388.
21. S. Muratsugu, K. Sodeyama, F. Kitamura, M. Sugimoto, S. Tsuneyuki, S. Miyashita, T. Kato, H. Nishihara, *J. Am. Chem. Soc.*, **1975**, *97*, 2285.
22. E. Y. Tsui, R. Tran, J. Yano, T. Agapie, *Nat. Chem.*, **2013**, *5*, 293.
23. D. E. Herbert, D. Lionetti, J. Rittle, T. Agapie, *J. Am. Chem. Soc.*, **2013**, *135*, 19075.
24. S. T. Wilson, R. F. Bondurant, T. J. Meyer, D. J. Salmon, *J. Am. Chem. Soc.*, **1975**, *97*, 2285.
25. T. Ito, T. Hamaguchi, H. Negino, T. Yamaguchi, J. Washington, C. P. Kubiak, *Science*, **1997**, *277*, 660.

26. T. Ito, T. Hamaguchi, H. Negino, T. Yamaguchi, H. Kido, I. Zavarine, T. Richmond, J. Washington, C. P. Kubiak, *J. Am. Chem. Soc.*, **1999**, *121*, 4625.
27. T. Lis, B. Jezowska-Trzebiatowska, *Acta Crystallogr.*, **1980**, *B33*, 2112.
28. A. Caneschi, D. Gatteschi, R. Sessoli, *J. Am. Chem. Soc.*, **1991**, *113*, 5873.
29. R. Sessoli, D. Gatteschi, A. Caneschi, M. A. Novak, *Nature*, **1993**, *365*, 141.
30. P. D. W. Boyd, Q. Li, J. B. Vincent, K. Folting, H.-R. Chang, W. E. Streib, J. C. Huffman, G. Christou, D. N. Hendrickson, *J. Am. Chem. Soc.*, **1988**, *110*, 5873.
31. J. R. Friedman, M. P. Sarachik, J. Tejada, R. Ziolo, *Phys. Rev. Lett.*, **1996**, *76*, 3830.
32. W. Vreugdenhil, J. G. Haasnoot, O. Kahn, P. Thuéry, J. Reedijk, *J. Am. Chem. Soc.*, **1987**, *109*, 5272.
33. M. Nihei, M. Ui, M. Yokota, L. Han, A. Maeda, H. Kishida, H. Okamoto, H. Oshio, *Angew. Chem. Int. Ed.*, **2005**, *44*, 6484.
34. Y. Garcia, O. Kahn, L. Rabardel, B. Chansou, L. Salmon, J. P. Tuchagues, *Inorg. Chem.*, **1999**, *38*, 4663.
35. J. A. Real, E. Andrés, M. C. Muñoz, M. Julve, T. Granier, A. Bousseksou, F. Varret, *Science*, **1995**, *268*, 265.
36. G. J. Halder, C. J. Kepert, B. Moubaraki, K. S. Murray, J. D. Cashion, *Science*, **2002**, *298*, 1762.
37. D. M. Roundhill, H. B. Gray, C.-M. Che, *Acc. Chem. Res.*, **1989**, *22*, 55.
38. Y. Ozawa, M. Terashima, M. Mitsumi, K. Toriumi, N. Yasuda, H. Uekusa, Y. Ohashi, *Chem. Lett.*, **2003**, *32*, 62.
39. S. B. Harkins, J. C. Peters, *J. Am. Chem. Soc.*, **2005**, *127*, 2030.
40. H. Xie, I. Kinoshita, T. Karasawa, K. Kimura, T. Nishioka, I. Akai, K. Kanemoto, *J. Phys. Chem. B*, **2005**, *109*, 9339.
41. Y.-Y. Lin, S.-W. Lai, C.-M. Che, W.-F. Fu, Z.-Y. Zhou, N. Zhu, *Inorg. Chem.*, **2005**, *44*, 1511.
42. P. C. Ford, E. Cariati, J. Bourassa, *Chem. Rev.*, **1999**, *99*, 3625.
43. C. L. Raston, A. H. White, *J. Chem. Soc. Dalton Trans.*, **1976**, 2153.
44. J. C. Dyason, P. C. Healy, L. M. Engelhardt, C. Pakawatchai, V. A. Patrick, C. L. Raston, A. H. White, *J. Chem. Soc. Dalton Trans.*, **1985**, 831.
45. C. K. Ryu, K. R. Kyle, P. C. Ford, *Inorg. Chem.*, **1991**, *30*, 3982.
46. H. Araki, K. Tsuge, Y. Sasaki, S. Ishizaka, N. Kitamura, *Inorg. Chem.*, **2005**, *44*, 9667.
47. D. Li, H.-K. Yip, C.-M. Che, Z.-Y. Zhou, T. C. W. Mak, S.-T. Liu, *J. Chem. Soc. Dalton Trans.*, **1992**, 2445.
48. K. Fujisawa, S. Imai, N. Kitajima, Y. Moro-oka, *Inorg. Chem.*, **1998**, *37*, 168.
49. F. Sabin, C. K. Ryu, P. C. Ford, A. Vogler, *Inorg. Chem.*, **1992**, *31*, 1941.

50. P. Buchwalter, J. Rosé, P. Braunstein, *Chem. Rev.*, **2015**, *115*, 28.
51. P. L. Arnold, D. Patel, C. Wilson, J. B. Love, *Nature*, **2008**, *451*, 315.
52. S. Ogo, K. Ichikawa, T. Kishima, T. Matsumoto, H. Nakai, K. Kusaka, T. Ohhara, *Science*, **2013**, *339*, 682.
53. S. W. Gersten, G. J. Samuels, T. J. Meyer, *J. Am. Chem. Soc.*, **1982**, *104*, 4029.
54. J. Limburg, J. S. Vrettos, L. M. Liable-Sands, A. L. Rheingold, R. H. Crabtree, G. W. Brudvig, *Science*, **1999**, *283*, 1524.
55. Y. Xu, A. Fischer, L. Duan, L. Tong, E. Gabrielsson, B. Åkermark, L. Sun, *Angew. Chem. Int. Ed. Engl.*, **2010**, *49*, 8934.
56. M. Okamura, M. Kondo, R. Kuga, Y. Kurashige, T. Yanai, S. Hayami, V. K. K. Praneeth, M. Yoshida, K. Yoneda, S. Kawata, S. Masaoka, *Nature*, **2016**, *530*, 465.
57. Y. Umena, K. Kawakami, J.-R. Shen, N. Kamiya, *Nature*, **2011**, *473*, 55.
58. M. Suga, F. Akita, K. Hirata, G. Ueno, H. Murakami, Y. Nakajima, T. Shimizu, K. Yamashita, M. Yamamoto, H. Ago, J.-R. Shen, *Nature*, **2015**, *517*, 99.
59. K. Brown, M. Tegoni, M. Prudêncio, A. S. Pereira, S. Besson, J. J. Moura, I. Moura, C. Cambillau, *Nat. Struct. Biol.*, **2000**, *7*, 191.
60. E. M. Johnston, S. Dell'Acqua, S. Ramos, S. R. Pauleta, I. Moura, E. I. Solomon, *J. Am. Chem. Soc.*, **2014**, *136*, 614.
61. K. M. Lancaster, M. Roemelt, P. Ettenhuber, Y. Hu, M. W. Ribbe, F. Neese, U. Bergmann, S. DeBeer, *Science*, **2011**, *334*, 974.
62. D. J. Vinyard, S. Khan, M. Askerka, V. S. Batista, G. W. Brudvig, *J. phys. Chem. B*, **2017**, *121*, 1020.
63. D. A. Pantazis, W. Ames, N. Cox, W. Lubitz, F. Neese, *Angew. Chem. Int. Ed.*, **2012**, *51*, 9935.
64. D. Bovi, D. Narzi, L. Guidoni, *Angew. Chem. Int. Ed.*, **2013**, *52*, 11744.
65. P. Chen, I. Cabrito, J. J. G. Moura, I. Moura, E. I. Solomon, *J. Am. Chem. Soc.*, **2002**, *124*, 10497.

Chapter 1

On-demand installation of metal ions into pentanuclear metal complexes

Introduction

Multinuclear metal complexes are an intriguing class of materials because the strong interaction between composed metal ions can provide unique electronic structure, which cannot be achieved in mononuclear metal complexes. Owing to their characteristic electronic structures, these complexes can exhibit excellent functions not only in artificial system but also nature system.¹⁻³⁵ These complexes potentially generate various kinds of electronic states, between which the number and/or the position of the oxidized metal centers are different, and the difference in the distribution of oxidation states largely affects the electronic structure and their functions. In other hands, the control over the redox property in multinuclear metal complex can be an important strategy for obtaining the material with the target functionality. However, these materials generally exhibit complicated redox behaviors because of the strong electronic interaction between composed metal ions. The strong interaction induces various electron transfer pathways and the prediction of the electronic structure generated upon such reactions becomes extremely difficult.

Given that the redox behavior of multinuclear metal complexes is determined both by the nature of each composed metal ion and the electronic interaction between the metal ions, the redox behavior of them can be controlled by installing the desired metal ions into specific position of them. In addition, systematic investigation on a series of them, in which the redox behavior of them is controllable with keeping the same molecular framework, is of great significance. This is because such systematic investigation would provide a comprehensive guideline to understand the redox behavior of multinuclear metal complexes. However, although studies on multinuclear metal complexes are abundant, such replacement of metal ions had been achieved mostly relying on the fruit of serendipity, and on-demand installation of metal ions into the

multinuclear metal complex with desired molecular framework is still challenging. Because of such lack in the rational synthetic route, the construction of definitive strategy to manipulate the redox behavior of multinuclear metal complexes had not been achieved.

This chapter describes the syntheses and characterization of a series of heterometallic pentanuclear complexes. A rational procedure enables the on-demand installation of metal ions into the multinuclear metal complex was successfully developed by utilizing the stepwise metalation method. As a result, the syntheses of a series of pentanuclear metal complexes which have different arrangement of metal ions with keeping the same molecular framework were achieved.

Experimental Section

Materials.

Mn(OAc)₂•4H₂O, Co(OAc)₂•4H₂O, NH₄PF₆ and NaOH were purchased from Wako Pure Chemical Industries, Ltd. Zn(OAc)₂•2H₂O was purchased from Kanto Chemical Co., Inc. RuCl₃•3H₂O was purchased from Tanaka Kikinzoku Kogyo K.K. 3,5-Bis(2-pyridyl)pyrazole, 1,8-diazabicyclo[5.4.0]undec-7-ene (DBU) and Fe(OAc)₂ and were purchased from Tokyo Chemical Industry Co., Ltd. NaClO₄ was purchased from Aldrich. All solvents and reagents are of the highest quality available and used as received. H₂O was purified using a Millipore MilliQ purifier, and was purged with argon before use.

Measurements Apparatus.

Elemental analyses were carried out on a J-SCIENCE LAB MICRO CORDER JM10 elemental analyser. ESI TOF-MS were recorded on a JEOL JMS-T100LP mass spectrometer.

X-ray Crystallography.

A crystal of the obtained complex was mounted in a loop. Diffraction data of **Ru₂Zn₃(ClO₄)₃**, **Ru₂Fe₃(ClO₄)₃**, **Ru₂Mn₃(ClO₄)₃**, **Zn₅(BF₄)₃**, **Co₅(BF₄)₃**, and **Mn₅(ClO₄)₃** at 123 K were measured on a Synergy Custom system CCD Plate diffractometer equipped with mirror monochromated Mo-K α radiation and data were processed using CrysAlisPro (Rigaku). Diffraction data of **[Ru(Hbpp)₃](PF₆)₂** and **Ru₂Co₃(PF₆)₃** at 123 K were measured on a RAXIS-RAPID Imaging Plate diffractometer equipped with a confocal monochromated Mo-K α radiation source, and data were processed using RAPID-AUTO (Rigaku). The structures were solved by direct method using *SIR-92*³⁶ and refined by the full-matrix least squares techniques on *F²* (*SHELXL-2014/7*)³⁷. All non-hydrogen atoms were refined anisotropically and refined with a riding model with U_{iso} constrained to be 1.2 times U_{eq} of the carrier atom. The diffused electron densities resulting from residual solvent molecules were removed from the data set using the SQUEEZE routine of PLATON³⁸ and refined further using the data generated. Crystallographic data have been deposited with Cambridge Crystallographic Data Centre: CCDC deposition numbers; 1949864 for **[Ru(Hbpp)₃](PF₆)₂**, 1949857 for **Ru₂Zn₃(ClO₄)₃**, 1949860 for **Ru₂Co₃(PF₆)₃**, 1949856 for **Ru₂Fe₃(ClO₄)₃**, 1949858 for

Ru₂Mn₃(ClO₄)₃, 1949861 for **Zn₅(BF₄)₃**, 1949862 for **Co₅(BF₄)₃**, and 1949859 for **Mn₅(ClO₄)₃**. Copies of the data can be obtained free of charge via www.ccdc.cam.ac.uk/data_request/cif.

Syntheses of homometallic pentanuclear complexes

Synthesis of [$\{\text{Zn}^{\text{II}}(\mu\text{-bpp})_3\}_2\text{Zn}^{\text{II}}(\mu\text{-OH})\}(\text{BF}_4)_3$ (**Zn₅(BF₄)₃**) was performed by modifying the procedure reported in the literatures.³⁹ Synthesis of [$\{\text{Fe}^{\text{II}}(\mu\text{-bpp})_3\}_2\text{Fe}^{\text{II}}\text{Fe}^{\text{III}}(\mu\text{-O})\}(\text{BF}_4)_3$ (**Fe₅(BF₄)₃**)²⁵, and [$\{\text{Mn}^{\text{II}}(\mu\text{-bpp})_3\}_2\text{Mn}^{\text{II}}\text{Mn}^{\text{III}}(\mu\text{-O})\}(\text{ClO}_4)_3$ (**Mn₅(ClO₄)₃**)⁴⁰ was performed according to the reported methods.

Synthesis of fac-[Ru(Hbpp)₃](ClO₄)₂.

RuCl₃·3H₂O (2.0 mmol) and 3,5-bis(2-pyridyl)pyrazole (Hbpp; 6.0 mmol) were suspended to 18.0 mL of ethanol. The reaction mixture was heated at 120°C for 9 hours by microwave reactor. The reaction mixture was filtered to remove undissolved residues and excess amount of saturated aqueous NaClO₄ solution was added to the filtrate, then the precipitate was collected by filtration. The obtained precipitate was dissolved in acetonitrile and a slow diffusion of diisopropylether at ambient temperature gave light orange crystals after a few days. The crystals were collected by filtration and dried under vacuum. Yield 265.31 mg (12.9%). Elemental analysis Calcd. for **[Ru(Hbpp)₃](ClO₄)₂·3.5H₂O**: C₃₉H₃₇Cl₂N₁₂O_{11.5}Ru₁: C, 45.49; H, 3.62; N, 16.32%. Found: C, 45.55; H 3.38; N 16.43%. ESI TOF-MS (positive ion, acetonitrile): m/z: 384.14 [Ru(Hbpp)₃]²⁺, 767.27 [Ru(Hbpp)₂(bpp)]⁺, 867.26 ([Ru(Hbpp)₃]²⁺+ClO₄⁻)⁺. ¹H NMR (400 MHz, CD₃CN): δ = 8.24 (t, *J* = 7.4 Hz, 1H), 7.95 (d, *J* = 8.2 Hz, 1H), 7.84 (t, *J* = 7.6 Hz, 1H), 7.45 (d, *J* = 7.8 Hz, 1H), 7.40 (d, *J* = 5.1 Hz, 1H), 7.19 (t, *J* = 6.4 Hz, 1H), 7.14 (t, *J* = 6.4 Hz, 1H), 7.08 (d, *J* = 5.0 Hz, 1H), 7.06 (s, 1H). **[Ru(Hbpp)₃](PF₆)₂** was prepared by adding excess amount of a saturated aqueous NH₄PF₆ solution instead of a saturated aqueous NaClO₄ solution to the filtrate obtained after the reaction. The formed precipitate was collected by filtration and dissolved in acetonitrile. Slow vapour diffusion of diethylether into the resultant solution affords the single crystals of **[Ru(Hbpp)₃](PF₆)₂** suitable for single crystal X-ray structural determination.

Synthesis of $[\{\text{Ru}^{\text{II}}(\mu\text{-bpp})_3\}_2\text{Zn}^{\text{II}}_3(\mu\text{-OH})](\text{ClO}_4)_3$ ($\text{Ru}_2\text{Zn}_3(\text{ClO}_4)_3$).

$\text{Ru}(\text{Hbpp})_3(\text{ClO}_4)_2 \cdot 3.5\text{H}_2\text{O}$ (0.03 mmol) and $\text{Zn}(\text{OAc})_2 \cdot 2\text{H}_2\text{O}$ (0.15 mmol) were dissolved in 3.0 mL of *N*-methylpyrrolidone. 1.0 M NaOH aqueous solution (300 μL) was added to the solution, and then it was heated at 80°C for 12 hours. The reaction mixture was filtered to remove undissolved residues and excess amount of saturated aqueous NaClO_4 solution and excess amount of H_2O were added to the filtrate, then the precipitate was collected by filtration. The obtained precipitate was dissolved in acetonitrile and a slow diffusion of diethylether at ambient temperature gave light red crystals after a few days. The crystals were collected by filtration and dried under vacuum. Yield 28.12 mg (85.1%). Elemental analysis Calcd. for $[\text{Ru}_2\text{Zn}_3(\text{OH})(\text{bpp})_6](\text{ClO}_4)_3 \cdot 8\text{H}_2\text{O}$: $\text{C}_{78}\text{H}_{70}\text{Cl}_3\text{N}_{24}\text{O}_{21}\text{Ru}_2\text{Zn}_3$: C, 42.87; H, 3.27; N, 15.38%. Found: C, 42.76; H 3.25; N 15.28%. ESI TOF-MS (positive ion, acetonitrile): m/z : 580.91 $[\{\text{Ru}^{\text{II}}(\mu\text{-bpp})_3\}_2\text{Zn}^{\text{II}}_3(\mu\text{-OH})]^{3+}$, 592.88 $([\{\text{Ru}^{\text{II}}(\mu\text{-bpp})_3\}_2\text{Zn}^{\text{II}}_3(\mu\text{-OH})]^{3+} + 2\text{H}_2\text{O})^{3+}$. ^1H NMR (400 MHz, CD_3CN): δ = 7.98-7.91 (m, 4H), 7.86 (d, J = 7.8 Hz, 2H), 7.47-7.41 (m, 3H), 7.38 (d, J = 8.2 Hz, 1H), 7.19 (t, J = 6.3 Hz, 2H), 6.98-6.92 (m, 2H), 6.69 (d, J = 4.8 Hz, 1H), 6.64 (d, J = 5.2 Hz, 1H), 6.55 (s, 1H), 6.51 (s, 1H). Single crystals of the complex suitable for single crystal X-ray structural determination were obtained by the slow vapour diffusion of diethylether into an acetonitrile solution of $[\{\text{Ru}^{\text{II}}(\mu\text{-bpp})_3\}_2\text{Zn}^{\text{II}}_3(\mu\text{-OH})](\text{ClO}_4)_3$.

Synthesis of $[\{\text{Ru}^{\text{II}}(\mu\text{-bpp})_3\}_2\text{Co}^{\text{II}}_3(\mu\text{-OH})](\text{ClO}_4)_3$ ($\text{Ru}_2\text{Co}_3(\text{ClO}_4)_3$).

$\text{Ru}(\text{Hbpp})_3(\text{ClO}_4)_2 \cdot 3.5\text{H}_2\text{O}$ (0.03 mmol) and $\text{Co}(\text{OAc})_2 \cdot 4\text{H}_2\text{O}$ (0.15 mmol) were dissolved in 3.0 mL of *N*-methylpyrrolidone. 1.0 M NaOH aqueous solution (300 μL) was added to the solution, and then it was heated at 80°C for 12 hours. The reaction mixture was filtered to remove undissolved residues and excess amount of saturated aqueous NaClO_4 solution was added to the filtrate, then the precipitate was collected by filtration. The obtained precipitate was dissolved in acetonitrile and a slow diffusion of *t*-butylmethylether at ambient temperature gave dark red crystals after a few days. The crystals were collected by filtration and dried under vacuum. Yield 27.35 mg (83.8%). Elemental analysis Calcd. for $[\text{Ru}_2\text{Co}_3(\text{OH})(\text{bpp})_6](\text{ClO}_4)_3 \cdot 8.5\text{H}_2\text{O}$: $\text{C}_{78}\text{H}_{72}\text{Cl}_3\text{Co}_3\text{N}_{24}\text{O}_{21.5}\text{Ru}_2$: C, 43.08; H, 3.34; N, 15.46%. Found: C, 42.98; H 3.26; N 15.43%. ESI TOF-MS (positive ion, acetonitrile): m/z : 574.58 $[\{\text{Ru}^{\text{II}}(\mu\text{-bpp})_3\}_2\text{Co}^{\text{II}}_3(\mu\text{-OH})]^{3+}$, 586.56 $([\{\text{Ru}^{\text{II}}(\mu\text{-bpp})_3\}_2\text{Co}^{\text{II}}_3(\mu\text{-OH})]^{3+} + 2\text{H}_2\text{O})^{3+}$. Single crystals of $[\{\text{Ru}^{\text{II}}(\mu\text{-bpp})_3\}_2\text{Co}^{\text{II}}_3(\mu\text{-OH})](\text{PF}_6)_3$ was prepared by adding excess amount of a saturated aqueous NH_4PF_6 solution instead of a saturated aqueous NaClO_4 solution to the filtrate obtained

after the reaction. The formed precipitate was collected by filtration and dissolved in acetonitrile. Slow vapour diffusion of diethylether into the resultant solution affords the single crystals of $[\{\text{Ru}^{\text{II}}(\mu\text{-bpp})_3\}_2\text{Co}^{\text{II}}_3(\mu\text{-OH})](\text{PF}_6)_3$ suitable for single crystal X-ray structural determination.

Synthesis of $[\{\text{Ru}^{\text{II}}(\mu\text{-bpp})_3\}_2\text{Fe}^{\text{II}}_2\text{Fe}^{\text{III}}(\mu\text{-O})](\text{ClO}_4)_3$ ($\text{Ru}_2\text{Fe}_3(\text{ClO}_4)$).

$\text{Ru}(\text{Hbpp})_3(\text{ClO}_4)_2 \cdot 3.5\text{H}_2\text{O}$ (0.03 mmol) and $\text{Fe}(\text{OAc})_2$ (0.5 mmol) were dissolved in 10.0 mL of *N*-methylpyrrolidone. DBU (0.60 mmol) was added to the solution, and then it was heated at 100°C for 12 hours. Excess amount of saturated aqueous NaClO_4 solution was added to the reaction mixture, then the mixture was sonicated for 20 minutes. The precipitate was obtained by addition of excess amount of H_2O , then the precipitate was collected by filtration. The obtained precipitate was washed with H_2O , then mixture of diethylether and small amount of methanol. The obtained brown powder was extracted with acetonitrile. The solution was concentrated and a slow diffusion of diethylether at ambient temperature gave dark brown crystals after a few days. The crystals were collected by filtration and dried under vacuum. Yield 24.40 mg (77.5%) Elemental analysis Calcd. for $[\text{Ru}_2\text{Fe}_3\text{O}(\text{bpp})_6](\text{ClO}_4)_3 \cdot 7\text{H}_2\text{O}$: $\text{C}_{78}\text{H}_{68}\text{Cl}_3\text{Fe}_3\text{N}_{24}\text{O}_{20}\text{Ru}_2$: C, 43.83; H, 3.21; N, 15.73%. Found: C, 43.74; H 3.20; N 15.58%. ESI TOF-MS (positive ion, acetonitrile): m/z : 570.26 $[\{\text{Ru}^{\text{II}}(\mu\text{-bpp})_3\}_2\text{Fe}^{\text{II}}_2\text{Fe}^{\text{III}}(\mu\text{-O})]^{3+}$, 583.25 $([\{\text{Ru}^{\text{II}}(\mu\text{-bpp})_3\}_2\text{Fe}^{\text{II}}_2\text{Fe}^{\text{III}}(\mu\text{-O})]^{3+} + 2\text{H}_2\text{O})^{3+}$. Single crystals of the complex suitable for single crystal X-ray structural determination were obtained by the slow vapour diffusion of diethylether into an acetonitrile solution of $[\{\text{Ru}^{\text{II}}(\mu\text{-bpp})_3\}_2\text{Fe}^{\text{II}}_2\text{Fe}^{\text{III}}(\mu\text{-O})](\text{ClO}_4)_3$.

Synthesis of $[\{\text{Ru}^{\text{II}}(\mu\text{-bpp})_3\}_2\text{Mn}^{\text{II}}_2\text{Mn}^{\text{III}}(\mu\text{-O})](\text{ClO}_4)_3$ ($\text{Ru}_2\text{Mn}_3(\text{ClO}_4)$).

$\text{Ru}(\text{Hbpp})_3(\text{ClO}_4)_2 \cdot 3.5\text{H}_2\text{O}$ (0.06 mmol) and $\text{Mn}(\text{OAc})_2 \cdot 4\text{H}_2\text{O}$ (1.0 mmol) were dissolved in 10.0 mL of *N*-methylpyrrolidone. DBU (0.60 mmol) was added to the solution, and then it was heated at 80°C for 8 hours. Excess amount of saturated aqueous NaClO_4 solution was added to the reaction mixture, then the mixture was sonicated for 20 minutes. The precipitate was obtained by addition of excess amount of H_2O , then the precipitate was collected by filtration. The obtained precipitate was washed with H_2O , then mixture of diethylether and small amount of methanol. The obtained brown colour powder was extracted with 15.0 mL of acetonitrile. The solution was concentrated to 8.0 mL and 1.0 M NaOH aqueous solution (30 μL) was added to the solution, and then it was stirred at ambient temperature. Excess amount of saturated aqueous NaClO_4 solution was

added to the reaction mixture, then the mixture was sonicated for 20 minutes. The precipitate was obtained by addition of excess amount of H₂O, then the precipitate was collected by filtration. The obtained precipitate was washed with H₂O, then mixture of diethylether and small amount of methanol. The obtained brown powder was extracted with acetonitrile. The solution was concentrated and a slow diffusion of diethylether at ambient temperature gave dark brown crystals after a few days. The crystals were collected by filtration and dried under vacuum. Yield 46.60 mg (72.1%) Elemental analysis Calcd. for [Ru₂Mn₃O(bpp)₆](ClO₄)₃·8H₂O: C₇₈H₇₀Cl₃Mn₃N₂₄O₂₁Ru₂: C, 43.52; H, 3.28; N, 15.61%. Found: C, 43.38; H 3.11; N 15.51%. ESI TOF-MS (positive ion, acetonitrile): m/z: 570.26 [$\{\text{Ru}^{\text{II}}(\mu\text{-bpp})_3\}_2\text{Mn}^{\text{II}}\text{Mn}^{\text{III}}(\mu\text{-O})\}^{3+}$, 582.24 ($[\{\text{Ru}^{\text{II}}(\mu\text{-bpp})_3\}_2\text{Mn}^{\text{II}}\text{Mn}^{\text{III}}(\mu\text{-O})\}^{3+} + 2\text{H}_2\text{O})^{3+}$) Single crystals of the complex suitable for single crystal X-ray structural determination were obtained by the slow vapour diffusion of diethylether into an acetonitrile solution of [$\{\text{Ru}^{\text{II}}(\mu\text{-bpp})_3\}_2\text{Mn}^{\text{II}}\text{Mn}^{\text{III}}(\mu\text{-O})\}(\text{ClO}_4)_3$].

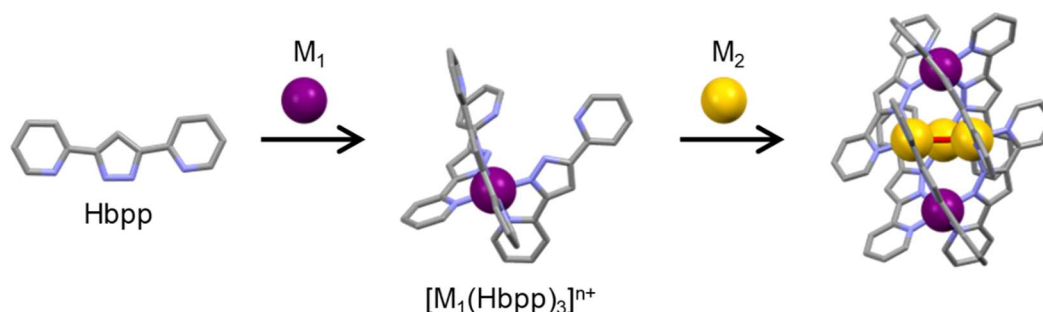
Synthesis of [$\{\text{Co}^{\text{II}}(\mu\text{-bpp})_3\}_2\text{Co}^{\text{II}}_3(\mu\text{-OH})\}(\text{BF}_4)_3 \cdot (\text{Co}_5(\text{BF}_4)_3)$].

Aqueous solution of NaOH (1 M, 0.48 mL) was added to the methanol solution (4 mL) of 3,5-bis(pyridyl)pyrazole (Hbpp, 0.48 mmol, 107 mg). Co(CH₃COO)₂·4H₂O (0.40 mmol, 100 mg) was then added to the reaction mixture and stirred at 40 °C for 10 minutes. A few drops of saturated aqueous NaBF₄ solution was added to the reaction mixture, and a small portion of water was added to the solution. The solution was kept in a refrigerator for 1 h to generate a brown precipitate. The precipitate was collected by filtration, washed with water and dried under vacuum. The obtained precipitate was dissolved in acetonitrile and subjected to vapor diffusion in diethyl ether to afford brown crystals of [$\{\text{Co}^{\text{II}}(\mu\text{-bpp})_3\}_2\text{Co}^{\text{II}}_3(\mu\text{-OH})\}(\text{BF}_4)_3 \cdot 2\text{H}_2\text{O}$]. The crystals were collected by filtration and dried under vacuum. Yield 80 mg (52%). Elemental analysis calcd for [$\{\text{Co}^{\text{II}}(\mu\text{-bpp})_3\}_2\text{Co}^{\text{II}}_3(\mu\text{-OH})\}(\text{BF}_4)_3 \cdot 2\text{H}_2\text{O}$]: C₇₈H₅₉Co₅F₁₂N₂₄O₃B₃: C, 48.40; H, 3.07; N, 17.37%. Found: C, 48.35; H, 3.13; N, 17.32%.

Strategy

Given that electron transfer reaction mainly occurs at metal centres in multinuclear metal complexes, the exclusive extraction of the effects of the metal ions on the electron transfer reactions should provide comprehensive guideline for elucidating the factors that determine the manner of the electron transfer reactions. In this context, the construction of a series of multinuclear metal complexes in which different kinds of metal ions are installed into the same molecular framework is of great significance. However, the on-demand installation of metal ions into the desired multinuclear structure is still challenging.

Based on the aforementioned background, the study started with the development of a rational synthetic strategy that enables the on-demand installation of metal ions into multinuclear metal complex. A pentanuclear complex composed of 3,5-bis(2-pyridyl)pyrazole (Hbpp) and metal ion was focused as a molecular scaffold. The electronic interactions occur among the metal ions in this class of complexes, and these interactions afford unique electronic^{40,41}/spin^{42,43} states and catalytic activities^{25,44}. To assemble metal ions into this pentanuclear scaffold in a controlled fashion, a new stepwise synthetic method shown in Scheme 1-1 was developed. In the strategy, a substitution-inert metal ion (M_1) is initially reacted with three equivalent of Hbpp under harsh condition to afford a mononuclear complex, $[M_1(\text{Hbpp})_3]^{n+}$. Subsequently, $[M_1(\text{Hbpp})_3]^{n+}$ is reacted with a substitution-labile metal ion (M_2) under milder condition. This strategy suppresses the scrambling of the metal ions and affords pentanuclear complex with the desired arrangement of metal ions.



Scheme 1-1 | Synthetic strategy for obtaining a series of heterometallic pentanuclear complexes. M_1 and M_2 represent substitution-inert metal ion and substitution-labile metal ion, respectively.

In this study, ruthenium ion was selected as M_1 because ruthenium-based complexes display redox activity, and their absorption properties are highly dependent on their oxidation states⁴¹, making them suitable for probing the electronic structure of the generated complex. A series of first-row transition metal ions with different redox activity (zinc, cobalt, iron and manganese ion) were employed as M_2 . Notably, the large difference in the number of electrons in M_1 and M_2 should allow the determination of the arrangement of the metal ions in the obtained complex by X-ray crystallographic technique.

Synthesis and Characterization

The initial step, the synthesis of a mononuclear ruthenium complex was performed by reacting RuCl_3 with 3 eq. of Hbpp in ethanol at $120\text{ }^\circ\text{C}$ for 9 hours. The anion exchange reaction and crystallization from a slow diffusion of diisopropylether to the acetonitrile solution at ambient temperature afforded red crystals. The composition of the red crystal was confirmed as $[\text{Ru}(\text{Hbpp})_3](\text{ClO}_4)_2$ by electro-spray ionization time-of-flight mass spectrometry (ESI TOF-MS) and elemental analysis (Figure 1-1). The single crystal X-ray structural analysis of the red crystal revealed that $[\text{Ru}(\text{Hbpp})_3](\text{ClO}_4)_2$ is a *facial* isomer (Figure 1-2 and Table 1-1), which is suitable for the formation of the target pentanuclear structure. It should be also noted that a *facial* structure of the complex is maintained in the solution state as evidenced by ^1H NMR spectroscopy (Figure 1-3). The yield of *fac*- $[\text{Ru}(\text{Hbpp})_3](\text{ClO}_4)_2$ was 13%, the preparation of the ruthenium mononuclear complex as a precursor of stepwise synthetic method was accomplished.

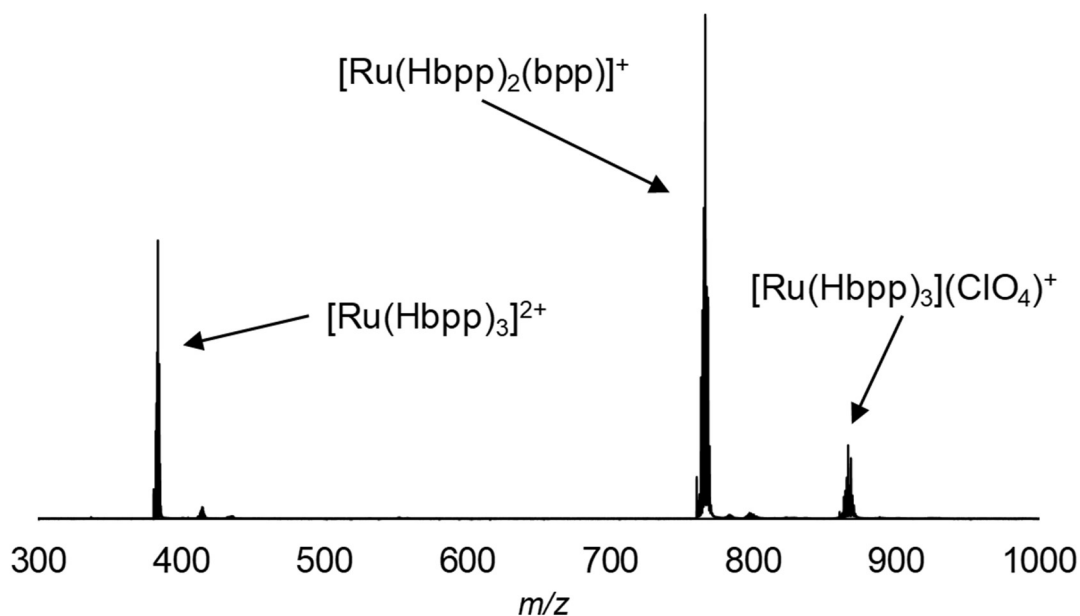


Figure 1-1 | ESI TOF-MS of *fac*- $[\text{Ru}(\text{Hbpp})_3](\text{ClO}_4)_2$ in acetonitrile.

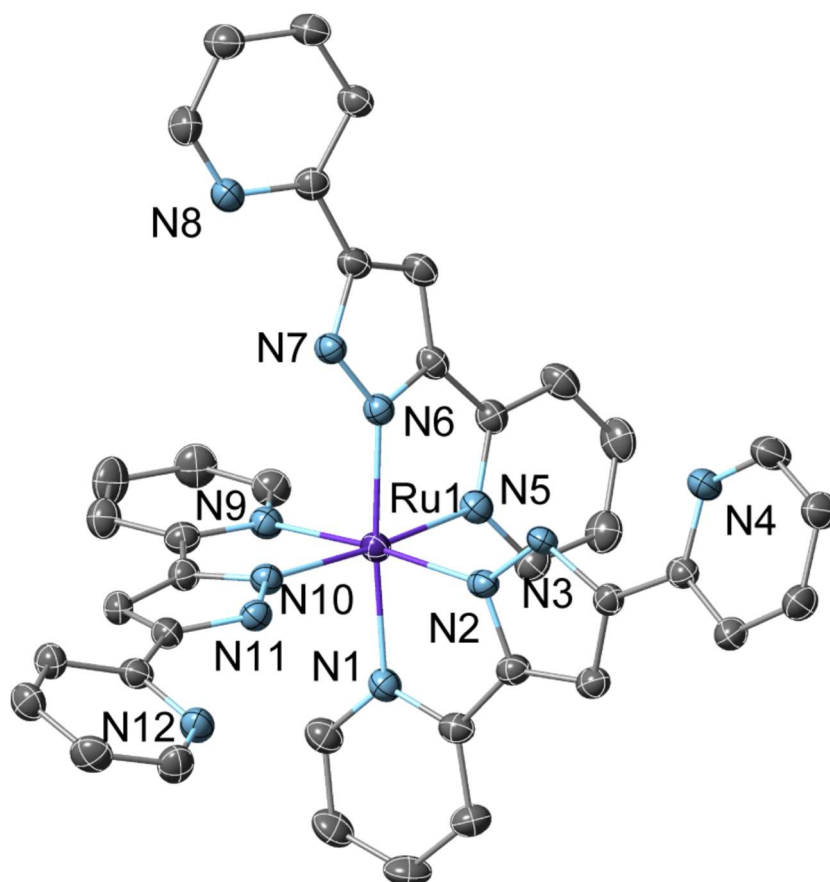


Figure 1-2 | An ORTEP drawing (50% probability ellipsoids) of a cationic moiety of *fac*-[Ru(Hbpp)₃](PF₆)₂. Hydrogen atoms are omitted clarity. C = grey, N = pale blue, and Ru = purple.

Table 1-1 | Summary of the crystallographic data for *fac*-[Ru(Hbpp)₃](PF₆)₂.

Formula	C ₄₅ H ₄₃ F ₁₂ N ₁₃ OP ₂ Ru
Fw	1172.93
Crystal color, habit	red, platelet
Crystal size, mm ³	0.54 × 0.30 × 0.19
Crystal system	monoclinic
Space group	<i>C</i> 2/c
<i>a</i> , Å	14.6835(3)
<i>b</i> , Å	25.0850(5)
<i>c</i> , Å	26.3732(5)
β , °	92.711(7)
<i>V</i> , Å ³	9703.3(3)
<i>Z</i>	8
<i>F</i> (000)	4752
<i>d</i> _{calc} , g/cm ³	1.606
μ (MoK α), mm ⁻¹	0.487
<i>T</i> , K	123
<i>R</i> ₁	0.045
w <i>R</i> ₂	0.0956
GOF	1.041

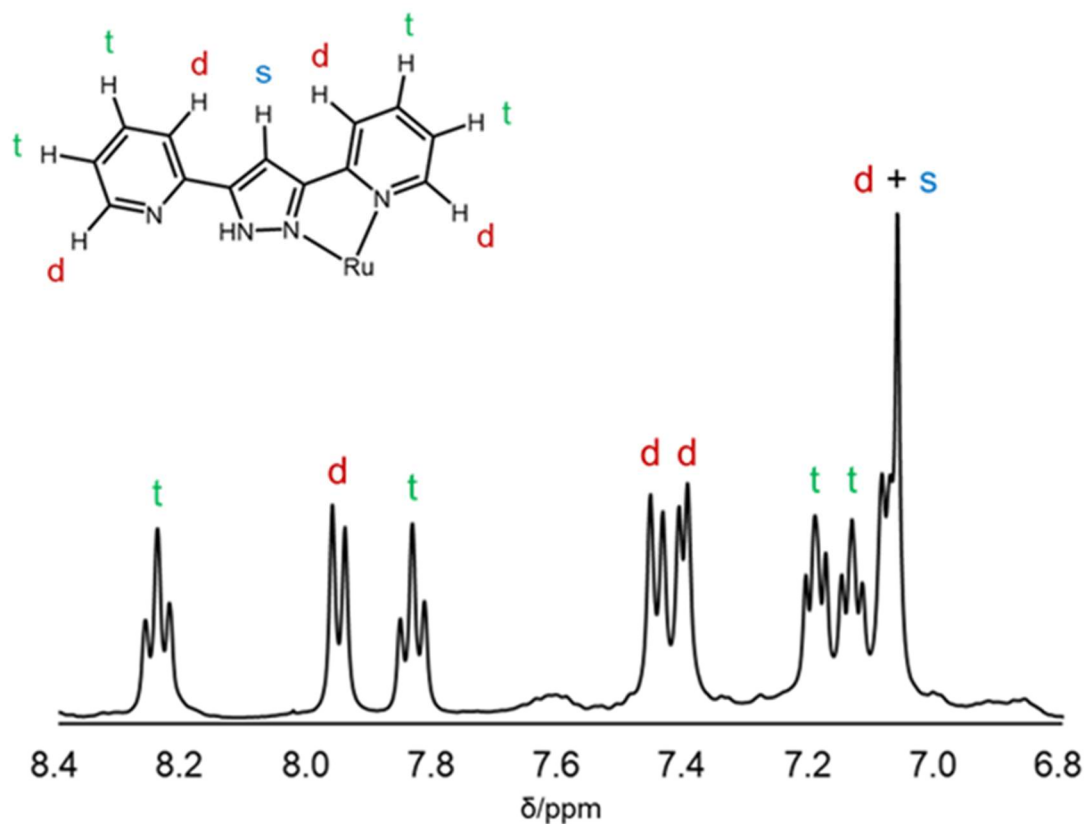


Figure 1-3 | A ^1H NMR spectrum of *fac*-[Ru(Hbpp) $_3$](ClO $_4$) $_2$ in MeCN- d_3 at 293 K.

Subsequently, the reactions of *fac*-[Ru(Hbpp) $_3$](ClO $_4$) $_2$ with first-row transition metal ion (Zinc, Cobalt, Iron and Manganese) were examined. Typically, *fac*-[Ru(Hbpp) $_3$](ClO $_4$) $_2$ was reacted with the appropriate metal ion source in the presence of base at 80-100 °C. The obtained complexes were characterized by ESI TOF-MS (Figure 1-4, 1-5, 1-6 and 1-7), elemental analyses and single crystal X-ray structural analyses. The yields for the second step are in the range of 72-85%, indicating the selective formation of the heterometallic pentanuclear complexes.

The relevant homometallic pentanuclear complexes, [$\{\text{Zn}^{\text{II}}(\mu\text{-bpp})_3\}_2\text{Zn}^{\text{II}}_3(\mu\text{-OH})\}^{3+}$ (**Zns**), [$\{\text{Co}^{\text{II}}(\mu\text{-bpp})_3\}_2\text{Co}^{\text{II}}_3(\mu\text{-OH})\}^{3+}$ (**Cos**), [$\{\text{Fe}^{\text{II}}(\mu\text{-bpp})_3\}_2\text{Fe}^{\text{II}}_2\text{Fe}^{\text{III}}(\mu\text{-O})\}^{3+}$ (**Fes**), and [$\{\text{Mn}^{\text{II}}(\mu\text{-bpp})_3\}_2\text{Mn}^{\text{II}}_2\text{Mn}^{\text{III}}(\mu\text{-O})\}^{3+}$ (**Mns**) were also prepared.

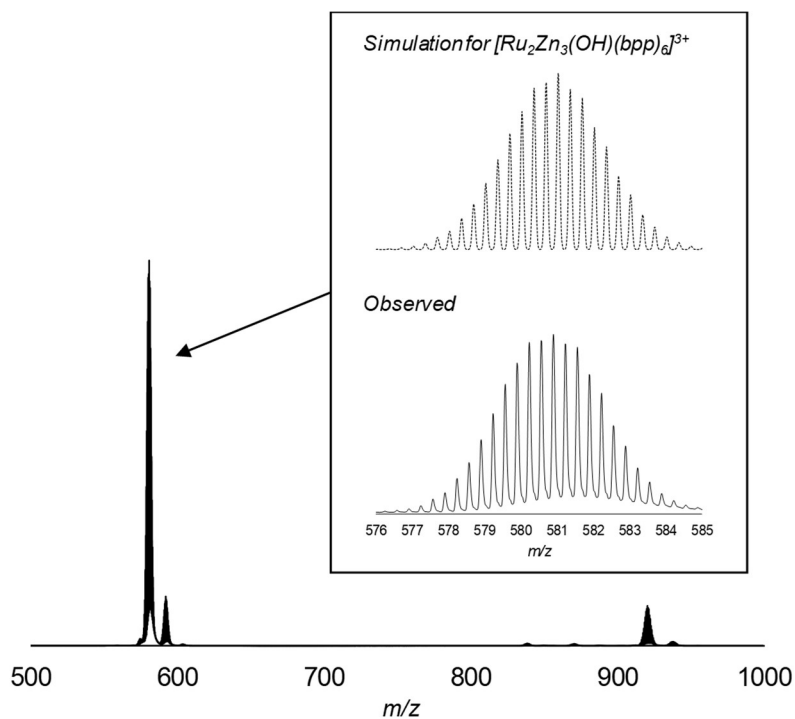


Figure 1-4 | ESI TOF-MS of $Ru_2Zn_3(ClO_4)_3$ in acetonitrile.

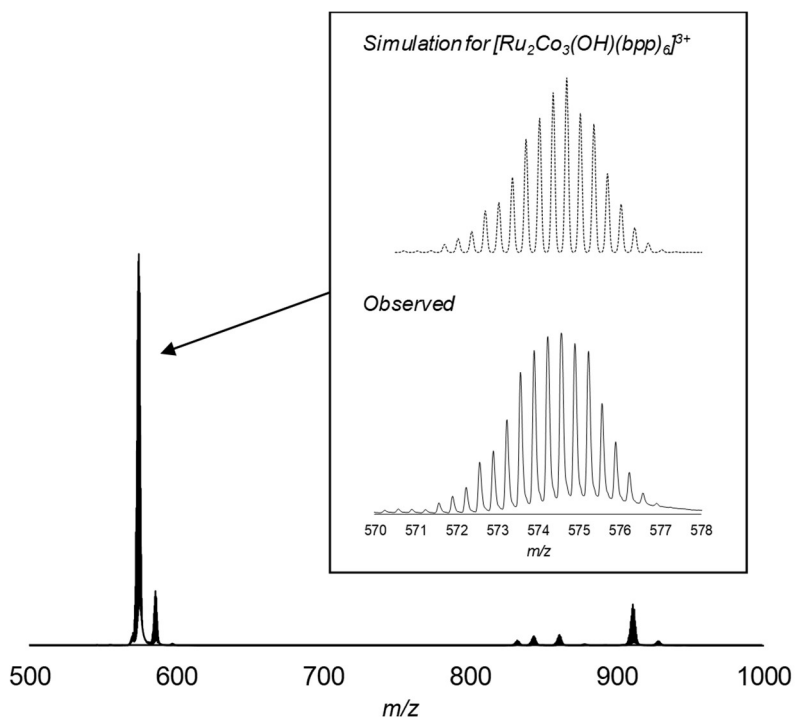


Figure 1-5 | ESI TOF-MS of $Ru_2Co_3(ClO_4)_3$ in acetonitrile.

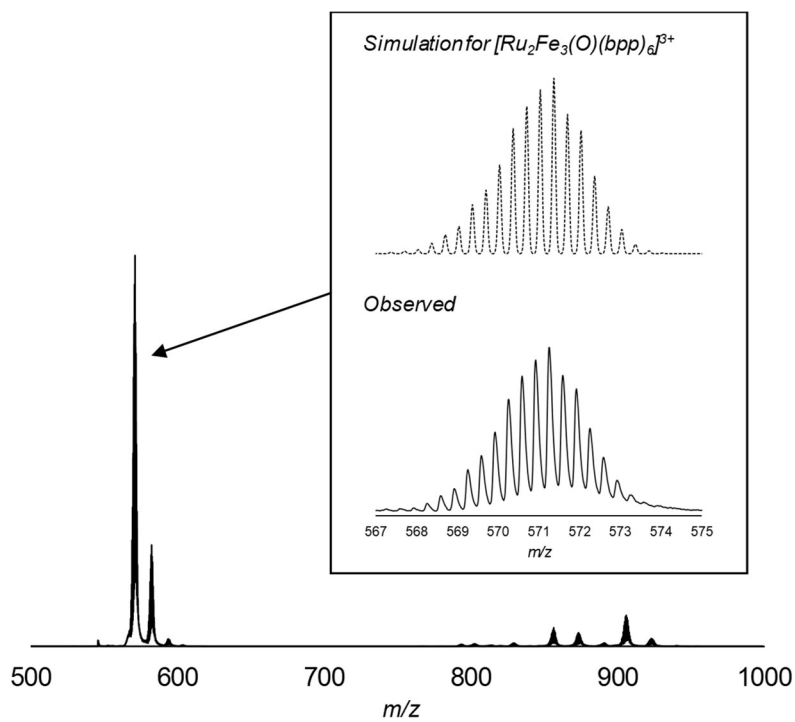


Figure 1-6 | ESI TOF-MS of $Ru_2Fe_3(ClO_4)_3$ in acetonitrile.

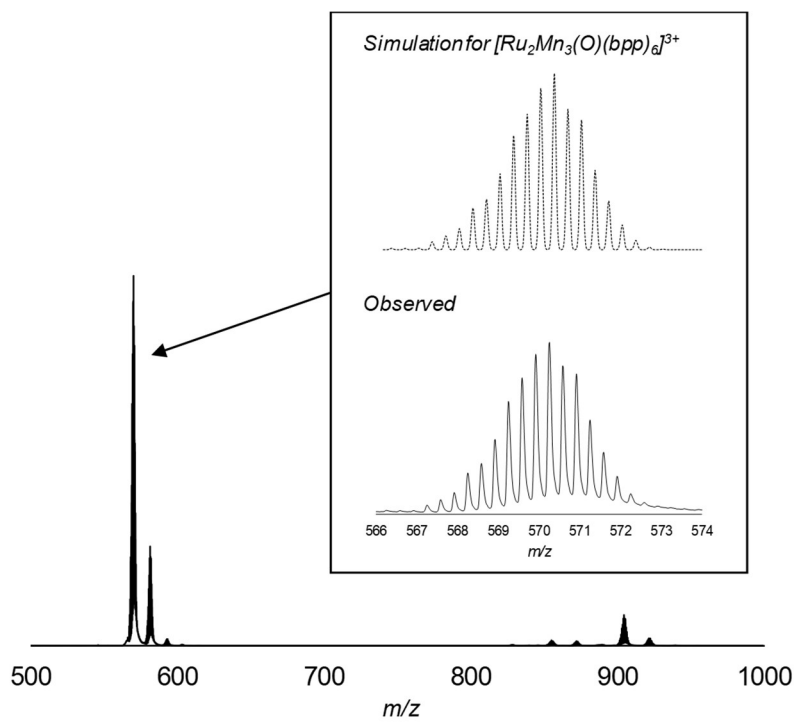


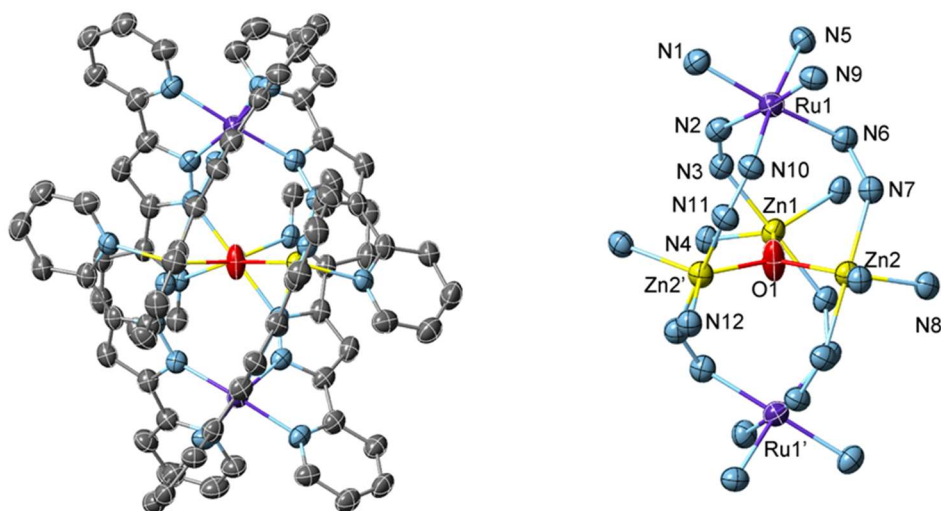
Figure 1-7 | ESI TOF-MS of $Ru_2Mn_3(ClO_4)_3$ in acetonitrile.

The crystal structures of the hetero/homometallic pentanuclear complexes are shown in Figure 1-8, 1-9, 1-10 and 1-11, and the crystallographic data are summarized in Table 1-2 and 1-3. All the complexes exhibit the desired pentanuclear structure with quasi- D_3 symmetry and consist of a triangular core wrapped by two $[M(\mu\text{-bpp})_3]$ units. The two metal ions at the apical position (M_{api}) are hexacoordinate with distorted octahedral geometry, whereas the three metal ions in the triangular core (M_{core}) are pentacoordinate with distorted trigonal bipyramidal geometry. The bond distances between M_{api} and the nitrogen atoms of the $[M(\mu\text{-bpp})_3]$ units ($d(M_{\text{api}}\text{-N})$) in the newly synthesized heterometallic complexes are significantly different from those in the corresponding homometallic complexes (Tables 1-4 and 1-5). In contrast, $d(M_{\text{api}}\text{-N})$ are almost constant in the heterometallic complexes. These observations strongly indicate that M_{api} in these heterometallic pentanuclear complexes are ruthenium ions.

The bond distances between M_{core} and the nitrogen atoms in the triangular core ($d(M_{\text{core}}\text{-N})$) are similar in the heterometallic and homometallic pentanuclear complexes containing the same first-row transition metal ion. Moreover, the bond distances between M_{core} and the oxygen atom in the triangular core ($d(M_{\text{core}}\text{-O})$) of the heterometallic complexes are quite similar to those in the corresponding homometallic complexes. Thus, the structures of the triangular cores in the heterometallic and homometallic complexes are identical.

Taken together, the structures of the heterometallic pentanuclear complexes in this series can be described as $[\{\text{Ru}^{\text{II}}(\mu\text{-bpp})_3\}_2\text{Zn}^{\text{II}}_3(\mu\text{-OH})]^{3+}$ (**Ru₂Zn₃**), $[\{\text{Ru}^{\text{II}}(\mu\text{-bpp})_3\}_2\text{Co}^{\text{II}}_3(\mu\text{-OH})]^{3+}$ (**Ru₂Co₃**), $[\{\text{Ru}^{\text{II}}(\mu\text{-bpp})_3\}_2\text{Fe}^{\text{II}}_2\text{Fe}^{\text{III}}(\mu\text{-O})]^{3+}$ (**Ru₂Fe₃**), and $[\{\text{Ru}^{\text{II}}(\mu\text{-bpp})_3\}_2\text{Mn}^{\text{II}}_2\text{Mn}^{\text{III}}(\mu\text{-O})]^{3+}$ (**Ru₂Mn₃**). These results indicate that the pentanuclear complexes with the desired arrangements of metal ions were successfully synthesized by the stepwise synthetic strategy.

(a)



(b)

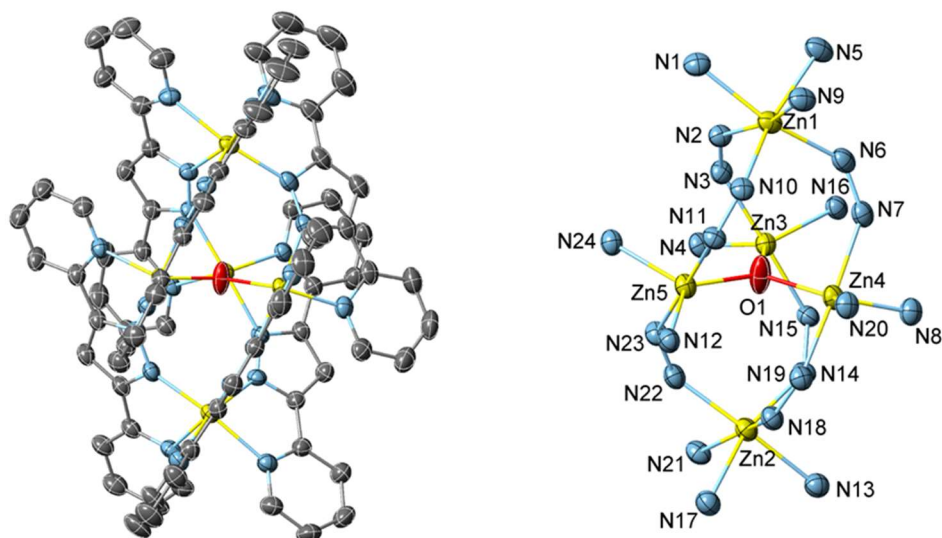
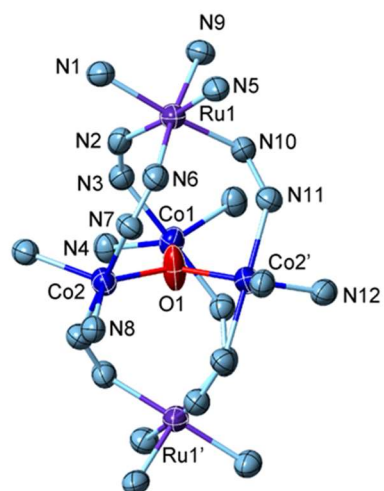
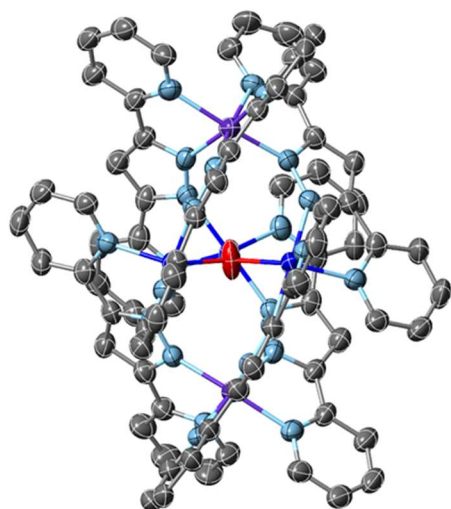


Figure 1-8 | The ORTEP drawings of the cationic moiety (left) and core structure (right) of (a) $\text{Ru}_2\text{Zn}_3(\text{ClO}_4)_3$ and (b) $\text{Zn}_5(\text{BF}_4)_3$ (50% probability ellipsoids). Hydrogen atoms are omitted for clarity. O = red, C = grey, N = pale blue, Ru = orchid and Zn = yellow.

(a)



(b)

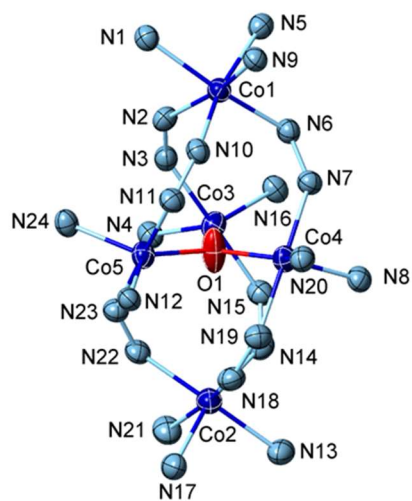
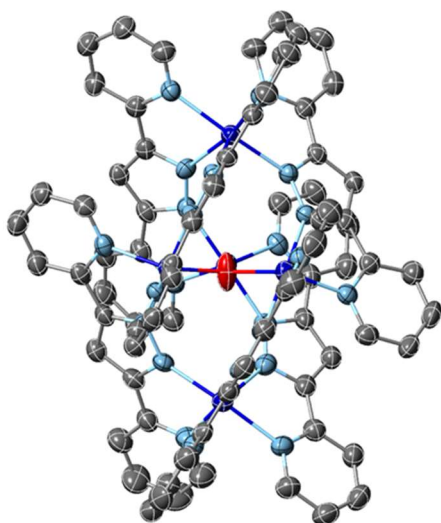
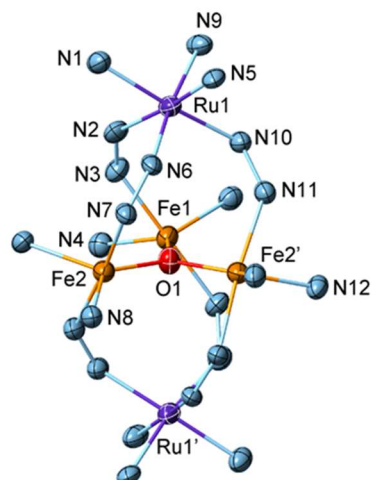
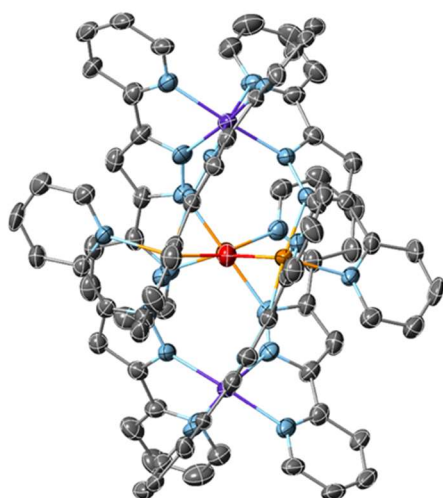


Figure 1-9 | The ORTEP drawings of the cationic moiety (left) and core structure (right) of (a) $\text{Ru}_2\text{Co}_3(\text{PF}_6)_3$ and (b) $\text{Co}_5(\text{BF}_4)_3$ (50% probability ellipsoids). Hydrogen atoms are omitted for clarity. O = red, C = grey, N = pale blue, Ru = orchid and Co = blue.

(a)



(b)

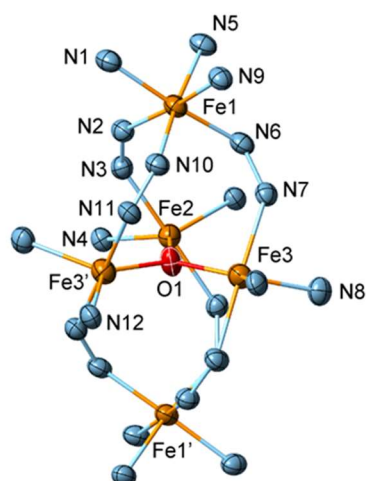
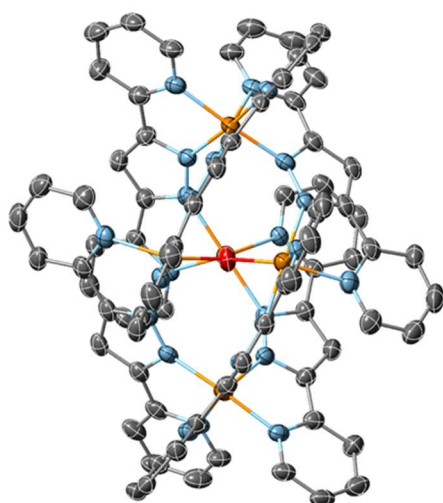
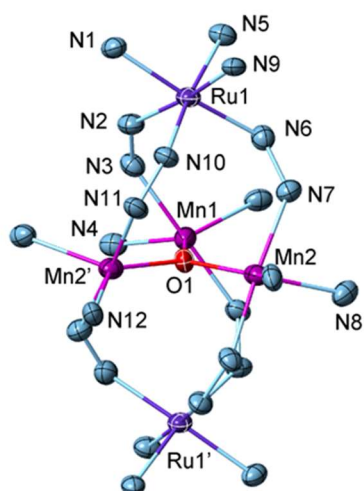
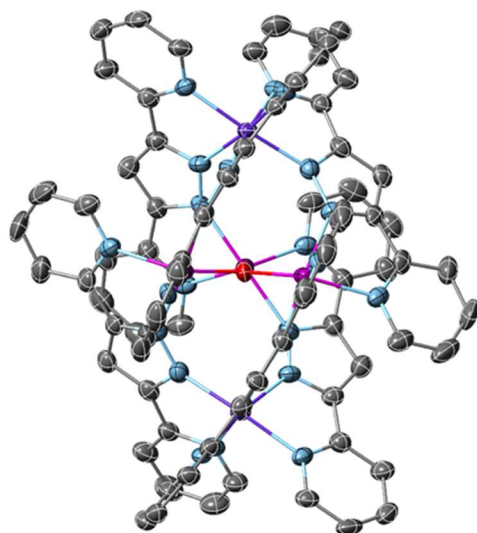


Figure 1-10 | The ORTEP drawings of the cationic moiety (left) and core structure (right) of (a) $\text{Ru}_2\text{Fe}_3(\text{ClO}_4)_3$ and (b) $\text{Fe}_5(\text{BF}_4)_3$ (50% probability ellipsoids). Hydrogen atoms are omitted for clarity. O = red, C = grey, N = pale blue, Ru = orchid and Fe = orange.

(a)



(b)

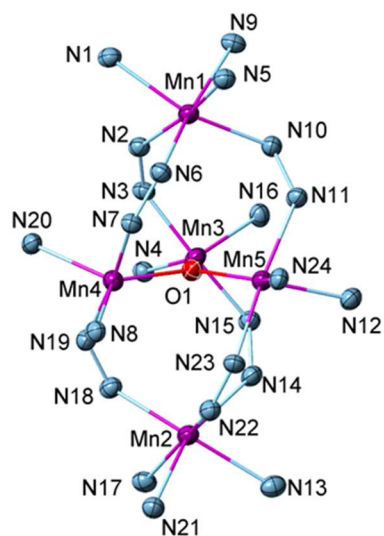
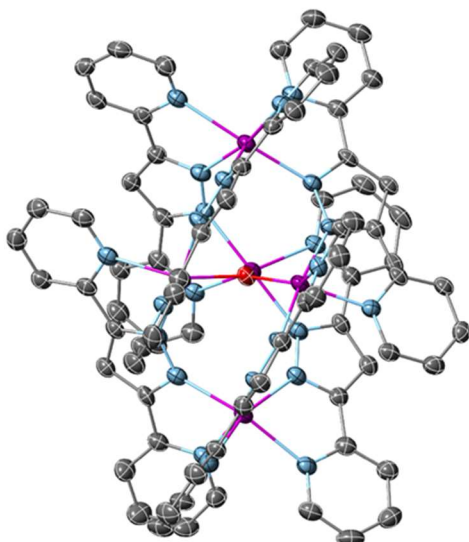


Figure 1-10 | The ORTEP drawings of the cationic moiety (left) and core structure (right) of (a) $\text{Ru}_2\text{Mn}_3(\text{ClO}_4)_3$ and (b) $\text{Mn}_5(\text{ClO}_4)_3$ (50% probability ellipsoids). Hydrogen atoms are omitted for clarity. O = red, C = grey, N = pale blue, Ru = orchid and Mn = magenta.

Table 1-2 | Summary of the crystallographic data for a series of heterometallic pentanuclear complexes.

	Ru₂Zn₃	Ru₂Co₃	Ru₂Fe₃	Ru₂Mn₃
formula	C ₇₈ H ₅₅ N ₂₄ O ₁₃ Ru ₂ Zn ₃ Cl ₃	C ₇₈ H ₅₅ N ₂₄ ORu ₂ Co ₃ F ₁₈ P ₃	C ₇₈ H ₅₄ N ₂₄ O ₁₃ Ru ₂ Fe ₃ Cl ₃	C ₇₈ H ₅₄ N ₂₄ O ₁₃ Ru ₂ Mn ₃ Cl ₃
fw	2041.06	2158.3	2011.49	2008.76
color, habit	clear orange, block	black, block	clear dark red, block	clear dark red, block
crystal size, mm ³	0.21 x 0.18 x 0.10	0.25 x 0.17 x 0.14	0.15 x 0.10 x 0.10	0.13 x 0.08 x 0.06
crystal system	tetragonal	tetragonal	tetragonal	tetragonal
space group	<i>I</i> -4	<i>I</i> -4	<i>I</i> -4	<i>I</i> -4
<i>a</i> / Å	16.6703(4)	16.8823(7)	16.6930(4)	16.7289(2)
<i>c</i> / Å	30.6322(9)	30.9672(7)	30.3629(11)	30.5241(8)
<i>V</i> / Å ³	8512.7(5)	8826.0(8)	8460.8(5)	8542.4(3)
<i>Z</i>	4	4	4	4
<i>F</i> (000)	4096	4300	4044	4032
<i>d</i> _{calc} , g/cm ³	1.593	1.624	1.579	1.562
μ (MoK α), mm ⁻¹	1.349	1.038	1.022	0.946
<i>T</i> , K	123(2)	123(2)	123(2)	123(2)
uniq reflns	9103	10034	10568	9854
<i>R</i> (int)	0.0333	0.0407	0.0565	0.0367
<i>R</i> ₁	0.0357	0.0481	0.056	0.0407
<i>wR</i> ₂	0.098	0.1319	0.1535	0.1186
GOF	1.067	1.047	0.995	1.032

Table 1-3 | Summary of the crystallographic data for a series of homometallic pentanuclear complexes.

	Zn₅	Co₅	Fe₅	Mn₅
formula	C ₇₈ H ₅₅ N ₂₄ OZn ₅ B ₃ F ₁₂	C ₈₈ H ₇₈ N ₂₅ O ₄ Co ₅ B ₃ F ₁₂	C ₇₈ H ₅₄ N ₂₄ OFe ₅ B ₃ F ₁₂	C ₇₈ H ₅₆ N ₂₄ O ₁₄ Mn ₅ Cl ₃
fw	1931.74	2104.83	1883.13	1934.51
color, habit	colourless, block	clear dark brown, block	red, block	clear dark brown, needle
crystal size, mm ³	0.38 x 0.3 x 0.24	0.15 x 0.13 x 0.09	0.22 x 0.1 x 0.08	0.34 x 0.07 x 0.06
crystal system	monoclinic	monoclinic	tetragonal	monoclinic
space group	<i>C2/c</i>	<i>P2₁/n</i>	<i>I-4</i>	<i>P2₁/n</i>
<i>a</i> / Å	25.2852(4)	15.2146(6)	16.6876(3)	14.8245(4)
<i>b</i> / Å	16.9146(2)	22.3485(8)	16.6876(3)	22.4761(4)
<i>c</i> / Å	46.9812(7)	26.8017(12)	30.1763(7)	24.0292(6)
α / deg	90	90	90	90
β / deg	98.6130(10)	102.122(4)	90	102.145(3)
γ / deg	90	90	90	90
<i>V</i> / Å ³	19866.7(5)	8910.0(6)	8403.4(3)	7827.3(3)
<i>Z</i>	8	4	4	4
<i>F</i> (000)	7776	4284	3804	3920
<i>d</i> _{calc} , g/cm ³	1.292	1.569	1.488	1.642
μ (MoK α), mm ⁻¹	1.263	1.004	0.929	0.971
<i>T</i> , K	123(2)	123(2)	123(2)	123(2)
uniq reflns	22740	20425	9596	17909
<i>R</i> (int)	0.0336	0.0954	0.033	0.0576
<i>R</i> ₁	0.0464	0.075	0.0526	0.0601
<i>wR</i> ₂	0.1246	0.228	0.1503	0.1779
GOF	1.055	1.03	1.099	1.025

Table 1-4 | Selected bond lengths and angles of a series of heterometallic pentanuclear complexes.

complex	Ru ₂ Zn ₃		Ru ₂ Co ₃		Ru ₂ Fe ₃		Ru ₂ Mn ₃	
	bond	length / Å	bond	length / Å	bond	length / Å	bond	length / Å
<i>d</i> (M _{api} -N)	Ru1-N1	2.092(4)	Ru1-N1	2.086(5)	Ru1-N1	2.089(6)	Ru1-N1	2.081(4)
	Ru1-N2	2.058(5)	Ru1-N2	2.056(6)	Ru1-N2	2.058(6)	Ru1-N2	2.060(4)
	Ru1-N5	2.084(4)	Ru1-N5	2.081(6)	Ru1-N5	2.067(6)	Ru1-N5	2.082(4)
	Ru1-N6	2.042(5)	Ru1-N6	2.048(6)	Ru1-N6	2.041(6)	Ru1-N6	2.045(4)
	Ru1-N9	2.067(5)	Ru1-N9	2.086(6)	Ru1-N9	2.087(6)	Ru1-N9	2.073(4)
	Ru1-N10	2.047(4)	Ru1-N10	2.042(5)	Ru1-N10	2.051(6)	Ru1-N10	2.054(4)
average		2.065(5)		2.067(6)		2.066(6)		2.066(4)
<i>d</i> (M _{core} -N)	Zn1-N3	2.071(4)	Co1-N3	2.064(5)	Fe1-N3	2.096(6)	Mn1-N3	2.092(4)
	Zn1-N4	2.104(4)	Co1-N4	2.104(6)	Fe1-N4	2.150(6)	Mn1-N4	2.220(5)
	Zn2-N7	2.097(5)	Co2-N7	2.081(5)	Fe2-N7	2.105(6)	Mn2-N7	2.104(4)
	Zn2-N8	2.081(5)	Co2-N8	2.085(6)	Fe2-N8	2.126(6)	Mn2-N8	2.194(5)
	Zn2-N11	2.096(5)	Co2-N11	2.070(5)	Fe2-N11	2.096(6)	Mn2-N11	2.092(4)
	Zn2-N12	2.096(4)	Co2-N12	2.083(6)	Fe2-N12	2.140(6)	Mn2-N12	2.195(5)
average		2.091(5)		2.081(6)		2.119(6)		2.150(5)
<i>d</i> (M _{core} -O)	Zn1-O1	2.057(5)	Co1-O1	2.035(8)	Fe1-O1	1.954(7)	Mn1-O1	1.972(5)
	Zn2-O2	2.036(3)	Co2-O2	2.023(4)	Fe1-O2	1.896(4)	Mn2-O1	1.928(3)
average		2.050(4)		2.031(7)		1.935(6)		1.957(4)
	bond	angle / deg	bond	angle / deg	bond	angle / deg	bond	angle / deg
core angle	Zn1-O1-Zn2	121.10(13)	Co1-O1-Co2	120.8(2)	Fe1-O1-Fe2	120.31(19)	Mn1-O1-Mn2	120.47(13)
	Zn2-O1-Zn2'	117.8(3)	Co2-O1-Co2'	118.4(4)	Fe2-O1-Fe2'	119.4(4)	Mn2-O1-Mn2'	119.1(3)
average		120.0(2)		120.0(3)		120.0(3)		120.0(2)

Table 1-5 | Selected bond lengths and angles of a series of homometallic pentanuclear complexes.

complex	Zn ₅		Co ₅		Fe ₅		Mn ₅	
	bond	length / Å	bond	length / Å	bond	length / Å	bond	length / Å
<i>d</i> (M _{api} -N)	Zn1-N1	2.230(3)	Co1-N1	2.198(5)	Fe1-N1	2.017(3)	Mn1-N1	2.276(3)
	Zn1-N2	2.124(2)	Co1-N2	2.108(5)	Fe1-N2	1.966(3)	Mn1-N2	2.201(4)
	Zn1-N5	2.242(3)	Co1-N5	2.186(5)	Fe1-N5	2.018(3)	Mn1-N5	2.324(4)
	Zn1-N6	2.110(3)	Co1-N6	2.103(4)	Fe1-N6	1.971(3)	Mn1-N6	2.175(3)
	Zn1-N9	2.261(2)	Co1-N9	2.182(5)	Fe1-N9	2.004(3)	Mn1-N9	2.394(4)
	Zn1-N10	2.112(2)	Co1-N10	2.104(4)	Fe1-N10	1.963(3)	Mn1-N10	2.156(3)
	Zn2-N13	2.233(2)	Co2-N13	2.195(5)			Mn2-N13	2.332(4)
	Zn2-M14	2.117(2)	Co2-N14	2.100(5)			Mn2-M14	2.217(3)
	Zn2-N17	2.252(3)	Co2-N17	2.175(5)			Mn2-N17	2.315(4)
	Zn2-N18	2.112(2)	Co2-N18	2.118(5)			Mn2-N18	2.171(3)
	Zn2-N21	2.260(2)	Co2-N21	2.195(5)			Mn2-N21	2.323(4)
	Zn2-N22	2.129(2)	Co2-N22	2.120(5)			Mn2-N22	2.192(4)
average		2.182(2)		2.149(5)		1.990(3)		2.256(4)
<i>d</i> (M _{core} -N)	Zn3-N3	2.092(2)	Co3-N3	2.054(5)	Fe2-N3	2.085(3)	Mn3-N3	1.962(3)
	Zn3-N4	2.082(2)	Co3-N4	2.072(5)	Fe2-N4	2.141(3)	Mn3-N4	2.151(3)
	Zn3-N15	2.083(2)	Co3-N15	2.055(5)	Fe3-N7	2.089(3)	Mn3-N15	1.963(3)
	Zn3-N16	2.100(2)	Co3-N16	2.086(4)	Fe3-N8	2.118(3)	Mn3-N16	2.173(3)
	Zn4-N7	2.102(2)	Co4-N7	2.049(4)	Fe3-N11	2.127(3)	Mn4-N7	2.138(4)
	Zn4-N8	2.068(2)	Co4-N8	2.073(5)	Fe3-N12	2.106(3)	Mn4-N8	2.246(3)
	Zn4-N19	2.096(2)	Co4-N19	2.073(5)			Mn4-N19	2.127(4)
	Zn4-N20	2.061(2)	Co4-N20	2.070(5)			Mn4-N20	2.246(3)
	Zn5-N11	2.082(2)	Co5-N11	2.055(4)			Mn5-N11	2.169(3)
	Zn5-N12	2.092(2)	Co5-N12	2.084(4)			Mn5-N12	2.230(3)
	Zn5-N23	2.074(2)	Co5-N23	2.056(4)			Mn5-N23	2.150(3)
	Zn5-N24	2.097(2)	Co5-N24	2.072(5)			Mn5-N24	2.254(4)
average		2.086(2)		2.067(5)		2.111(3)		2.151(3)
<i>d</i> (M _{core} -O)	Zn3-O1	2.016(2)	Co3-O1	1.997(4)	Fe2-O1	1.983(4)	Mn3-O1	1.779(3)
	Zn4-O1	2.030(2)	Co4-O1	2.017(4)	Fe3-O1	1.9183(19)	Mn4-O1	2.036(3)
	Zn5-O1	2.041(2)	Co5-O1	2.014(4)			Mn5-O1	2.027(3)
average		2.029(2)		2.009(4)		1.961(3)		1.947(3)
core angle	bond	angle / deg	bond	angle / deg	bond	angle / deg	bond	angle / deg
	Zn3-O1-Zn4	116.3(1)	Co3-O1-Co4	120.4(2)	Fe2-O1-Fe3	120.69(9)	Mn3-O1-Mn4	116.72(14)
	Zn3-O1-Zn5	122.5(1)	Co3-O1-Co5	120.3(2)	Fe3-O1-Fe3'	118.63(18)	Mn3-O1-Mn5	123.97(14)
	Zn4-O1-Zn5	121.2(1)	Co4-O1-Co5	118.7(2)			Mn4-O1-Mn5	119.02(13)
average		120.1(1)		119.8(2)		120.0(1)		119.90(14)

Conclusion

The author succeeded in the establishment of the rational synthetic strategy of heterometallic pentanuclear complex. The strategy is constructed by two step complexations. The first step is preparation of a ruthenium mononuclear complex, *fac*-[Ru(Hbpp)₃](ClO₄)₂, as a precursor. The second step is the reaction between *fac*-[Ru(Hbpp)₃](ClO₄)₂ and another metal ion. This stepwise synthetic route allowed the on-demand installation of two kinds of metal ions into the pentanuclear scaffold. In addition, the comparisons of the bond distances between heterometallic and homometallic pentanuclear complexes revealed that metal installation into the specific position without the scrambling of metal ions was achieved. Judging these experimental results, it is indicated that a series of heterometallic pentanuclear complexes, **Ru₂Zn₃(ClO₄)₃**, **Ru₂Co₃(ClO₄)₃**, **Ru₂Fe₃(ClO₄)₃**, and **Ru₂Mn₃(ClO₄)₃**, were successfully constructed with keeping the same molecular framework.

References

1. R. Chakrabarty, P. S. Mukherjee, P. J. Stang, *Chem. Rev.*, **2011**, *111*, 6810.
2. L.-J. Chen, H.-B. Yang, M. Shionoya, *Chem. Soc. Rev.*, **2017**, *46*, 2555.
3. Q.-F. Sun, J. Iwasa, D. Ogawa, Y. Ishido, S. Sato, T. Ozeki, Y. Sei, K. Yamaguchi, M. Fujita, *Science*, **2010**, *328*, 1144.
4. J. S. Kanady, E. Y. Tsui, M. W. Day, T. Agapie, *Science*, **2011**, *333*, 733.
5. S. H. Lim, Y. Su, S. M. Cohen, *Angew. Chem. Int. Ed.*, **2012**, *51*, 5106.
6. S. Horiuchi, Y. Tachibana, M. Yamashita, K. Yamamoto, K. Masai, K. Takase, T. Matsutani, S. Kawamata, Y. Kurashige, T. Yanai, T. Murahashi, *Nat. Commun.*, **2015**, *6*, 6742.
7. M. Teramoto, K. Iwata, H. Yamaura, K. Kurashima, K. Miyazawa, Y. Kurashige, K. Yamamoto, T. Murahashi, *J. Am. Chem. Soc.*, **2018**, *140*, 12682.
8. D. Fujita, Y. Ueda, S. Sato, N. Mizuno, T. Kumasaka, M. Fujita, *Nature*, **2016**, *540*, 563.
9. H. Ube, K. Endo, H. Sato, M. Shionoya, *J. Am. Chem. Soc.*, **2019**, *141*, 10384.
10. B.-H. Zhu, Y. Shibata, S. Muratsugu, Y. Yamanoi, H. Nishihara, *Angew. Chem. Int. Ed.*, **2009**, *48*, 3858.
11. R. H. Ismayilov, W.-Z. Wang, G.-H. Lee, C.-Y. Yeh, S.-A. Hua, Y. Song, M.-M. Rohmer, M. Bénard, S.-M. Peng, *Angew. Chem. Int. Ed.*, **2011**, *50*, 2045.
12. S. Muratsugu, K. Sodeyama, F. Kitamura, S. Tsukada, M. Tada, S. Tsuneyuki, H. Nishihara, *Chem. Sci.*, **2011**, *2*, 1960.
13. T. Murahashi, K. Shirato, A. Fukushima, K. Takase, T. Suenobu, S. Fukuzumi, S. Ogoshi, H. Kurosawa, *Nat. Chem.*, **2012**, *4*, 52.
14. E. Y. Tsui, R. Tran, J. Yano, T. Agapie, *Nat. Chem.*, **2013**, *5*, 293.
15. B. Rausch, M. D. Symes, G. Chisholm, L. Cronin, *Science*, **2014**, *345*, 1326.
16. R. Sessoli, H.-L. Tsai, A. R. Schake, S. Wang, J. B. Vincent, K. Folting, D. Gatteschi, G. Christou, D. N. Hendrickson, *J. Am. Chem. Soc.*, **1993**, *115*, 1804.
17. R. Sessoll, D. Gatteschi, A. Caneschi, M. A. Novak, *Nature*, **1993**, *365*, 141.
18. T. Matsumoto, G. N. Newton, T. Shiga, S. Hayami, Y. Matsui, H. Okamoto, R. Kumai, Y. Murakami, H. Oshio, *Nat. Commun.*, **2014**, *5*, 3865.
19. V. W.-W. Yam, V. K.-M. Au, S. Y.-L. Leung, *Chem. Rev.*, **2015**, *115*, 7589.
20. J. Rohacova, O. Ishitani, *Chem. Sci.*, **2016**, *7*, 6728.
21. P. Buchwalter, J. Rosé, P. Braunstein, *Chem. Rev.*, **2015**, *115*, 28.
22. P. L. Arnold, D. Patel, C. Wilson, J. B. Love, *Nature*, **2008**, *451*, 315.

23. P. L. Arnold, G. M. Jones, S. O. Odoh, G. Schreckenbach, N. Magnani, J. B. Love, *Nat. Chem.*, **2012**, *4*, 221.
24. S. Ogo, K. Ichikawa, T. Kishima, T. Matsumoto, H. Nakai, K. Kusaka, T. Ohhara, *Science*, **2013**, *339*, 682.
25. M. Okamura, M. Kondo, R. Kuga, Y. Kurashige, T. Yanai, S. Hayami, V. K. K. Praneeth, M. Yoshida, K. Yoneda, S. Kawata, S. Masaoka, *Nature*, **2016**, *530*, 465.
26. X. Jiang, J. Li, B. Yang, X.-Z. Wei, B.-W. Dong, Y. Kao, M.-Y. Huang, C.-H. Tung, L.-Z. Wu, *Angew. Chem. Int. Ed.*, **2018**, *57*, 7850.
27. K. M. Lancaster, M. Roemelt, P. Ettenhuber, Y. Hu, M. W. Ribbe, F. Neese, U. Bergmann, S. DeBeer, *Science*, **2011**, *334*, 974.
28. Y. Umena, K. Kawakami, J.-R. Shen, N. Kamiya, *Nature*, **2011**, *473*, 55.
29. M. Suga, F. Akita, K. Hirata, G. Ueno, H. Murakami, Y. Nakajima, T. Shimizu, K. Yamashita, M. Yamamoto, H. Ago, J.-R. Shen, *Nature*, **2015**, *517*, 99.
30. K. Brown, M. Tegoni, M. Prudêncio, A. S. Pereira, S. Besson, J. J. Moura, I. Moura, C. Cambillau, *Nat. Struct. Biol.*, **2000**, *7*, 191.
31. J. M. Clemente-Juan, E. Coronado, A. Gaita-Ariño, *Chem. Soc. Rev.*, **2012**, *41*, 7464.
32. L.-Y. Hsu, B.-Y. Jin, C. Chen, S.-M. Peng, *Chem*, **2017**, *3*, 373.
33. C. Busche, L. Vilá-Nadal, J. Yan, H. N. Miras, D.-L. Long, V. P. Georgiev, A. Asenov, R. H. Pedersen, N. Gadegaard, M. M. Mirza, D. J. Paul, J. M. Poblet, L. Cronin, *Nature*, **2014**, *515*, 545.
34. Y. Zhao, L. Zhang, X. Li, Y. Shi, R. Ding, M. Teng, P. Zhang, C. Cao, P. J. Stang, *Proc. Natl. Acad. Sci. USA*, **2019**, *116* (10), 4090.
35. D. J. Vinyard, S. Khan, M. Askerka, V. S. Batista, G. W. Brudvig, *J. Phys. Chem. B*, **2017**, *121*, 1020.
36. A. Altomare, G. Cascarano, C. Giacovazzo, A. Guagliardi, *J. Appl. Cryst.*, **1993**, *26*, 343.
37. G. M. Sheldrick, *Acta Cryst.*, **2015**, *C71*, 3.
38. A. L. Spek, *Acta Cryst.*, **2009**, *D65*, 148.
39. J.-Z. Hou, M. Li, Z. Li, S.-Z. Zhan, X.-C. Huang, D. Li, *Angew. Chem. Int. Ed.*, **2008**, *47*, 1711.
40. S. Romain, J. Rich, C. Sens, T. Stoll, J. Benet-Buchholz, A. Llobet, M. Rodriguez, I. Romero, R. Clérac, C. Mathonière, C. Duboc, A. Deronzier, M.-N. Collomb, *Inorg. Chem.*, **2011**, *50*, 8427.
41. E. Gouré, B. Gery, M. Clémancey, J. Pécaut, F. Molton, J.-M. Latour, G. Blondin, M.-N. Collomb, *Inorg. Chem.*, **2016**, *55*, 9178.

42. K. Yoneda, K. Adachi, K. Nishio, M. Yamasaki, A. Fuyuhiko, M. Katada, S. Kaizaki, S. Kawata, *Angew. Chem. Int. Ed.*, **2006**, *45*, 5459.
43. R. Ishikawa, M. Nakano, A. Fuyuhiko, T. Takeuchi, S. Kimura, T. Kashiwagi, M. Hagiwara, K. Kindo, S. Kaizaki, S. Kawata, *Chem. Eur. J.*, **2010**, *16*, 11139.
44. V. K. K. Praneeth, M. Kondo, M. Okamura, T. Akai, H. Izu, S. Masaoka, *Chem. Sci.*, **2019**, *10*, 4628.
45. S. Bellinger-Buckley, T.-C. Chang, S. Bag, D. Schweinfurth, W. Zhou, B. Torok, B. Sarkar, M.-K. Tsai, J. Rochford, *Inorg. Chem.*, **2014**, *53*, 5556.

Chapter 2

Electron Juggling in Clustered Five Redox Sites

Introduction

Incorporation of multiple redox active centers into a finite structure such as multinuclear metal complexes is an attractive strategy for obtaining artificial materials with unique functions. A significant feature of this class of materials is their potential ability to generate various kinds of electronic states via oxidation/reduction reactions, and the formed species exhibit the distinct electronic structures with unique physical properties. For instance, in the reaction catalyzed by the metalloenzymes, the existence of the several species with distinct electronic states greatly contributes to the promotion of the reaction with high efficiency. Therefore, the control over the redox behavior in redox-core-assembled structures can be an important strategy for obtaining the materials with the target functionality. However, these materials generally exhibit complicated redox behavior because of the strong electronic interactions between redox cores. The strong interactions induce intramolecular electron transfer between redox centers and the prediction of the electronic structure generated upon the complicated electron transfer reactions becomes extremely difficult.

Given that the redox behavior of redox-core-assembled structures is determined both by the nature of each redox core and the electronic interactions between the cores, systematic investigation on a series of redox-core-assembled structure, in which the redox activity of the cores are controllable with keeping the same molecular framework, is of great significance. This is because such systematic investigation would provide a comprehensive guideline to understand the redox behavior of the redox-core-assembled structure.

Here, the control of the distribution of oxidation states by the precise arrangement of redox active sites was shown. A rational synthetic procedure to enable on-demand installation of redox cores was successfully developed by utilizing the stepwise synthetic strategy, which affords a series of heterometallic pentanuclear complexes that have different arrangement of metal ions with keeping the same molecular framework.

The global investigation of electron transfer reactions of the obtained complexes clarified that flexible electron transfer reactions of redox cores afford the various kinds of chemical species with distinct distribution of oxidation states, and the redox behavior is dependent on the arrangement of metal ions. The investigation provide new insight for the deeper understanding to control the distribution of oxidation states in the multinuclear metal complexes, which would lead to the construction of novel strategy to develop a new class of functional materials.

Experimental Section

Materials.

Ferrocene was purchased from Wako Pure Chemical Industries, Ltd. tetra-*n*-butylammonium perchlorate (TBAP) was purchased from Tokyo Chemical Industry Co., Ltd. All solvents and reagents are of the highest quality available and used as received except for TBAP. TBAP was recrystallized from absolute ethanol.

Electrochemical and UV-Vis Spectral Measurements.

All experimental procedures were conducted at ambient temperature, 20 °C, under argon. A standard three-electrode configuration was employed in conjunction with a Bio-Logic-Science Instruments potentiostat interfaced to a computer with SP-50 software. In all cases, a platinum auxiliary electrode and Ag/Ag⁺ reference electrode were used. Cyclic voltammetry was performed using a GC disk working electrode (diameter 3 mm, from BAS Inc.). The working electrode was treated between scans by means of polishing with 0.05 μm alumina paste (from BAS Inc.) and washing with purified H₂O. Ferrocene was used as an internal standard, and all potentials reported within this work are referenced to the ferrocenium/ferrocene couple at 0 V. UV-vis spectral measurements were recorded using SHIMADZU UV-3600 UV-VIS spectrophotometer with a conventional quartz cuvette (path length, $l = 1$ cm). Spectroelectrolysis was performed using a BAS Inc. spectroelectrochemical quartz cell ($l = 1$ mm) containing a Pt gauze (working electrode), Pt wire (auxiliary electrode) and Ag/Ag⁺ (reference electrode) in conjunction with the CH Instruments potentiostat, and UV-vis spectra were recorded using DH-2000-BAL from Ocean Optics in UL-1000A from UNICO under an Ar atmosphere.

Synthesis.

Synthesis of **Ru₂Zn₃(ClO₄)₃**, **Ru₂Co₃(ClO₄)₃**, **Ru₂Fe₃(ClO₄)₃**, **Ru₂Mn₃(ClO₄)₃**, **Zn₅(BF₄)₃**, **Co₅(BF₄)₃**, **Fe₅(BF₄)₃** and **Mn₅(ClO₄)₃** were performed in chapter 1, and the detailed synthetic procedurs are in chapter 1.

Redox Behaviors of the Pentanuclear Metal Complexes

Electrochemical measurement of the series of pentanuclear complexes was made to elucidate their redox behaviors. Although no redox wave was observed in **Zn₅** due to the redox inactivity of zinc ion, all other complexes displayed several redox waves reflecting the number of redox-active centers (Figure 2-1, 2-2, 2-3, 2-4 and Table 2-1). Therefore, all redox waves can be regarded as one-electron transfer process. **Ru₂Zn₃** exhibited two reversible oxidation waves at $E_{1/2} = 0.35$ and 0.51 V (vs. ferrocene/ferrocenium (Fc/Fc⁺)), and these waves were attributed to the sequential oxidations of the ruthenium ions at the apical position.

In the CVs of **Ru₂Co₃** and **Co₅**, two reversible oxidation waves and three reversible reduction waves were observed. The $E_{1/2}$ values of the oxidation waves of **Ru₂Co₃** (0.36 and 0.52 V) are almost identical to those of **Ru₂Zn₃**, indicating that these can be attributed to the oxidations of the ruthenium ions. The redox potentials of the reduction waves of **Ru₂Co₃** and **Co₅** were also quite similar ($E_{1/2} = -1.71$, -1.98 , and -2.24 V for **Ru₂Co₃** and -1.72 , -1.96 , and -2.19 V for **Co₅**), and thus, these waves are assignable to the reductions of the cobalt ions in the triangular core. Accordingly, the oxidation waves of **Co₅** at -0.42 and -0.31 V were assigned as the oxidations of the Co ions at the apical position.

The CV of **Ru₂Fe₃** exhibited one reversible reduction wave ($E_{1/2} = -0.52$ V) and four reversible oxidation waves ($E_{1/2} = 0.17$, 0.56 , 0.75 , and 1.10 V). Although the oxidation waves corresponding to the oxidations of the ruthenium ions were observed potentials similar to those of **Ru₂Zn₃** and **Ru₂Co₃** (*vide supra*), the oxidation potentials of **Ru₂Fe₃** were not located in the same region. In addition, when comparing the redox potentials of **Ru₂Fe₃** and **Fe₅**, only the potential of the second oxidation wave was substantially different, and it had shifted to a more positive value ($E_{1/2} = 0.56$ V for **Ru₂Fe₃** and 0.29 V for **Fe₅**).

Similarly, **Ru₂Mn₃** exhibited one reversible reduction wave ($E_{1/2} = -0.65$ V) and four sequential oxidation waves ($E_{1/2} = 0.09$, 0.58 , 0.78 , and 1.19 V), and the observed waves were not in regions similar to those of the waves of **Ru₂Zn₃** and **Ru₂Co₃**. In the case of **Ru₂Mn₃**, however, only the potential of the third oxidation wave was shifted to a more negative potential ($E_{1/2} = 0.78$ V) compared to that of **Mn₅** ($E_{1/2} = 1.11$ V), and this trend is different from that of **Ru₂Fe₃**. These observed redox behaviors of **Ru₂Fe₃** and **Ru₂Mn₃** imply that the electronic interactions between the different kinds of metal ions alter the nature of the electron transfer reactions. This result prompted to further explore the redox behavior of these complexes.

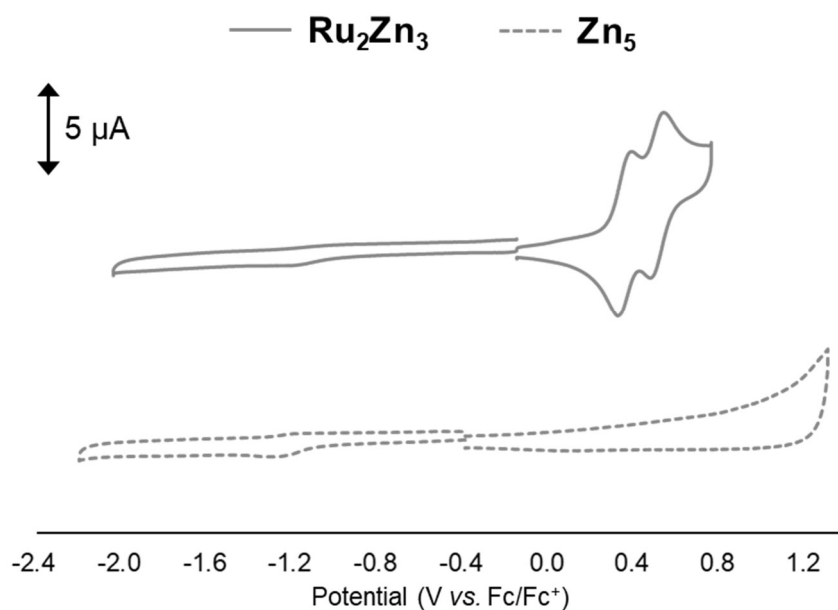


Figure 2-1 | Cyclic voltammograms of Ru_2Zn_3 (0.2 mM, solid lines) and Zn_5 (0.2 mM, dashed lines) in acetonitrile solutions containing TBAP (0.1 M) at a scan rate of 100 mV/s.

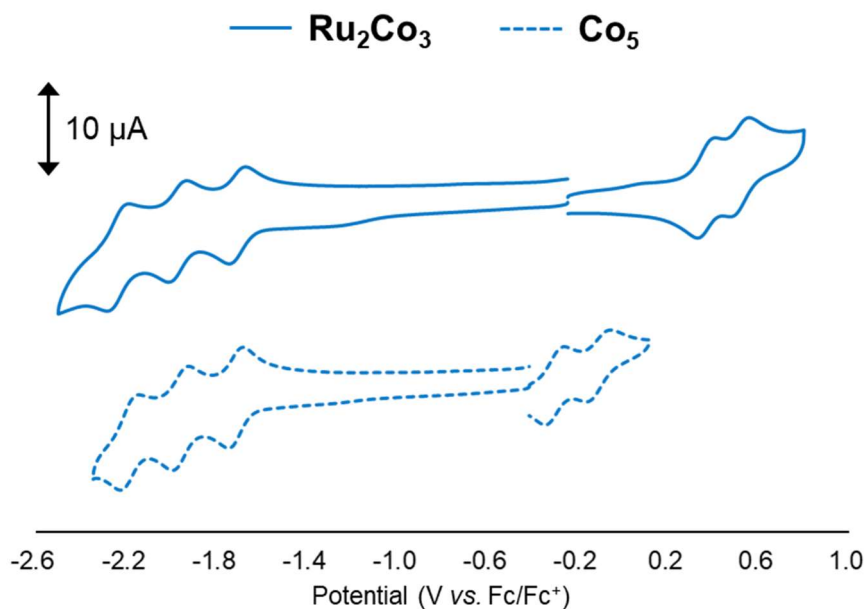


Figure 2-2 | Cyclic voltammograms of Ru_2Co_3 (0.2 mM, solid lines) and Co_5 (0.2 mM, dashed lines) in acetonitrile solutions containing TBAP (0.1 M) at a scan rate of 100 mV/s.

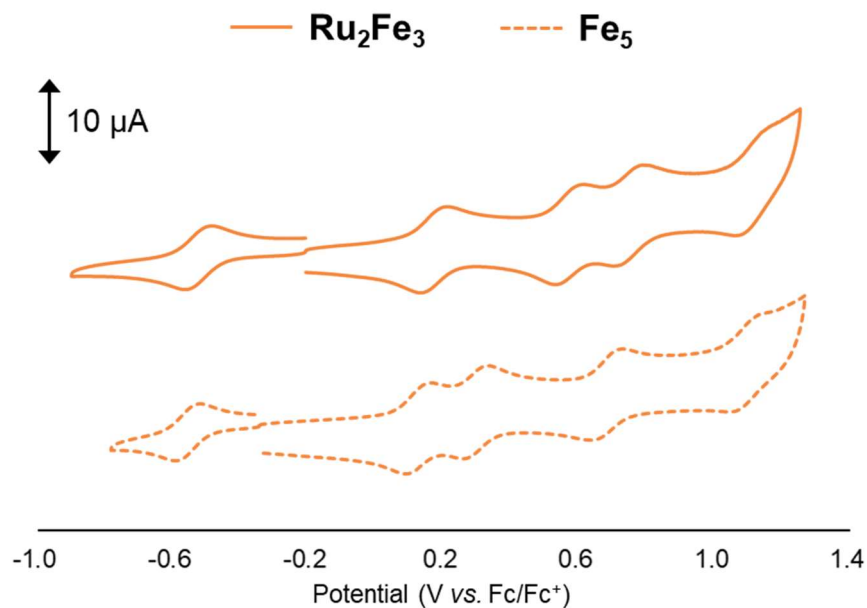


Figure 2-3 | Cyclic voltammograms of **Ru₂Fe₃** (0.2 mM, solid lines) and **Fe₅** (0.2 mM, dashed lines) in acetonitrile solutions containing TBAP (0.1 M) at a scan rate of 100 mV/s.

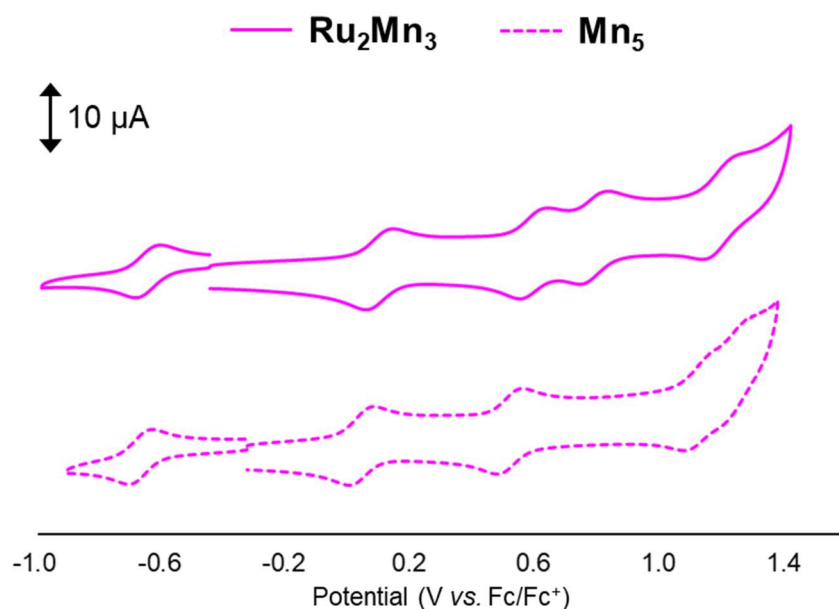


Figure 2-4 | Cyclic voltammograms of **Ru₂Mn₃** (0.2 mM, solid lines) and **Mn₅** (0.2 mM, dashed lines) in acetonitrile solutions containing TBAP (0.1 M) at a scan rate of 100 mV/s.

Table 2-1 | Summary of redox potentials of a series of pentanuclear metal complexes.

complex	$E_{1/2} / V$ (vs. Fc/Fc^+)						
	red(3)	red(2)	red(1)	ox(1)	ox(2)	ox(3)	ox(4)
Zn₅	-	-	-	-	-	-	-
Ru₂Zn₃	-	-	-	0.35	0.51	-	-
Co₅	-2.19	-1.96	-1.72	-0.42	-0.31	-	-
Ru₂Co₃	-2.24	-1.98	-1.71	0.36	0.52	-	-
Fe₅	-	-	-0.56	0.12	0.29	0.68	1.10
Ru₂Fe₃	-	-	-0.52	0.17	0.56	0.75	1.10
Mn₅	-	-	-0.67	0.04	0.51	1.11	1.24
Ru₂Mn₃	-	-	-0.65	0.09	0.58	0.78	1.19

Electron Transfers in the Pentanuclear Complexes

To unveil the details of the electron transfer reactions in **Ru₂Fe₃** and **Ru₂Mn₃**, UV-vis absorption spectroscopic and UV-vis spectroelectrochemical (UV-SEC) measurements were taken. The UV-vis absorption spectra of the heterometallic pentanuclear complexes before oxidation are shown in Figure 2-5. All the complexes exhibited intense band in the visible region (Table 2-2), and the band can be assigned to the metal-to-ligand charge transfer (MLCT) transition of the ruthenium centers by comparison with the UV-vis absorption spectra of the corresponding homometallic complexes (Figure 2-5).

Table 2-2 | Summary of UV-vis absorption spectra of a series of heterometallic pentanuclear complexes.

complex	$\lambda_{\text{max}}(\text{MLCT}) / \text{nm}$	$\epsilon(\text{MLCT}) \times 10^{-6} / \text{mol}^{-1}\text{Lcm}^{-1}$
Ru₂Zn₃	394	0.244
Ru₂Co₃	389	0.211
Ru₂Fe₃	390	0.253
Ru₂Mn₃	380	0.228

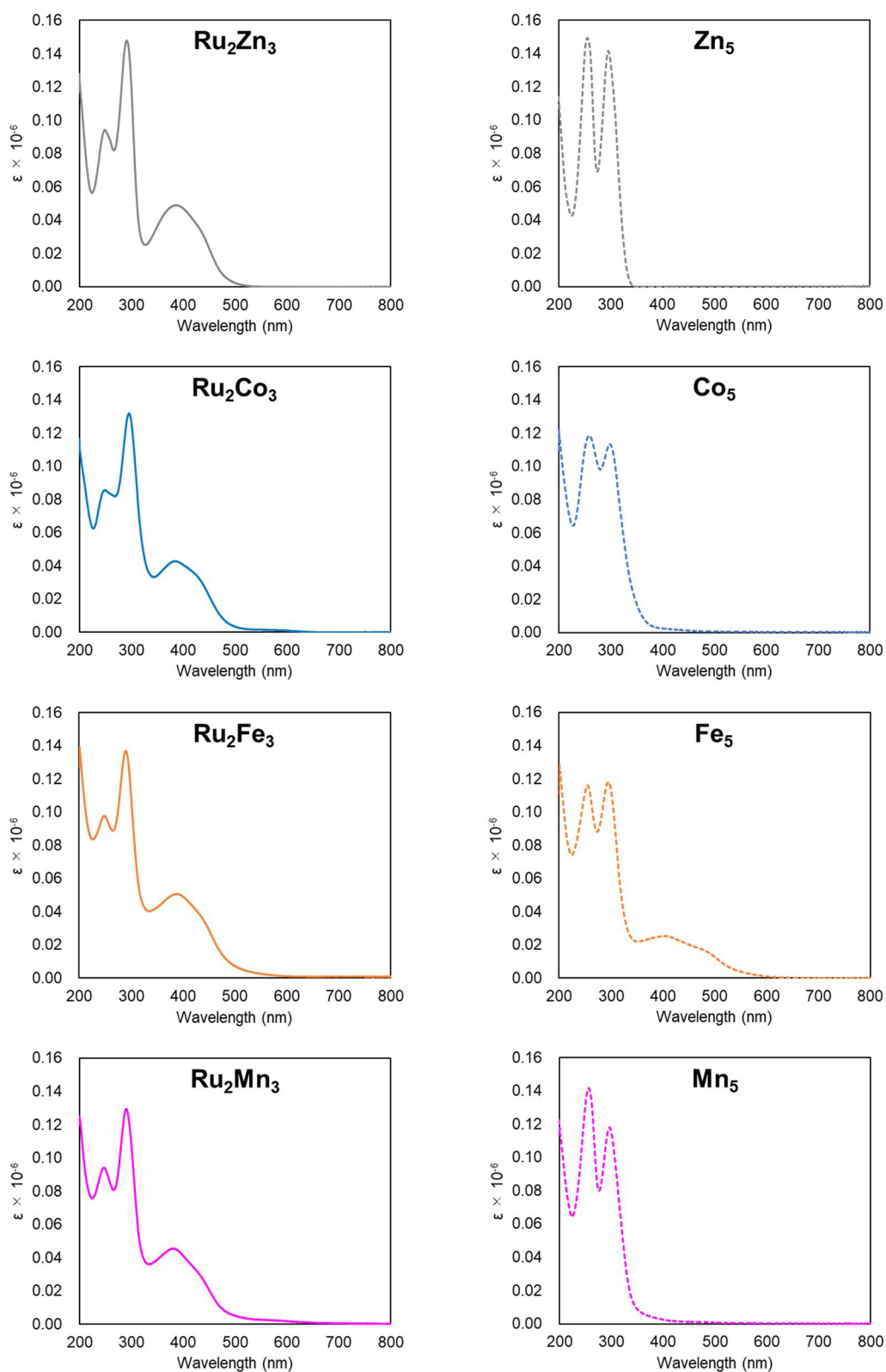


Figure 2-5 | UV-vis absorption spectra of a series of heterometallic pentanuclear complexes (5 μM) and homometallic pentanuclear complexes (5 μM) in acetonitrile.

It should be noted that the bleaching ratio of the MLCT band upon each oxidation wave is used in order to see each MLCT change as comparable value. The bleaching ratios of the MLCT band upon each oxidation wave were calculated by using the absorbance (A_k) at the absorption maximum of the MLCT band (λ_{max}) of each heterometallic pentanuclear complex. Here, the state before oxidation is defined as $k = 0$, and the states generated by the first, second, third, and fourth oxidations are defined as $k = 1, 2, 3$, and 4 , respectively. Initially, the absorbance of the fully oxidized state (A_2 for **Ru₂Zn₃** and **Ru₂Co₃** and A_4 for **Ru₂Fe₃** and **Ru₂Mn₃**) was used as the baseline and was subtracted from A_k , and the obtained values were defined as A'_k . Second, the decreases in the intensity of the MLCT band upon oxidation were calculated as $\Delta A'_k = A'_{k-1} - A'_k$. Finally, the bleaching ratios of the MLCT band were determined by using the following equation: $(\Delta A'_k / A'_0) \times 100$, ($k = 1-4$). The results of the calculations are summarized in Table 2-3.

Table 2-3 | Summary of the estimation of the bleaching ratios of the MLCT band upon each oxidation wave in a series of heterometallic pentanuclear complexes.

complex	$\lambda_{\text{max}}(\text{MLCT}) / \text{nm}$		before oxidation ($k = 0$)	1st oxidation ($k = 1$)	2nd oxidation ($k = 2$)	3rd oxidation ($k = 3$)	4th oxidation ($k = 4$)
Ru₂Zn₃	394	A_n	0.553	0.377	0.175	-	-
		A'_n	0.379	0.202	0.000	-	-
		$\Delta A'_n$	-	0.177	0.202	-	-
		bleaching ratio of MLCT band /%	-	46.6	53.4	-	-
Ru₂Co₃	389	A_n	0.494	0.355	0.237	-	-
		A'_n	0.257	0.118	0.000	-	-
		$\Delta A'_n$	-	0.138	0.118	-	-
		bleaching ratio of MLCT band /%	-	53.9	46.1	-	-
Ru₂Fe₃	390	A_n	0.523	0.510	0.460	0.221	0.186
		A'_n	0.337	0.324	0.275	0.035	0.000
		$\Delta A'_n$	-	0.013	0.049	0.240	0.035
		bleaching ratio of MLCT band /%	-	3.9	14.6	71.1	10.4
Ru₂Mn₃	380	A_n	0.504	0.533	0.524	0.316	0.236
		A'_n	0.268	0.297	0.288	0.080	0.000
		$\Delta A'_n$	-	-0.029	0.009	0.208	0.080
		bleaching ratio of MLCT band /%	-	-10.7	3.2	77.6	30.0

Initially, UV-SEC experiments with **Ru₂Zn₃** and **Ru₂Co₃** were performed. The intensity of the MLCT band of these complexes decreased in a stepwise manner with isosbestic points corresponding to the first and second oxidation steps (Figures 2-6, 2-7 and Table 2-4). The bleaching ratios of the MLCT band of **Ru₂Zn₃** and **Ru₂Co₃** for the first oxidation step were calculated to be 46.6 and 53.9%, respectively, and those for the second oxidation step were 53.4 and 46.1% (Table 2-3). This result indicates that each ruthenium center in these complexes undergoes a one-electron oxidation, which is consistent with the electrochemical measurements (*vide supra*). Based on these results, it is revealed that the observed MLCT band can provide information on the oxidation states of the ruthenium centers due to the drastic change in the intensity of the band as a response to the oxidation states of the ruthenium centers.

Table 2-4 | Summary of isosbestic points observed during UV-SEC measurements of a series of heterometallic pentanuclear complexes.

complex	isosbestic point / nm			
	1st oxidation	2nd oxidation	3rd oxidation	4th oxidation
Ru₂Zn₃	302, 340, 503	341, 497	-	-
Ru₂Co₃	309, 342, 512	304, 342, 503	-	-
Ru₂Fe₃	321, 336, 488	309, 340, 493	338, 497	333, 493
Ru₂Mn₃	321, 408, 538	318, 375, 534	329, 487	325, 449

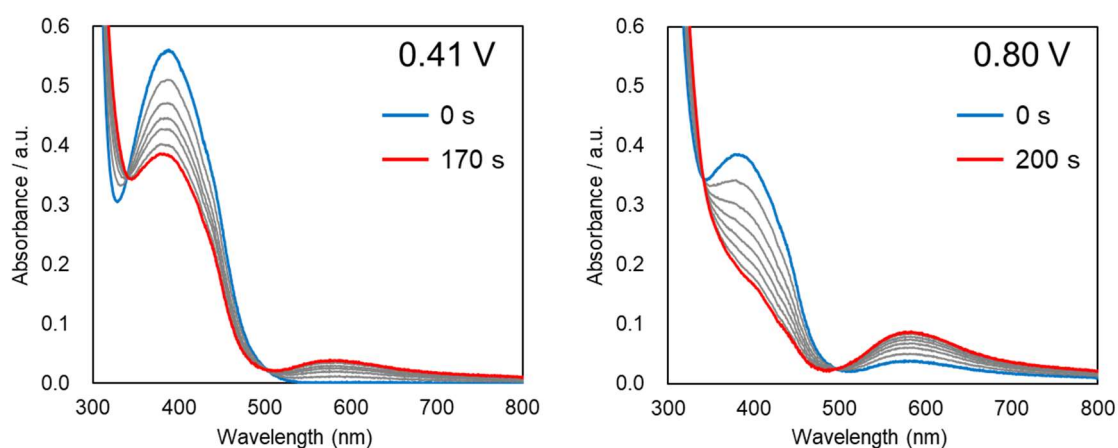


Figure 2-6 | The results of UV-SEC of Ru_2Zn_3 (0.1 mM) in 0.1 M TBAP/MeCN. Applied potentials are (left) 0.41 and (right) 0.80 V (vs. Fc/Fc^+), respectively. All measurements were performed under an Ar atmosphere.

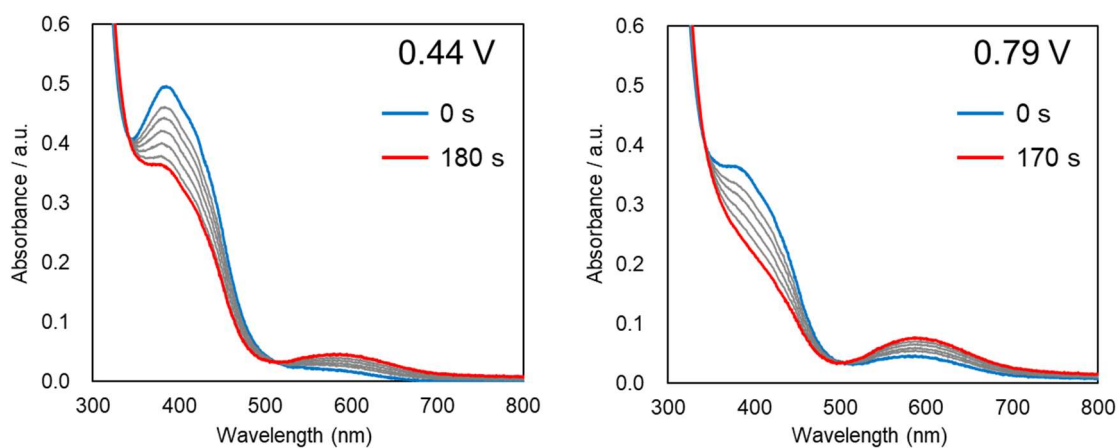


Figure 2-7 | The results of UV-SEC of Ru_2Co_3 (0.1 mM) in 0.1 M TBAP/MeCN. Applied potentials are (left) 0.44 and (right) 0.79 V (vs. Fc/Fc^+), respectively. All measurements were performed under an Ar atmosphere.

Subsequently, UV-SEC measurement on **Ru₂Fe₃** was performed by oxidizing the complex at 0.40, 0.60, 1.00 and 1.30 V. In all steps, spectral change with clear isosbestic points was observed (Figure 2-8 and Table 2-4), which suggests the formation of a single product at each oxidation step. In the first step and the second step, the bleaching of the MLCT band was not significant. In contrast, in the third step, the intensity of the MLCT band decreased drastically. In the fourth step, the bleaching of the MLCT band was again rather small. The bleaching ratios of the MLCT band in these steps were 3.9 (1st), 14.6 (2nd), 71.1 (3rd), and 10.4 (4th)%. These observations imply that the two Ru ions in **Ru₂Fe₃** were simultaneously oxidized in the third oxidation step, although the result of the electrochemical measurement indicates that this step is a one-electron oxidation process (*vide supra*).

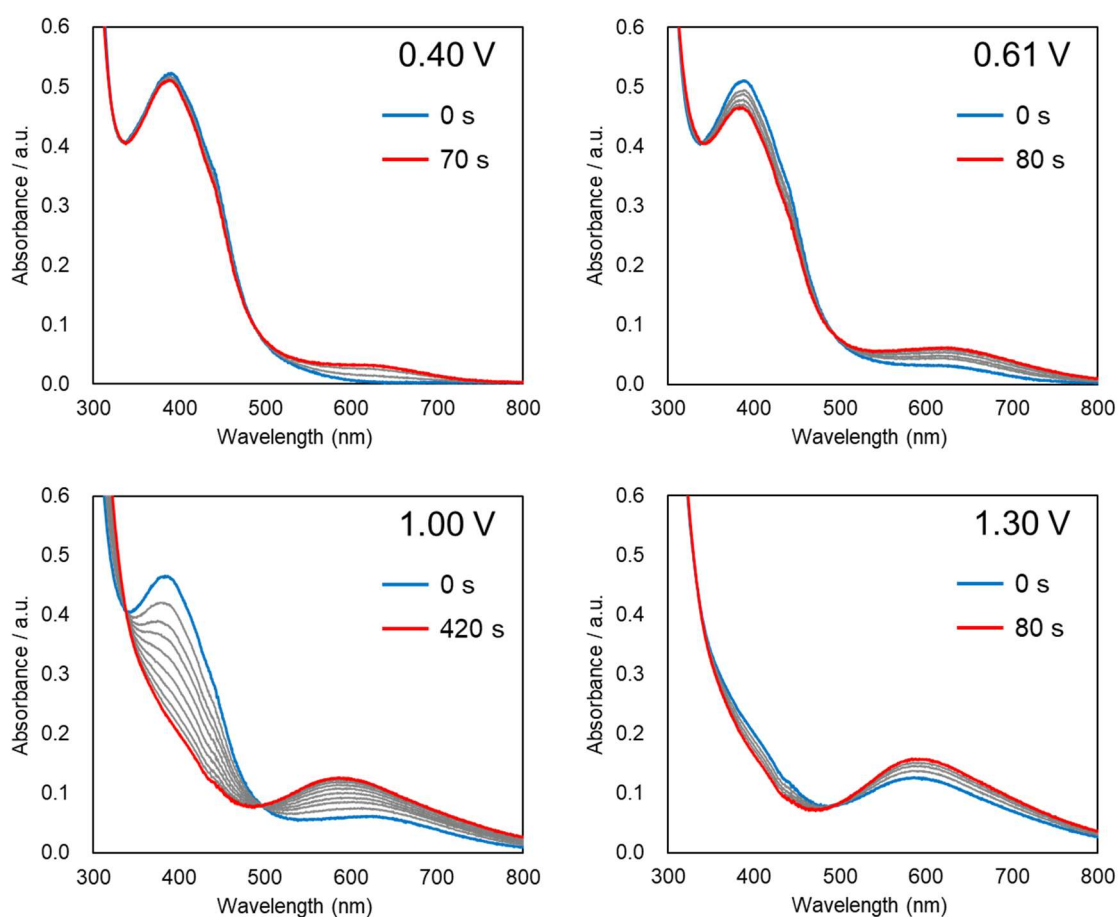
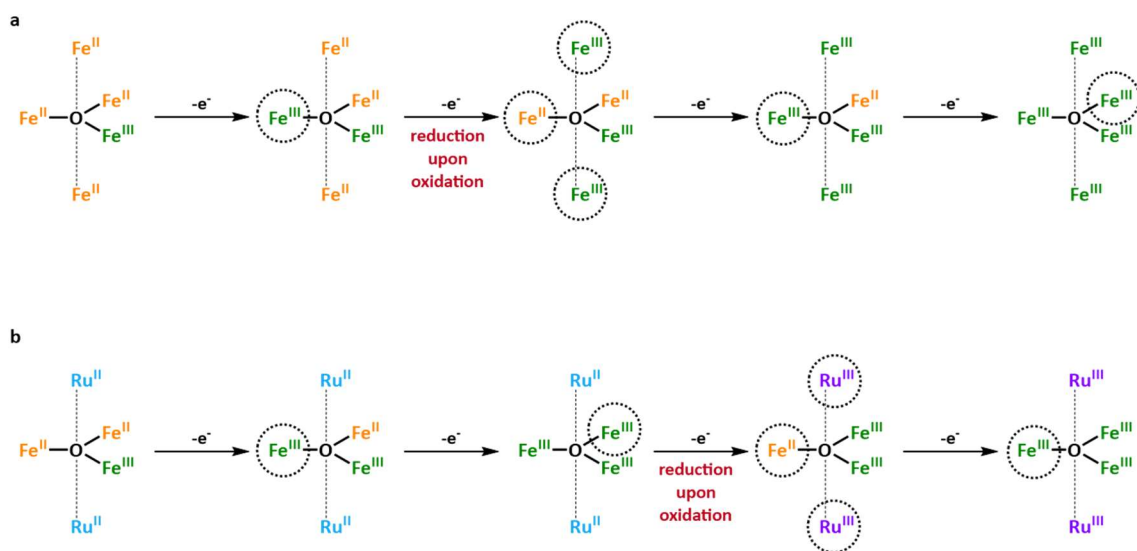


Figure 2-8 | The results of UV-SEC of **Ru₂Fe₃** (0.1 mM) in 0.1 M TBAP/MeCN. Applied potentials are (left, top) 0.40, (right, top) 0.61, (left, bottom) 1.00 and (right, bottom) 1.30 V (*vs.* Fc/Fc⁺), respectively. All measurements were performed under an Ar atmosphere.

A reasonable interpretation of the aforementioned discrepancy in the results of the UV-SEC and electrochemical measurement is provided by comparing the redox behavior of Ru_2Fe_3 with one of Fe_5 . We previously clarified the redox behavior of Fe_5 by UV-SEC measurement, ^{57}Fe Mössbauer spectroscopy, and quantum chemical calculation^{ref} (Scheme 2-1a). A notable electron transfer process was observed in the second oxidation. In this step, the one-electron oxidation of the overall complex induces the reduction of one of the Fe^{III} ions in the triangular core to the Fe^{II} state (a “reduction-upon-oxidation” reaction). Simultaneously, the two iron ions in the apical position were oxidized to the Fe^{III} state, and the apparent change in the overall charge due to this oxidation step is one. In other words, the reduction of the triangular core upon oxidation of the complex allows the simultaneous oxidation of the two metal centers at the apical position. Therefore, the results suggest a similar reduction-upon-oxidation process occurs in Ru_2Fe_3 , although the third oxidation step involves the corresponding reaction (Scheme 2-1b). These results indicate that the substitution of iron ions for ruthenium ions can change the step corresponding to the reduction-upon-oxidation reaction.



Scheme 2-1 | Electron transfer processes of (a) Fe_5 and (b) Ru_2Fe_3 . The metal centers which undergo electron transfer reaction are circled.

For Ru_2Mn_3 , the result of UV-SEC measurement was in a manner similar to that of Ru_2Fe_3 ; the remarkable bleaching of the MLCT band was observed only at the third oxidation step (Figure 2-9). Therefore, Ru_2Mn_3 can also undergo a reduction-upon-oxidation reaction at the triangular core (Scheme 2-2). Note that each oxidation of the relevant homometallic complex, Mn_5 , does not involve such a process¹. Therefore, the unique electron transfer process can be induced by the installation of ruthenium ion in the case of a manganese-based complex.

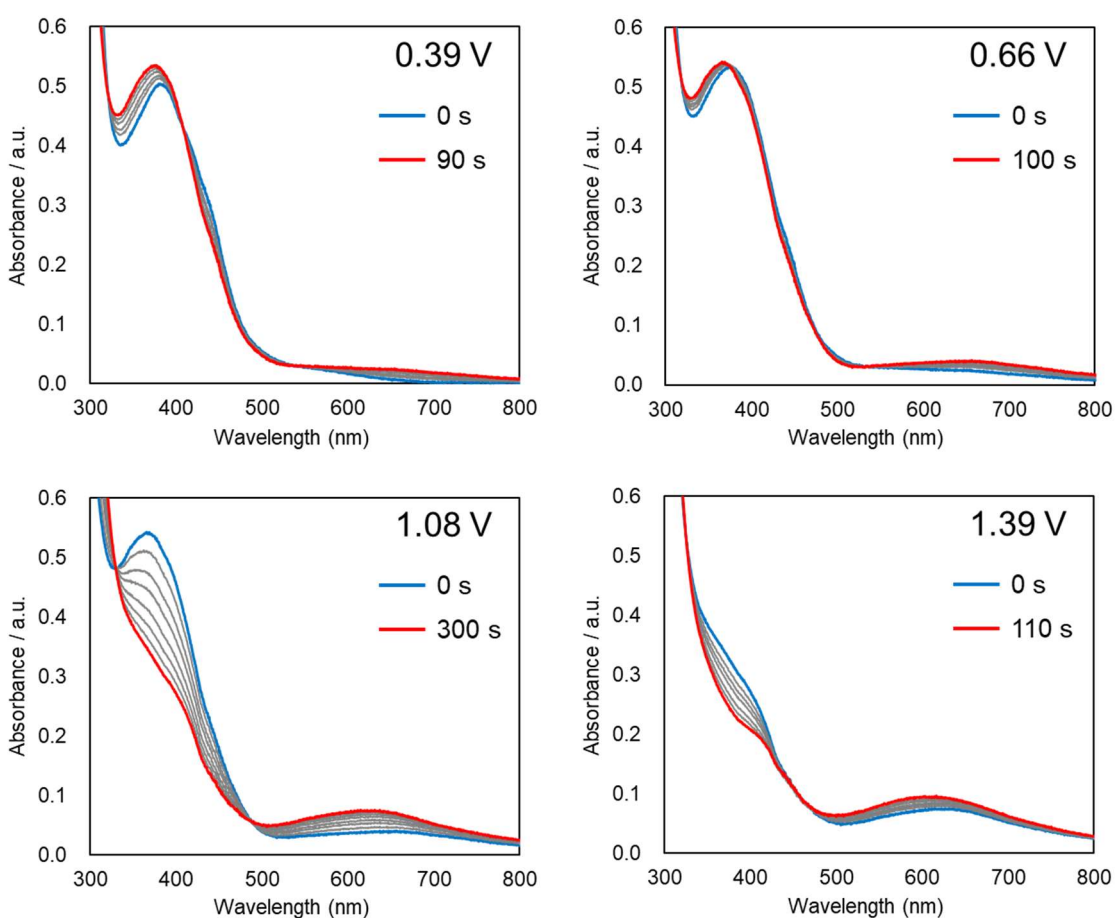
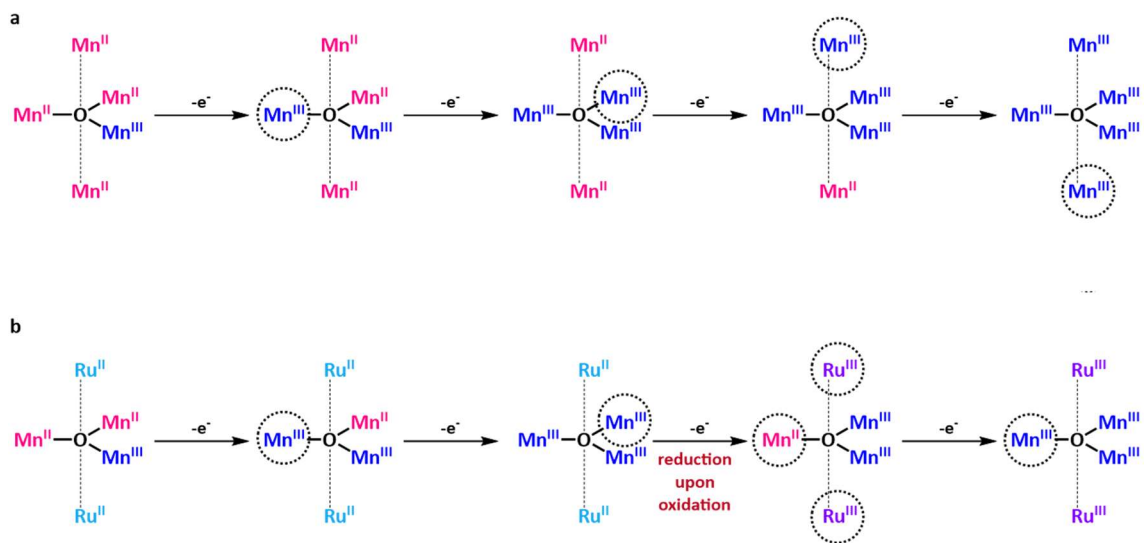


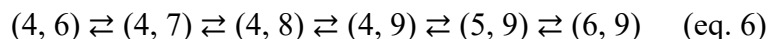
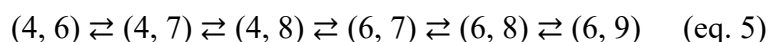
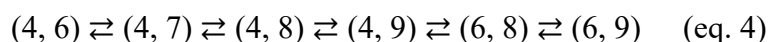
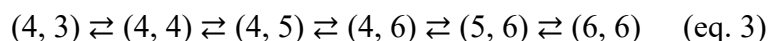
Figure 2-9 | The results of UV-SEC of Ru_2Mn_3 (0.1 mM) in 0.1 M TBAP/MeCN. Applied potentials are (left, top) 0.39, (right, top) 0.66, (left, bottom) 1.08 and (right, bottom) 1.39 V (vs. Fc/Fc^+), respectively. All measurements were performed under an Ar atmosphere.



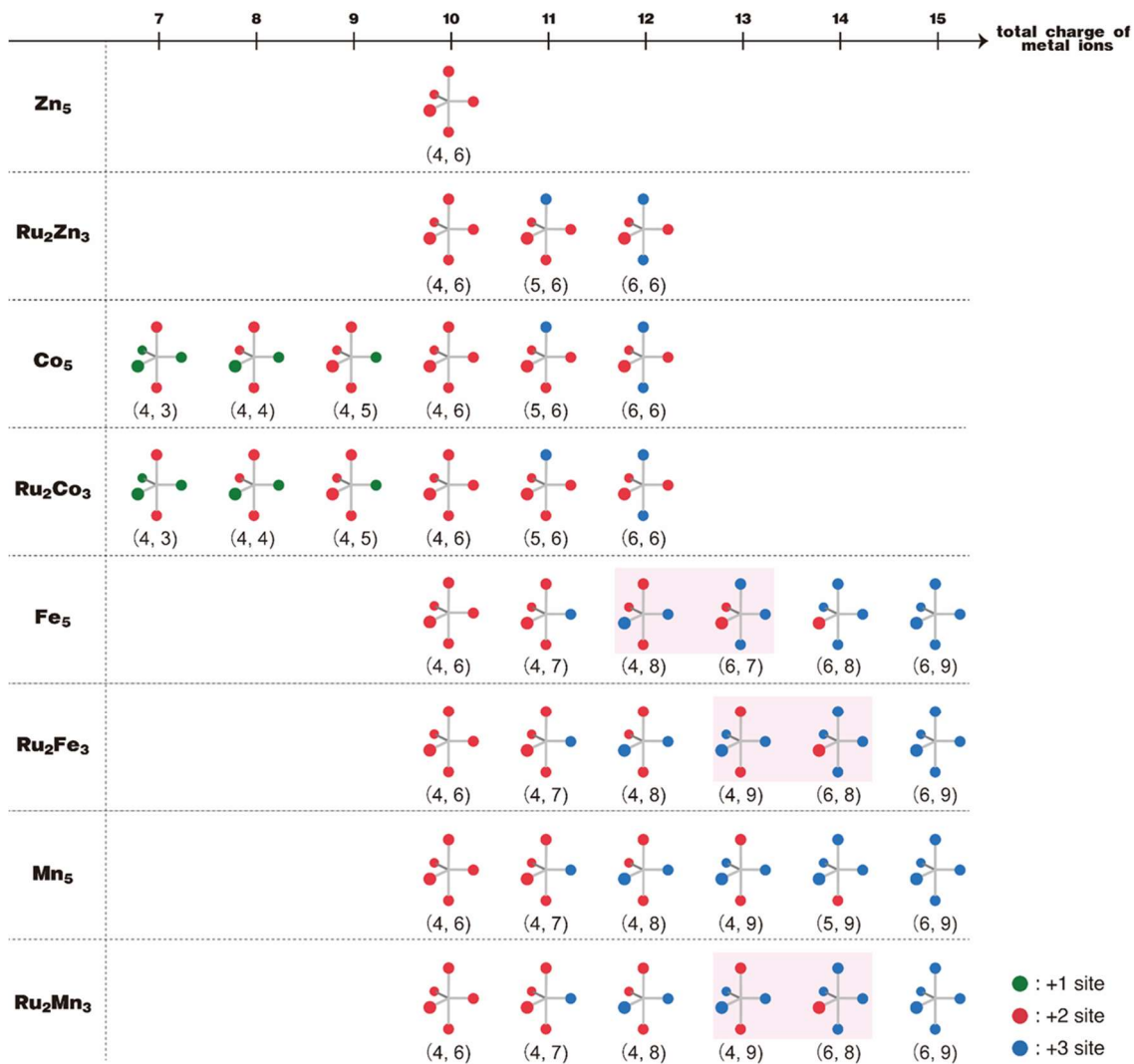
Scheme 2-2 | Electron transfer processes of (a) Mn_5 and (b) Ru_2Mn_3 . The metal centers which undergo electron transfer reaction are circled.

Key Factors Controlling the Electron Transfers in Pentanuclear Metal Complexes

The investigation of a series of pentanuclear metal complexes provide a map of their electron transfer reactions, as shown in Scheme 2-3. The electron transfer reactions in the complexes in this series can be categorized into the following six processes (eqs. 1-6). Note that in these equations, the first and second digits in brackets represent the sum of the charges of metal ions at apical positions (M_{api}) and a triangular core (M_{core}), respectively (for instance, (4, 6) corresponds to the $M_{\text{api}}^{\text{II}}M_{\text{core}}^{\text{II}}_3$ state).



Due to the redox inactivity of the constituent metal ions, no electron transfer reaction occurs in **Zn5** (eq. 1). **Ru2Zn3** undergoes two-step oxidation reactions of the apical position due to the installation of redox-active ruthenium ions (eq. 2). **Co5** and **Ru2Co5** undergo similar electron transfer processes (eq. 3), which involve the formations of monovalent metal ion, reflecting the reductive nature of cobalt centers installed in the triangular core. The electron transfer process in the heterometallic complexes **Ru2Fe3** and **Ru2Mn3** follow eq. 4 and involve the reduction-upon-oxidation reaction of the triangular core, denoted (4, 9) \rightleftharpoons (6, 8). The behavior is different from the one of the corresponding homometallic complexes, **Fe5** and **Mn5**; **Fe5** undergoes electron transfer reactions with the reduction-upon-oxidation reaction given by (4, 8) \rightleftharpoons (6, 7) (eq. 5), and **Mn5** undergoes five sequential one-electron transfer processes without the reduction-upon-oxidation reaction (eq. 6).



Scheme 2-3 | Summary of electron transfer reactions of a series of pentanuclear metal complexes.

(1) Electrostatic Repulsion between Oxidized Metal Centers

To verify the origin of this unique electron transfer reaction, the reduction-upon-oxidation reaction, the electrostatic repulsions between oxidized metal centers were considered. In the series of pentanuclear complexes investigated in this study, the electrostatic repulsions between metal centers should increase upon oxidations of the metal centers. There exist three kinds of electrostatic repulsions (denoted A, B and C) between oxidized (M^{III}) metal centers, as shown in Figure 2-10. A, B, and C correspond to the electrostatic repulsion between $M_{core}-M_{core}$, $M_{core}-M_{api}$, and $M_{api}-M_{api}$, respectively. The strengths of the electrostatic repulsions ($E_{rep}(A)$, $E_{rep}(B)$, and $E_{rep}(C)$) should be in the order $E_{rep}(A) > E_{rep}(B) > E_{rep}(C)$, reflecting the distances between the corresponding oxidized cores.

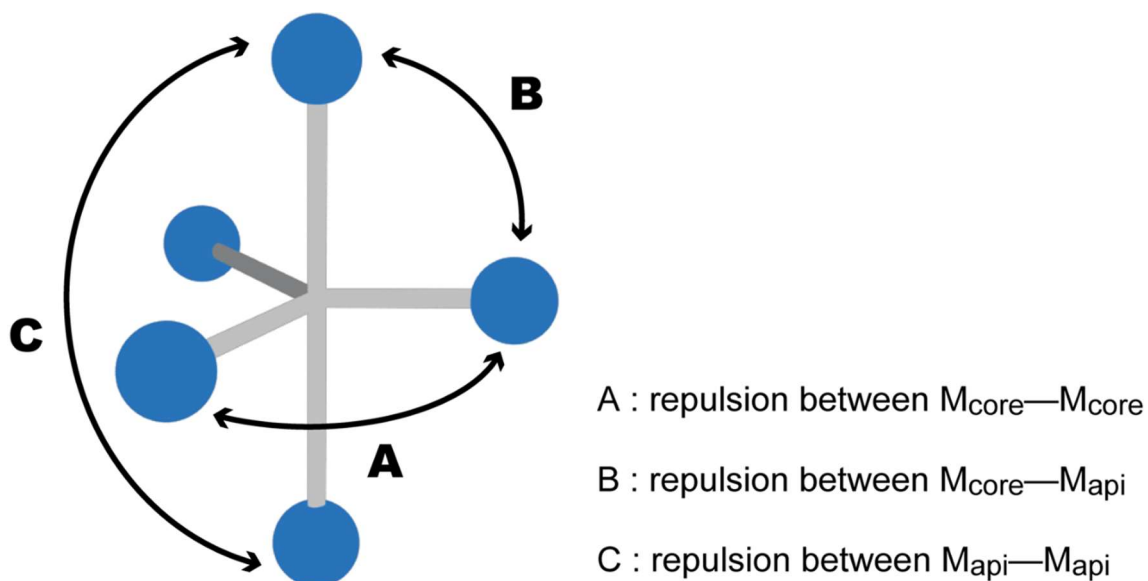
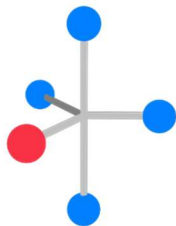
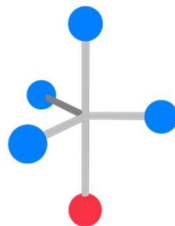


Figure 2-10 | Schematic of the three kinds of electrostatic interactions between oxidized cores in the pentanuclear system.

Based on this consideration, we initially investigated the (4, 9) \rightarrow (6, 8) process, which was observed in **Ru₂Fe₃** and **Ru₂Mn₃**. There exists a valence tautomer of (6, 8), (5, 9), which can be formed from the oxidation of (4, 9) without the reduction-upon-oxidation reaction. As shown in Table 2-5, the total strength of the electrostatic repulsion between oxidised metal centers (E_{reptotal}) is $E_{\text{reptotal}}(6, 8) = E_{\text{rep}}(\text{A}) + 4 E_{\text{rep}}(\text{B}) + E_{\text{rep}}(\text{C})$ and $E_{\text{reptotal}}(5, 9) = 3E_{\text{rep}}(\text{A}) + 3E_{\text{rep}}(\text{B})$ for (6, 8) and (5, 9). By considering the fact that $E_{\text{rep}}(\text{A}) > E_{\text{rep}}(\text{B}) > E_{\text{rep}}(\text{C})$, the following relationship can be obtained: $E_{\text{reptotal}}(6, 8) - E_{\text{reptotal}}(5, 9) = E_{\text{rep}}(\text{B}) + E_{\text{rep}}(\text{C}) - 2E_{\text{rep}}(\text{A}) < 0$. As a result, $E_{\text{reptotal}}(6, 8)$ becomes smaller than $E_{\text{reptotal}}(5, 9)$, which indicates that (6, 8) has less electrostatic repulsion compared to (5, 9), and thus should be favored.

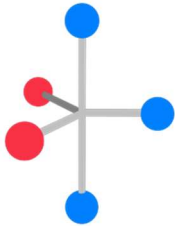
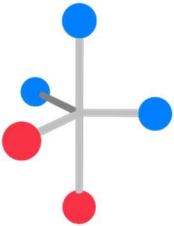
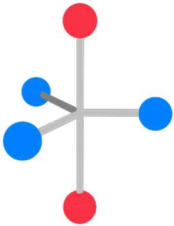
Table 2-5 | Electrostatic repulsion between the oxidized metal centers in (6, 8) and (5, 9).

State	 (6, 8)	 (5, 9)
E_{reptotal}	$E_{\text{rep}}(\text{A}) + 4E_{\text{rep}}(\text{B}) + E_{\text{rep}}(\text{C})$	$3E_{\text{rep}}(\text{A}) + 3E_{\text{rep}}(\text{B})$

Similarly, the relative stabilities of the valence tautomers (6, 7), (5, 8), and (4, 9) in the (4, 8) \rightarrow (6, 7) process, which occurs in **Fe₅**, are discussed. As shown in Table 2-6, the E_{reptotal} of these states can be described as $E_{\text{reptotal}}(6, 7) = 2E_{\text{rep}}(\text{B}) + E_{\text{rep}}(\text{C})$, $E_{\text{reptotal}}(5, 8) = E_{\text{rep}}(\text{A}) + 2E_{\text{rep}}(\text{B})$, and $E_{\text{reptotal}}(4, 9) = 3E_{\text{rep}}(\text{A})$. Based on the following relationship, $E_{\text{rep}}(\text{A}) > E_{\text{rep}}(\text{B}) > E_{\text{rep}}(\text{C})$, the order of the values of E_{reptotal} for these states is $E_{\text{reptotal}}(6, 7) < E_{\text{reptotal}}(5, 8) < E_{\text{reptotal}}(4, 9)$. Therefore, the relative stability of these three valence tautomers is in the order of (6, 7) $>$ (5, 8) $>$ (4, 9), and thus (4, 9) should be favored.

These results indicate that the reduction-upon-oxidation reaction reduces the electrostatic repulsion and contributes to the formation of more energetically favorable species.

Table 2-6 | Electrostatic repulsion between the oxidized metal centers in (6, 7), (5, 8) and (4, 9).

State			
	(6, 7)	(5, 8)	(4, 9)
E_{reptotal}	$2E_{\text{rep}}(\text{B}) + E_{\text{rep}}(\text{C})$	$E_{\text{rep}}(\text{A}) + 2E_{\text{rep}}(\text{B})$	$3E_{\text{rep}}(\text{A})$

(2) Redox Potential of the Metal Ions at the Apical Positions

However, the explanation, based solely on the effect of electrostatic repulsions, cannot justify the existence of the various states that form without the reduction-upon-oxidation reaction, *e.g.*, (4, 9) in **Ru₂Fe₃** and **Ru₂Mn₃**. In principle, the reduction-upon-oxidation reaction of the triangular core should be accompanied by the oxidation of M_{api}. Therefore, the redox potentials of M_{api} should influence the occurrence of reduction-upon-oxidation reaction. Actually, the emergence of reduction-upon-oxidation reaction in pentanuclear complexes is largely dependent on M_{api}; the reduction-upon-oxidation reaction of **Fe₅** occurs in the oxidation of (4, 8), that of **Ru₂Fe₃** and **Ru₂Mn₃** is in the oxidation of (4, 9), and **Mn₅** does not exhibit a reduction-upon-oxidation reaction.

As evidenced by the UV-SEC measurements, the redox potentials that involve the oxidation of M_{api} are largely dependent on the identity of M_{api}; **Fe₅** (0.29 V), **Ru₂Fe₃** (0.75 V), **Ru₂Mn₃** (0.78 V), and **Mn₅** (1.11 and 1.24 V). These results indicate that the potential required to oxidise M_{api} may be in the order of Fe_{api} < Ru_{api} < Mn_{api}.²⁻⁷ To further confirm this explanation, we compared the redox potentials of several mononuclear metal complexes that contain Fe²⁺, Ru²⁺ or Mn²⁺ as the metal ion and six nitrogen donor atoms, as shown in Table 2-7. These complexes are representative hexacoordinate metal centers with octahedral geometry and can thus be regarded as model compounds that mimic the structure around the M_{api} centers of the pentanuclear complexes. In these complexes, the order of the redox potentials is Fe < Ru < Mn, which is consistent with the order of the oxidation potentials of M_{api}, Fe_{api} < Ru_{api} < Mn_{api}.

Table 2-7 | Comparison of oxidation potentials of mononuclear metal complexes containing M (M = Fe²⁺, Ru²⁺, Mn²⁺) and six nitrogen donor atoms.

Complex	Potential	Condition
[Fe(bpy) ₃] ²⁺	1.06 V (vs. SCE)	0.1 M TEAP in MeCN
[Ru(bpy) ₃] ²⁺	1.26 V (vs. SCE)	0.1 M TBAP in MeCN
[Mn(bpy) ₃] ²⁺	1.36 V (vs. SCE)	0.1 M TPAP in MeCN
[Fe(tacn) ₂] ²⁺	0.13 V (vs. NHE)	0.1 M KCl in water
[Ru(tacn) ₂] ²⁺	0.37 V (vs. NHE)	0.1 M CF ₃ SO ₃ H in water
[Mn(tacn) ₂] ²⁺	0.62 V (vs. NHE)	0.1 M KCl in water
[Fe(Tp) ₂]	-0.27 V (vs. Fc/Fc ⁺)	0.1 M TBAPF ₆ in DCE
[Ru(Tp) ₂]	-0.21 V (vs. Fc/Fc ⁺)	0.1 M TBAPF ₆ in DCE
[Mn(Tp) ₂]	0.06 V (vs. Fc/Fc ⁺)	0.1 M TBAPF ₆ in DCE

bpy = 2,2-bipyridine, tacn = 1,4,7-triazacyclononane, Tp = hydrotris(pyrazolyl)borate
 TEAP = tetraethylammonium perchlorate, TPAP = tetra-n-propylammonium perchlorate
 TBAPF₆ = tetra-n-butylammonium hexafluorophosphate, DCE = 1,2-dichloroethane
 SCE = saturated calomel electrode, NHE = normal hydrogen electrode

Summary of the Reduction-Upon-Oxidation Process in Pentanuclear Metal Complexes

As described before, the reduction-upon-oxidation reaction can generate species with the lowest electrostatic repulsion. However, there are several cases in which the reduction-upon-oxidation reaction is suppressed: (i) the formation of (4, 8) instead of (6, 6) by the oxidation of (4, 7) in **Fe₅**, **Ru₂Fe₃**, **Ru₂Mn₃**, and **Mn₅**; (ii) the formation of (4, 9) instead of (6, 7) by the oxidation of (4, 8) in **Ru₂Fe₃**, **Ru₂Mn₃**, and **Mn₅**; and (iii) the formation of (5, 9) instead of (6, 8) by the oxidation of (4, 9) in **Mn₅**.

In the oxidation of (4, 7), the oxidation of the core proceeds in all four complexes because the potentials are not enough to oxidise M_{api} . In the oxidation of (4, 8), **Fe₅** can undergo reduction-upon-oxidation reaction to minimize electrostatic repulsion because Fe_{api} is readily oxidised. However, for **Ru₂Fe₃**, **Ru₂Mn₃**, and **Mn₅**, the reduction-upon-oxidation reaction is suppressed because Ru_{api} and Mn_{api} are hardly oxidised in this potential region. In the oxidation of (4, 9), **Ru₂Fe₃** and **Ru₂Mn₃** can undergo reduction-upon-oxidation reaction by the oxidations of Ru_{api} and the reduction of the M_{core} . In contrast, in the case of **Mn₅**, the reduction-upon-oxidation reaction cannot proceed because the high potential required to oxidise Mn_{api} prevents the reduction of Mn_{core} in this potential range. As a result, (5, 9) forms instead of (6, 8) in this oxidation step of **Mn₅**.

Therefore, the electrostatic repulsion between the oxidized cores and the ease of the oxidation of M_{api} are the dominant factors that determine the reduction-upon-oxidation reaction of the pentanuclear system. These results clearly demonstrate that complicated redox behavior of multinuclear metal complexes can be rationally understood by systematic investigation.

Conclusion

The author succeeded in systematic investigation for the redox behaviour of a series of heterometallic and homometallic pentanuclear complexes by electrochemical measurement, UV-vis absorption spectroscopy and UV-SEC measurement. As a result, a general picture of the electron transfer reactions in the system was unveiled, and unique electron transfer reaction, in which a metal center is reduced during oxidation of the complex, was discovered. Furthermore, the two factors that impact the redox behaviour of the complexes were determined. Collectively, the systematic investigation of a series of pentanuclear complexes demonstrated that the flexible transfer of electrons in clustered redox-active sites can be programmed by the precise arrangement of the metal ions.

References

1. S. Romain, J. Rich, C. Sens, T. Stoll, J. Benet-Buchholz, A. Llobet, M. Rodriguez, I. Romero, R. Clérac, C. Mathonière, C. Duboc, A. Deronzier, M.-N. Collomb, *Inorg. Chem.*, **2011**, *50*, 8427.
2. S. A. Richert, P. K. S. Tsang, D. T. Sawyer, *Inorg. Chem.*, **1989**, *28*, 2471.
3. A. W. Wallace, Jr. W. R. Murphy, J. D. Petersen, *Inorg. Chim. Acta.*, **1989**, *166*, 41.
4. M. M. Morrison, D. T. Sawyer, *Inorg. Chem.*, **1978**, *17*, 333.
5. K. Wieghardt, W. Schmidt, W. Herrmann, H.-J. Küppers, *Inorg. Chem.*, **1983**, *22*, 2953.
6. P. Bernhard, A. M. Sargeson, *Inorg. Chem.*, **1988**, *27*, 2582.
7. D. C. L. D. Alwis, F. A. Schultz, *Inorg. Chem.*, **2003**, *42*, 3616.

Chapter 3

Rational Synthetic Strategy for Heterometallic Tetranuclear Complexes

Introduction

Multinuclear metal complexes have received considerable attention due to their unique physical and chemical properties such as redox¹⁻⁶, photochemical^{7,8} and magnetic properties⁹⁻¹² and reactivity¹³⁻¹⁸ as well as their attractive structures.¹⁹⁻²⁴ In particular, heterometallic multinuclear complexes, which contains more than two kinds of metal ions in the structure, exhibit various functions owing to the cooperative effect between different kinds of metal ions, as can be found in natural biological system.²⁵⁻²⁸ In this context, the precise arrangement of distinct metal ions in multinuclear metal complex is of great significance to develop artificial functional materials. However, the rational synthetic strategy of heterometallic multinuclear complex to achieve such precise arrangement of metal ions is rather limited.²⁹

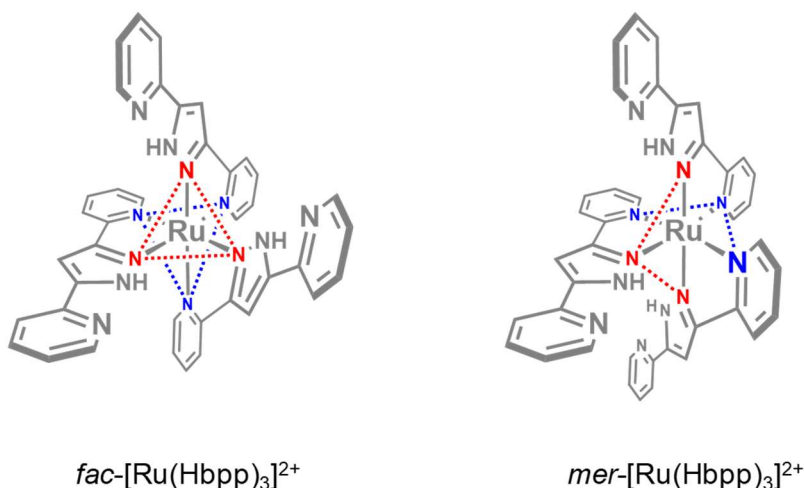
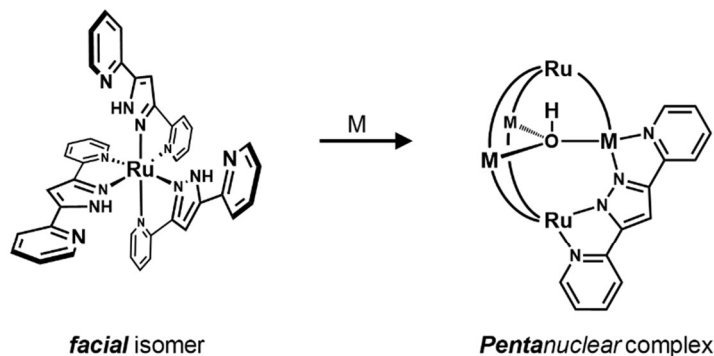


Figure 3-1 | Chemical structure of *fac*-[Ru(Hbpp)₃]²⁺ (left) and *mer*-[Ru(Hbpp)₃]²⁺ (right), in which configuration of six coordinating nitrogen atoms around each ruthenium ion center are emphasized.

(a) Synthetic strategy for heterometallic *pentanuclear* complexes (Chapter 1)



(b) Synthetic strategy for heterometallic *tetranuclear* complexes (Chapter 3)

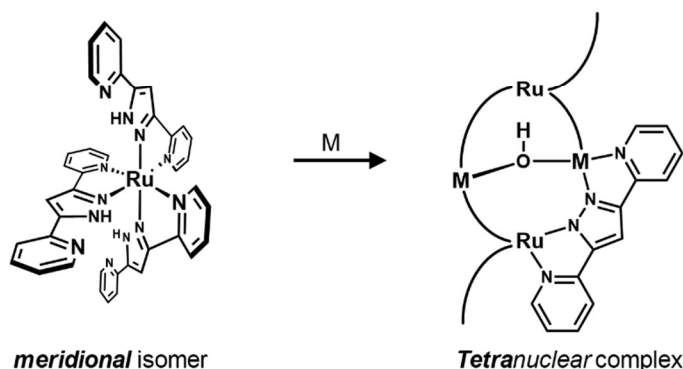


Figure 3-2 | Schematic illustration of the strategy for the rational synthesis of (a) heterometallic pentanuclear complexes and (b) heterometallic tetranuclear complexes.

In this study, it was found that two different series of heterometallic multinuclear complexes can rationally and selectively be synthesized from the same components, ruthenium ion, first-row transition metal ion, and 3,5-bis(2-pyridyl)pyrazole (Hbpp) ligand. A key to success is the use of geometrical isomers of the ruthenium mononuclear complex, *fac*-[Ru(Hbpp)₃]²⁺ and *mer*-[Ru(Hbpp)₃]²⁺ (Figure 3-1). Whereas the treatment of *fac*-[Ru(Hbpp)₃]²⁺ with each first-row transition metal ion afforded a series of heterometallic *pentanuclear* complexes, as is described in chapter 1 (Figure 3-2a), the reaction of *mer*-[Ru(Hbpp)₃]²⁺ gave a series of heterometallic *tetranuclear* complexes (Figure 3-2b).

This chapter focuses on the development of tetranuclear metal complexes constructed via the stepwise complexations of ruthenium ion and first-row transition metal ion to Hbpp ligand. The result presented in this chapter offers a powerful and rational strategy to enable the precise arrangement of metal ions in multinuclear metal complex.

Experimental Section

Materials.

NH₄PF₆ and NaOH were purchased from Wako Pure Chemical Industries, Ltd. Zn(OAc)₂•2H₂O and Cu(OAc)₂•H₂O were purchased from Kanto Chemical Co., Inc. RuCl₃•3H₂O was purchased from Tanaka Kikinzoku Kogyo K.K. 3,5-Bis(2-pyridyl)pyrazole, lithium bis(trifluoromethanesulfonyl)imide (LiTFSI) and 1,8-diazabicyclo[5.4.0]undec-7-ene (DBU) were purchased from Tokyo Chemical Industry Co., Ltd. Co(ClO₄)•6H₂O was purchased from Aldrich. All solvents and reagents are of the highest quality available and used as received. H₂O was purified using a Millipore MilliQ purifier, and was purged with argon before use.

Measurement Apparatus.

Elemental analysis was carried out on a J-SCIENCE LAB MICRO CORDER JM10 elemental analyser. ESI TOF-MS were recorded on a JEOL JMS-T100LP mass spectrometer. ¹H NMR spectra were acquired on a Bruker AVANCE III spectrometer.

X-ray Crystallography.

A crystal of the obtained complex was mounted in a loop. Diffraction data of **Ru₂Zn₂(PF₆)** and **Ru₂Co₂(TFSI)** at 123 K were measured on a Synergy Custom system CCD Plate diffractometer equipped with mirror monochromated Mo-K α radiation and data were processed using CrysAlisPro (Rigaku). Diffraction data of **Ru₂Cu₂(TFSI)** at 123 K were measured on a XtaLAB Synergy CCD Plate diffractometer equipped with mirror monochromated Mo-K α radiation and data were processed using CrysAlisPro (Rigaku). The structures were solved by direct method using *SIR-92* [S1] and refined by the full-matrix least squares techniques on *F*² (*SHELXL-2014/7* [S2]). All non-hydrogen atoms were refined anisotropically and refined with a riding model with *U*_{iso} constrained to be 1.2 times *U*_{eq} of the carrier atom. The diffused electron densities resulting from residual solvent molecules were removed from the data set using the SQUEEZE routine of PLATON [S3] and refined further using the data generated. Crystallographic data have been deposited with Cambridge Crystallographic Data Centre: CCDC deposition numbers; 1960443 for **Ru₂Zn₂(PF₆)**, 1960444 for **Ru₂Co₂(TFSI)** and 1960445 for **Ru₂Cu₂(TFSI)**. Copies of the data can be obtained free of charge via www.ccdc.cam.ac.uk/data_request/cif.

Synthesis of mer-[Ru(Hbpp)₃](TFSI)₂.

RuCl₃·3H₂O (1.0 mmol) and 3,5-bis(2-pyridyl)pyrazole (Hbpp; 3.0 mmol) were suspended in 18.0 mL of ethanol. The reaction mixture was heated at 120 °C for 9 hours by microwave reactor. The reaction mixture was filtered to remove undissolved residues and excess amount of saturated aqueous NaClO₄ solution was added to the filtrate, then the precipitate was collected by filtration. The obtained precipitate was dissolved in acetonitrile and slow diffusion of diisopropylether at ambient temperature gave yellow powder after a few days. The yellow powder was collected by filtration and then dissolved in acetonitrile. The excess amount of saturated aqueous LiTFSI solution was added to the solution, then the precipitate was collected by filtration. The formed precipitate was dissolved in mixed solvent of acetonitrile and H₂O, then slow evaporation of acetonitrile at ambient temperature gave light orange crystals after a few days. The crystals were collected by filtration and dried under vacuum. Yield 353.72 mg (27.9%). Elemental analysis Calcd. for [Ru(Hbpp)₃](TFSI)₂·H₂O: C₄₃H₃₂F₁₂N₁₄O₉Ru₁S₄: C, 38.37; H, 2.40; N, 14.57%. Found: C, 38.61; H 2.54; N 14.72%. ESI-TOF MS (positive ion, acetonitrile): m/z: 384.10 [Ru(Hbpp)₃]²⁺, 767.19 [Ru(Hbpp)₂(bpp)₃]⁺, 1048.13 ([Ru(Hbpp)₃]²⁺+TFSI⁻)⁺. ¹H NMR (600 MHz, DMSO-*d*₆): δ = 8.64-8.59 (m, 3H), 8.37 (d, *J* = 7.9 Hz, 1H), 8.30 (t, *J* = 7.7 Hz, 2H), 8.16-8.08 (m, 4H), 8.05-7.98 (m, 5H), 7.96-7.91 (m, 3H), 7.64 (d, *J* = 5.4 Hz, 1H), 7.56 (d, *J* = 5.4 Hz, 1H), 7.48-7.41 (m, 5H), 7.34 (t, *J* = 6.4 Hz, 1H), 7.29 (t, *J* = 6.6 Hz, 1H).

Synthesis of [Ru^{II}(μ-bpp)₃]₂Zn^{II}₂(μ-OH)](PF₆) (Ru₂Zn₂(PF₆)).

mer-Ru(Hbpp)₃(TFSI)₂·H₂O (0.03 mmol) and Zn(OAc)₂·2H₂O (0.15 mmol) were dissolved in 3.0 mL of *N*-methylpyrrolidone. A 1.0 M NaOH aqueous solution (300 μL) was added to the solution, and then it was heated at 80 °C for 12 hours. The reaction mixture was filtered to remove undissolved residues and excess amount of saturated aqueous NH₄PF₆ solution and excess amount of H₂O were added to the filtrate, then the precipitate was collected by filtration. The obtained precipitate was dissolved in acetonitrile and then 50 μL of DBU was added to the solution. The solution was heated at 50 °C for 1 hour, then the solution was concentrated. Excess amount of diethylether was added to the solution, and then the formed precipitate was collected by filtration. The precipitate was dissolved in acetonitrile and slow diffusion of diethylether at ambient temperature gave light red crystals after a few days. The crystals were collected by filtration and dried under vacuum. Yield 19.9 mg (73.0%). Elemental analysis Calcd. for [Ru₂Zn₂(OH)(bpp)₆](PF₆)₃·2H₂O: C₇₈H₅₉F₆N₂₄O₃P₁Ru₂Zn₂: C, 50.41; H, 3.20; N,

18.09%. Found: C, 50.20; H 3.47; N 18.03%. ESI-TOF MS (positive ion, acetonitrile): m/z: 1677.13 [$\{\text{Ru}^{\text{II}}(\mu\text{-bpp})_3\}_2\text{Zn}^{\text{II}}_2(\mu\text{-OH})^+$]. ^1H NMR (600 MHz, DMSO- d_6): δ = 8.44 (s, 1H), 8.05 (d, J = 7.9 Hz, 1H), 8.00 (t, J = 7.7 Hz, 1H), 7.88 (t, J = 7.7, 2H), 7.83 (t, J = 7.7, 1H), 7.80-7.76 (m, 3H), 7.61 (d, J = 4.2 Hz, 3H), 7.56 (d, J = 5.5 Hz, 1H), 7.48 (s, 1H), 7.42 (d, J = 8.1 Hz, 1H), 7.38 (d, J = 5.5 Hz, 1H), 7.19-7.14 (m, 2H), 7.11-7.03 (m, 4H), 6.96 (t, J = 7.7 Hz, 1H), 6.74 (d, J = 5.0 Hz, 1H), 6.65 (t, J = 6.1 Hz, 1H), 6.63 (s, 1H), 6.57 (t, J = 6.4 Hz, 1H).

Synthesis of [$\{\text{Ru}^{\text{II}}(\mu\text{-bpp})_3\}_2\text{Cu}^{\text{II}}_2(\mu\text{-OH})$](TFSI) ($\text{Ru}_2\text{Cu}_2(\text{TFSI})$).

mer-Ru(Hbpp) $_3$ (TFSI) $_2$ ·H $_2$ O (0.03 mmol) and Cu(OAc) $_2$ ·H $_2$ O (0.15 mmol) were dissolved in 3.0 mL of *N*-methylpyrrolidone. A 1.0 M NaOH aqueous solution (300 μ L) was added to the solution, and then it was heated at 100 °C for 12 hours. The reaction mixture was filtered to remove undissolved residues and excess amount of saturated aqueous LiTFSI solution and excess amount of H $_2$ O were added to the filtrate, then the precipitate was collected by filtration. The obtained precipitate was dissolved in acetonitrile and then 50 μ L of DBU was added to the solution. The solution was heated at 50 °C for 1 hour, then the solution was concentrated. Excess amount of diethylether was added to the solution, and then the formed precipitate was collected by filtration. The precipitate was dissolved in dichloromethane and slow diffusion of diethylether at ambient temperature gave dark red crystals after a few days. The crystals were collected by filtration and dried under vacuum. Yield 18.0 mg (60.4%). Elemental analysis Calcd. for [$\text{Ru}_2\text{Cu}_2(\text{OH})(\text{bpp})_6$](TFSI)·4H $_2$ O: C $_{80}$ H $_{63}$ Cu $_2$ F $_6$ N $_2$ S $_2$ O $_9$ Ru $_2$ S $_2$: C, 47.43; H, 3.13; N, 17.28%. Found: C, 47.42; H 3.32; N 17.30%. ESI-TOF MS (positive ion, acetonitrile): m/z: 1675.14 [$\{\text{Ru}^{\text{II}}(\mu\text{-bpp})_3\}_2\text{Cu}^{\text{II}}_2(\mu\text{-OH})^+$].

Synthesis of [$\{\text{Ru}^{\text{II}}(\mu\text{-bpp})_3\}_2\text{Co}^{\text{II}}_2(\mu\text{-OH})$](PF $_6$) ($\text{Ru}_2\text{Co}_2(\text{PF}_6)$).

mer-Ru(Hbpp) $_3$ (TFSI) $_2$ ·H $_2$ O (0.03 mmol) and Co(ClO $_4$) $_2$ ·6H $_2$ O (0.45 mmol) were dissolved in 3.0 mL of *N*-methylpyrrolidone. A 1.0 M NaOH aqueous solution (300 μ L) was added to the solution, and then it was heated at 100 °C for 12 hours. The reaction mixture was filtered to remove undissolved residues and excess amount of saturated aqueous NH $_4$ PF $_6$ solution and excess amount of H $_2$ O were added to the filtrate, then the precipitate was collected by filtration. The obtained precipitate was dissolved in acetonitrile and then 50 μ L of DBU was added to the solution. The solution was heated at 50 °C for 1 hour, then the solution was concentrated. Excess amount of diethylether

was added to the solution, and then the formed precipitate was collected by filtration. The precipitate was dissolved in dichloromethane and slow diffusion of diethylether at ambient temperature gave dark red crystals after a few days. The crystals were collected by filtration and dried under vacuum. Yield 20.7 mg (74.1%). Elemental analysis Calcd. for $[\text{Ru}_2\text{Co}_2(\text{OH})(\text{bpp})_6](\text{PF}_6)\cdot 6\text{H}_2\text{O}$: $\text{C}_{78}\text{H}_{67}\text{Co}_2\text{F}_6\text{N}_{24}\text{O}_7\text{P}_1\text{Ru}_2$: C, 48.86; H, 3.52; N, 17.53%. Found: C, 49.01; H 3.68; N 17.28%. ESI-TOF MS (positive ion, acetonitrile): m/z : 1665.14 [$\{\text{Ru}^{\text{II}}(\mu\text{-bpp})_3\}_2\text{Co}^{\text{II}}_2(\mu\text{-OH})^+$]. $[\text{Ru}_2\text{Co}_2(\text{bpp})_6](\text{TFSI})$ was prepared by adding excess amount of a saturated aqueous LiTFSI solution instead of a saturated aqueous NH_4PF_6 solution to the filtrate obtained after the reaction. The obtained precipitate was dissolved in acetonitrile and then 50 μL of DBU was added to the solution. The solution was heated at 50 $^\circ\text{C}$ for 1 hour, then the solution was concentrated. Excess amount of diethylether was added to the solution, and then the obtained precipitate was collected by filtration. The precipitate was dissolved in dichloromethane and slow diffusion of diethylether into the solution at ambient temperature afforded the single crystals of $[\text{Ru}_2\text{Co}_2(\text{bpp})_6](\text{TFSI})$ suitable for single crystal X-ray structural determination.

Synthesis and Characterization

The syntheses of mononuclear ruthenium complexes were performed by reacting RuCl_3 with 3 eq. of Hbpp in ethanol at $120\text{ }^\circ\text{C}$ for 9 hours, and the addition of a saturated aqueous solution of NaClO_4 to the reaction mixture afforded precipitate. The precipitate was then dissolved in acetonitrile and slow diffusion of diisopropylether to the resultant solution at ambient temperature afforded yellow powder. Further diffusion of diisopropylether to the solution afforded red crystals. The red crystals were characterized as *fac*- $[\text{Ru}(\text{Hbpp})_3](\text{ClO}_4)_2$ by ^1H NMR and electro-spray ionization time-of-flight mass spectrometry (ESI TOF-MS), elemental analysis and single crystal X-ray structural analysis in chapter 1. Subsequently, the yellow powder was collected by filtration and dissolved in acetonitrile. To this solution, an excess amount of a saturated aqueous solution of lithium bis(trifluoromethanesulfonyl)imide (LiTFSI) was added and precipitate formed. The precipitate was dissolved in a mixed solvent of acetonitrile and H_2O , and slow evaporation of acetonitrile at ambient temperature gave light orange crystals after a few days.

The characterization of the orange crystals was performed by elemental analysis and ESI TOF-MS and ^1H NMR spectroscopy. The results of elemental analysis and ESI TOF-MS (Figure 3-3) revealed that the orange crystals have the composition of $[\text{Ru}(\text{Hbpp})_3](\text{TFSI})_2$. In the ^1H NMR spectrum of the orange crystals (Figure 3-4a), the larger number of peaks were observed compared to the ^1H NMR spectrum of *fac*- $[\text{Ru}(\text{Hbpp})_3](\text{ClO}_4)_2$ (Figure 3-4b), indicating that the complex has more unsymmetrical structure than *fac*- $[\text{Ru}(\text{Hbpp})_3]^{2+}$. This observation strongly supports that the orange crystals are *mer*- $[\text{Ru}(\text{Hbpp})_3](\text{TFSI})_2$ in conjunction with the aforementioned results of ESI TOF-MS and elemental analysis.

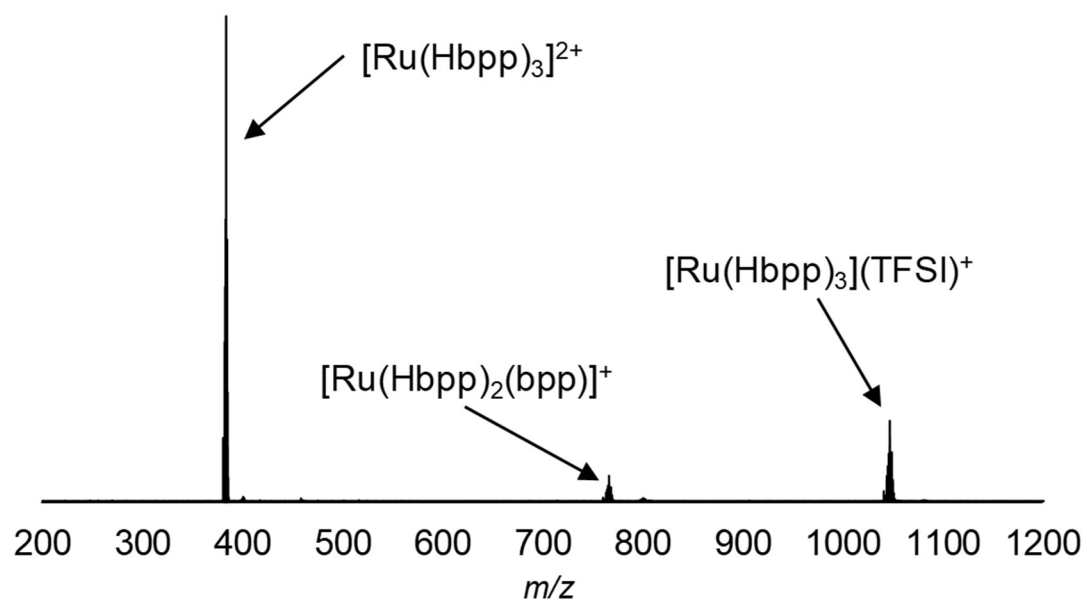
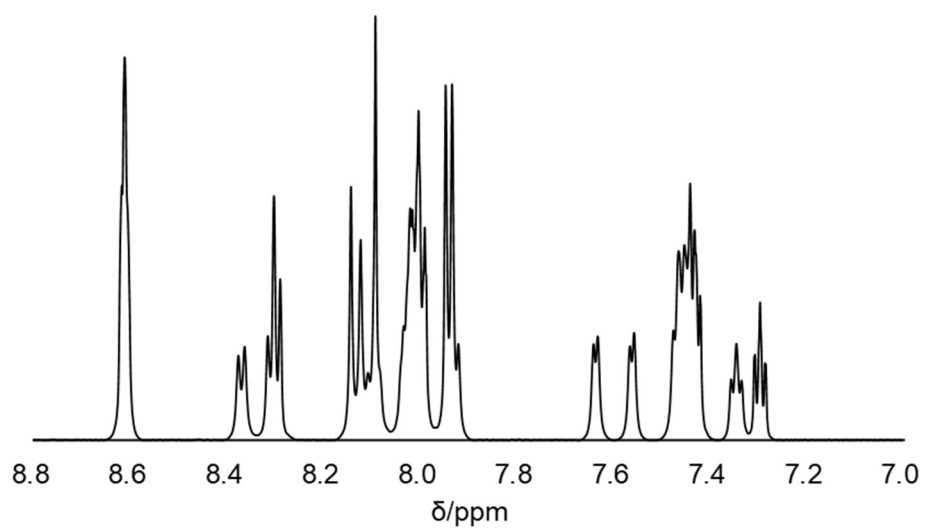


Figure 3-3 | ESI TOF-MS of *mer*- $[\text{Ru}(\text{Hbpp})_3](\text{TFSI})_2$ in acetonitrile.

(a)



(b)

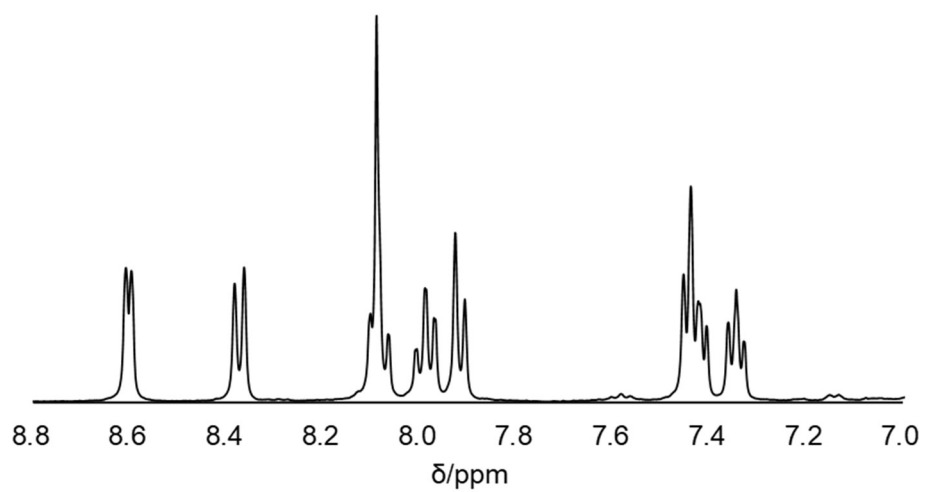


Figure 3-4 | ^1H NMR spectra of (a) *mer*- $[\text{Ru}(\text{Hbpp})_3](\text{TFSI})_2$ and (b) *fac*- $[\text{Ru}(\text{Hbpp})_3](\text{ClO}_4)_2$ in $\text{DMSO-}d_6$ at 293 K.

Subsequently, the reaction of *mer*-[Ru(Hbpp)₃](TFSI)₂ with first-row transition metal ion was examined. As an initial trial, Zn²⁺ was employed as a first-row transition metal ion because the diamagnetic d¹⁰ nature of Zn²⁺ enables the characterization of the formed complex by ¹H NMR spectroscopy. *mer*-[Ru(Hbpp)₃](TFSI)₂ was reacted with 5.0 eq. of Zn(OAc)₂·2H₂O in the presence of base at 80 °C for 12 hours. After the reaction, a saturated aqueous solution of NH₄PF₆ was added to the reaction mixture, and the formed precipitate was collected by filtration. The precipitate was dissolved into acetonitrile and the resultant solution was heated in the presence of 50 μL of 1,8-diazabicyclo[5.4.0]undec-7-ene (DBU) at 50 °C for 1 hour. Subsequently, diethylether was added to the solution until precipitate formed, and the formed precipitate was recrystallized from acetonitrile/diethylether to give orange crystals. The ESI TOF-MS of the crystals (Figure 3-5) exhibited a peak corresponds to [Ru₂Zn₂(OH)(bpp)₆]⁺ (m/z = 1677.13). Furthermore, the elemental analysis revealed that the composition of the crystals are [Ru₂Zn₂(OH)(bpp)₆](PF₆)·2H₂O. These results indicate that the reaction between *mer*-[Ru(Hbpp)₃](TFSI)₂ and Zn²⁺ ion affords the selective formation of one product with a tetranuclear structure. In the ¹H NMR spectrum of the obtained crystals (Figure 3-6), three singlet peaks attributed to pyrazole moiety of bpp were observed, which suggests that there exists three kinds of bpp ligands in the structure. This result supports the formation of the tetranuclear complex in which two meridional Ru(bpp)₃ units were connected by a Zn-(μ-OH)-Zn core moiety.

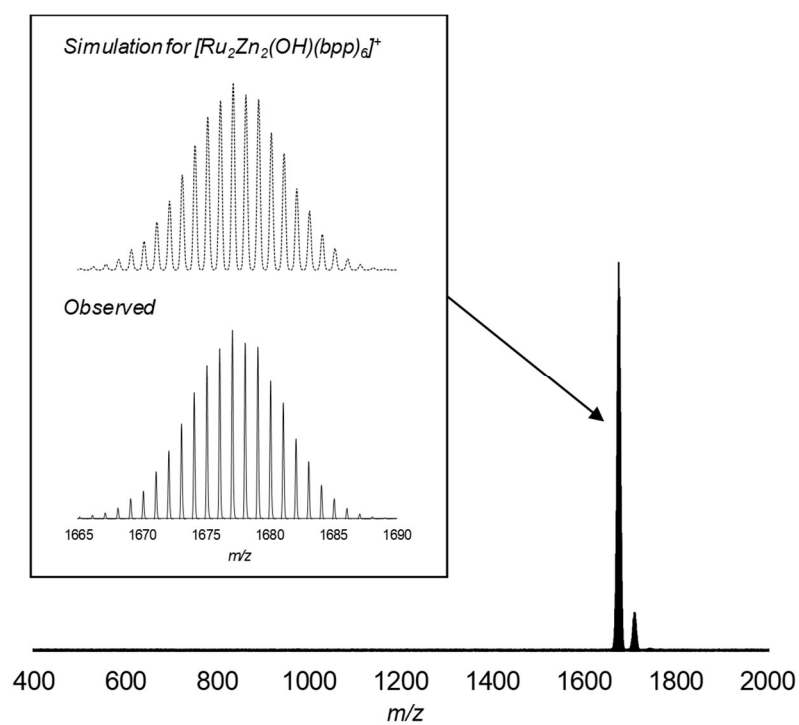


Figure 3-5 | ESI TOF-MS of $[\text{Ru}_2\text{Zn}_2(\text{OH})(\text{bpp})_6](\text{PF}_6)$ in acetonitrile.

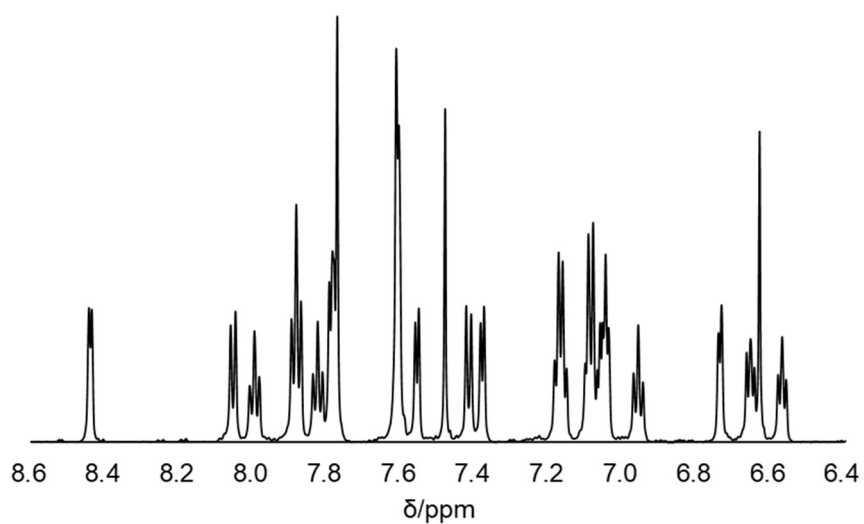


Figure 3-6 | ^1H NMR spectrum of $[\text{Ru}_2\text{Zn}_2(\text{OH})(\text{bpp})_6](\text{PF}_6)$ in $\text{DMSO}-d_6$ at 293 K.

To further unveil the structure of the complex, single crystal X-ray structural analysis was performed. The structure of the cationic moiety of the complex is shown in Figure 3-7. As expected, the complex has a tetranuclear structure that consists of a dinuclear core bridged by hydroxyl ligand sandwiched by two *mer*-[M(μ -bpp)₃] units. The two metal ions in the dinuclear core (M_{core}) are pentacoordinate with distorted trigonal bipyramidal geometry, whereas metal ions at the apical position (M_{api}) are hexacoordinate with distorted octahedral geometry. The average bond distance between M_{api} and the coordinating six nitrogen atoms of the *mer*-[M_{api}(μ -bpp)₃] units ($d(M_{\text{api}}-N)$) is 2.063(3) Å (Table 3-2), and is the typical value for the hexacoordinated ruthenium polyimine complexes³³. Therefore, M_{api} and M_{core} in this tetranuclear complex can be assigned to ruthenium ion and zinc ion, respectively. In other words, the structure of the complex is as [$\{\text{Ru}^{\text{II}}(\mu\text{-bpp})_3\}_2\text{Zn}^{\text{II}}_2(\mu\text{-OH})$]⁺ (**Ru₂Zn₂**). These results strongly suggest that *mer*-[Ru(Hbpp)₃]²⁺ did not isomerize nor decompose in the solution during the reaction, and it can work as a robust building block of the stepwise synthetic strategy.

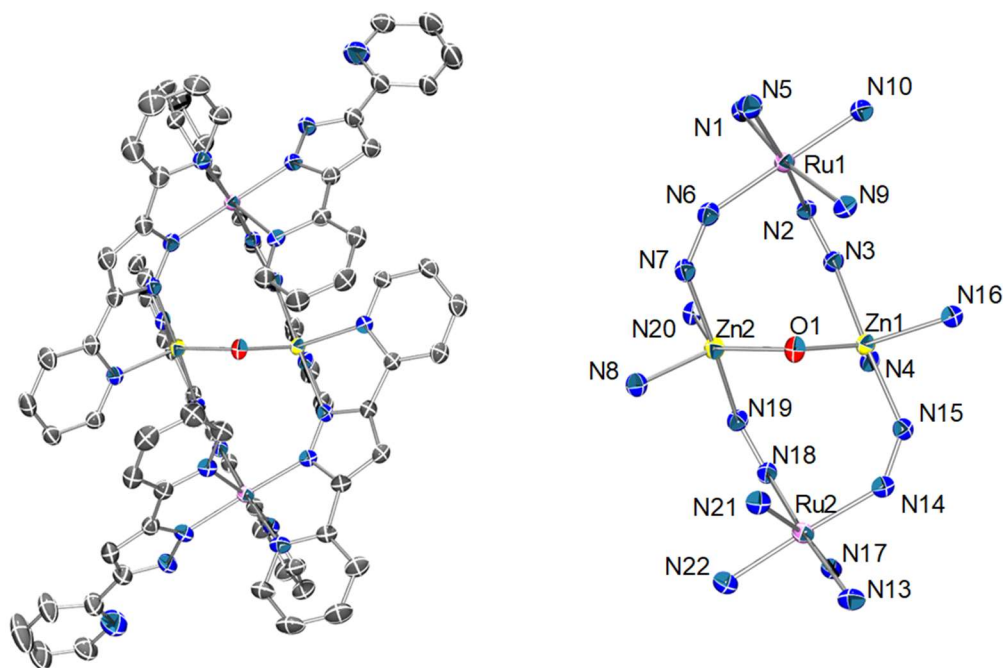


Figure 3-7 | The ORTEP drawing of cationic moiety (left) and core structure (right) of [Ru₂Zn₂(OH)(bpp)₆](PF₆) (50% probability ellipsoids). Hydrogen atoms are omitted for clarity. O = red, C = gray, N = blue, Zn = yellow and Ru = orchid.

Table 3-1 | Summary of the crystallographic data for [Ru₂Zn₂(OH)(bpp)₆](PF₆).

formula	C ₇₈ H ₅₅ F ₆ N ₂₄ OPRu ₂ Zn ₂
fw	1822.31
color, habit	clear light orange, plate
crystal size, mm ³	0.149 x 0.110 x 0.039
crystal system	triclinic
space group	<i>P</i> -1
<i>a</i> / Å	15.7383(3)
<i>b</i> / Å	18.0021(3)
<i>c</i> / Å	19.5479(3)
<i>α</i> / °	107.8620(10)
<i>β</i> / °	112.201(2)
<i>γ</i> / °	101.8210(10)
<i>V</i> / Å ³	4545.82(15)
<i>Z</i>	2
<i>F</i> (000)	1832
<i>d</i> _{calc} , g/cm ³	1.331
<i>μ</i> (MoK α), mm ⁻¹	0.931
<i>T</i> , K	123(2)
uniq reflns	24898
<i>R</i> _{int}	0.0360
<i>R</i> ₁	0.0533
<i>wR</i> ₂	0.1507
GOF	1.033

Table 3-2 | Selected bond lengths of [Ru₂Zn₂(OH)(bpp)₆](PF₆).

	bond	length / Å
M _{api} -N	Ru1-N1	2.067(3)
	Ru1-N2	2.080(3)
	Ru1-N5	2.060(3)
	Ru1-N6	2.064(3)
	Ru1-N9	2.087(4)
	Ru1-N10	2.026(3)
	Ru2-N13	2.069(4)
	Ru2-N14	2.057(3)
	Ru2-N17	2.069(3)
	Ru2-N18	2.069(3)
	Ru2-N21	2.084(3)
	Ru2-N22	2.028(3)
average		2.063(3)

	bond	length / Å
M _{core} -N	Zn1-N3	2.132(3)
	Zn1-N4	2.102(3)
	Zn1-N15	2.108(3)
	Zn1-N16	2.105(3)
	Zn2-N7	2.123(2)
	Zn2-N8	2.094(3)
	Zn2-N19	2.115(2)
	Zn2-N20	2.103(4)
average		2.110(3)

	bond	length / Å
M _{core} -O	Zn1-O1	1.940(3)
	Zn2-O1	1.943(3)
average		1.942(3)

The stepwise synthetic strategy was adopted for the synthesis of tetranuclear complexes containing other first-row transition metal ions, Cu^{2+} and Co^{2+} . The synthetic procedure for these tetranuclear complexes is similar to that for **Ru₂Zn₂**. *mer*-[Ru(Hbpp)₃](TFSI)₂ was reacted with 5.0 eq. of Cu^{2+} or 15.0 eq. of Co^{2+} in the presence of base at 100 °C, and the obtained compounds were further treated with DBU at 50 °C. These reactions afforded the selective formation of [Ru₂M₂(OH)(bpp)₆]⁺ (M = Cu or Co) species, as evidenced by ESI TOF-MS (Figure 3-8 and 3-9) and elemental analysis. The structures of the complexes were also clarified by single crystal X-ray structural analysis. As shown in Figure 3-10 and 3-11, both complexes exhibited structure similar to **Ru₂Zn₂**. Note that in the crystal structure of the complex containing Cu ions, two crystallographically independent complexes were observed (Figure 3-12). The average $d(\text{M}_{\text{api}}\text{-N})$ of these complexes is 2.058(4) Å ([Ru₂Cu₂(OH)(bpp)₆]⁺, Table 3-4) and 2.059(4) Å ([Ru₂Co₂(OH)(bpp)₆]⁺, Table 3-4), and is quite similar to average $d(\text{M}_{\text{api}}\text{-N})$ of **Ru₂Zn₂** (2.063(3) Å, *vide supra*). Therefore, M_{api} and M_{core} in these tetranuclear complexes are assignable to ruthenium ion and first-row transition metal ion, respectively, and the structure of the complexes can be described as [$\{\text{Ru}^{\text{II}}(\mu\text{-bpp})_3\}_2\text{Cu}^{\text{II}}_2(\mu\text{-OH})$]⁺ (**Ru₂Cu₂**) and [$\{\text{Ru}^{\text{II}}(\mu\text{-bpp})_3\}_2\text{Co}^{\text{II}}_2(\mu\text{-OH})$]⁺ (**Ru₂Co₂**). Collectively, the stepwise synthetic strategy using *mer*-[Ru(Hbpp)₃]²⁺ can lead the selective formation of a series of heterometallic complexes which have tetranuclear structure.

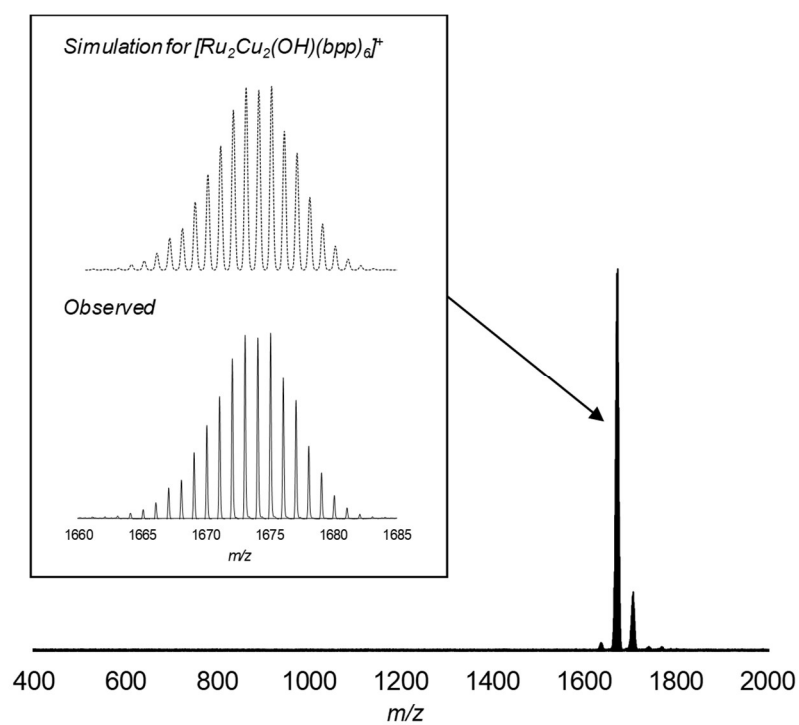


Figure 3-8 | ESI TOF-MS of $[Ru_2Cu_2(OH)(bpp)_6](TFSI)$ in acetonitrile.

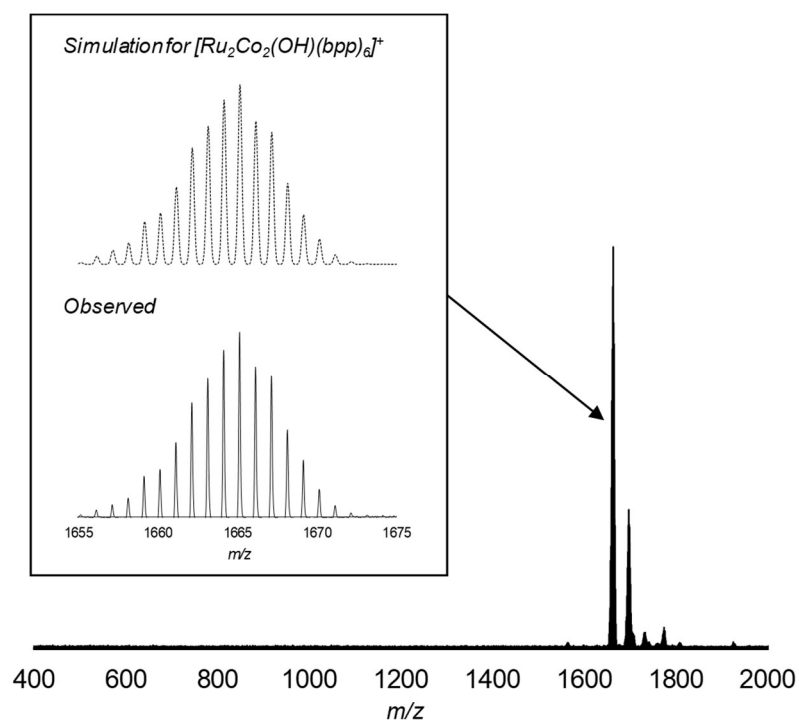


Figure 3-9 | ESI TOF-MS of $[Ru_2Co_2(OH)(bpp)_6](PF_6)$ in acetonitrile.

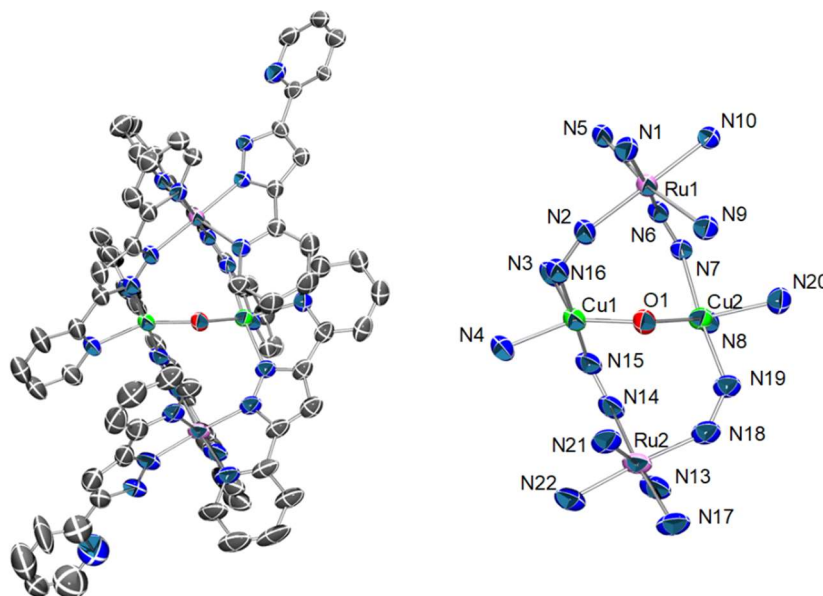


Figure 3-10 | The ORTEP drawing of cationic moiety (left) and core structure (right) of $[\text{Ru}_2\text{Cu}_2(\text{OH})(\text{bpp})_6](\text{TFSI})$ (50% probability ellipsoids). Hydrogen atoms are omitted for clarity. O = red, C = gray, N = blue, Cu = green and Ru = orchid. One out of two crystallographically independent cationic moieties was presented (see also Figure 3-12).

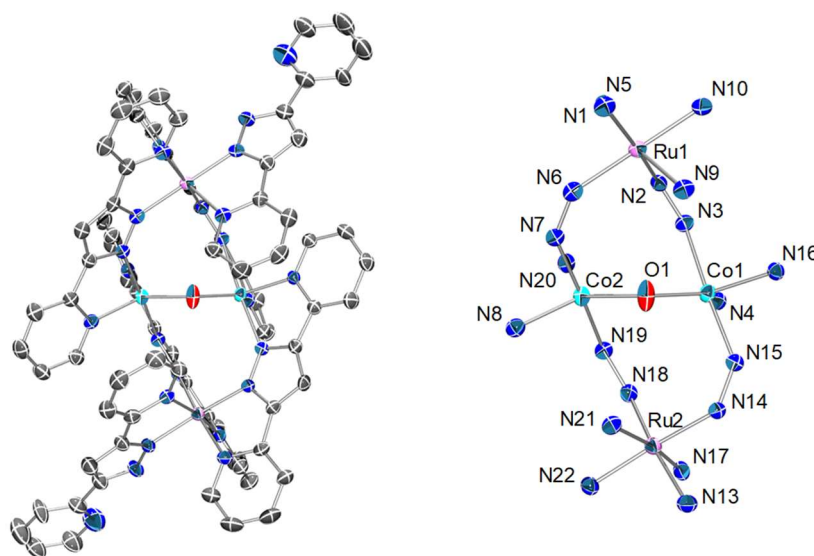


Figure 3-11 | The ORTEP drawing of cationic moiety (left) and core structure (right) of $[\text{Ru}_2\text{Co}_2(\text{OH})(\text{bpp})_6](\text{TFSI})$ (50% probability ellipsoids). Hydrogen atoms are omitted for clarity. O = red, C = gray, N = blue, Co = cyan and Ru = orchid.

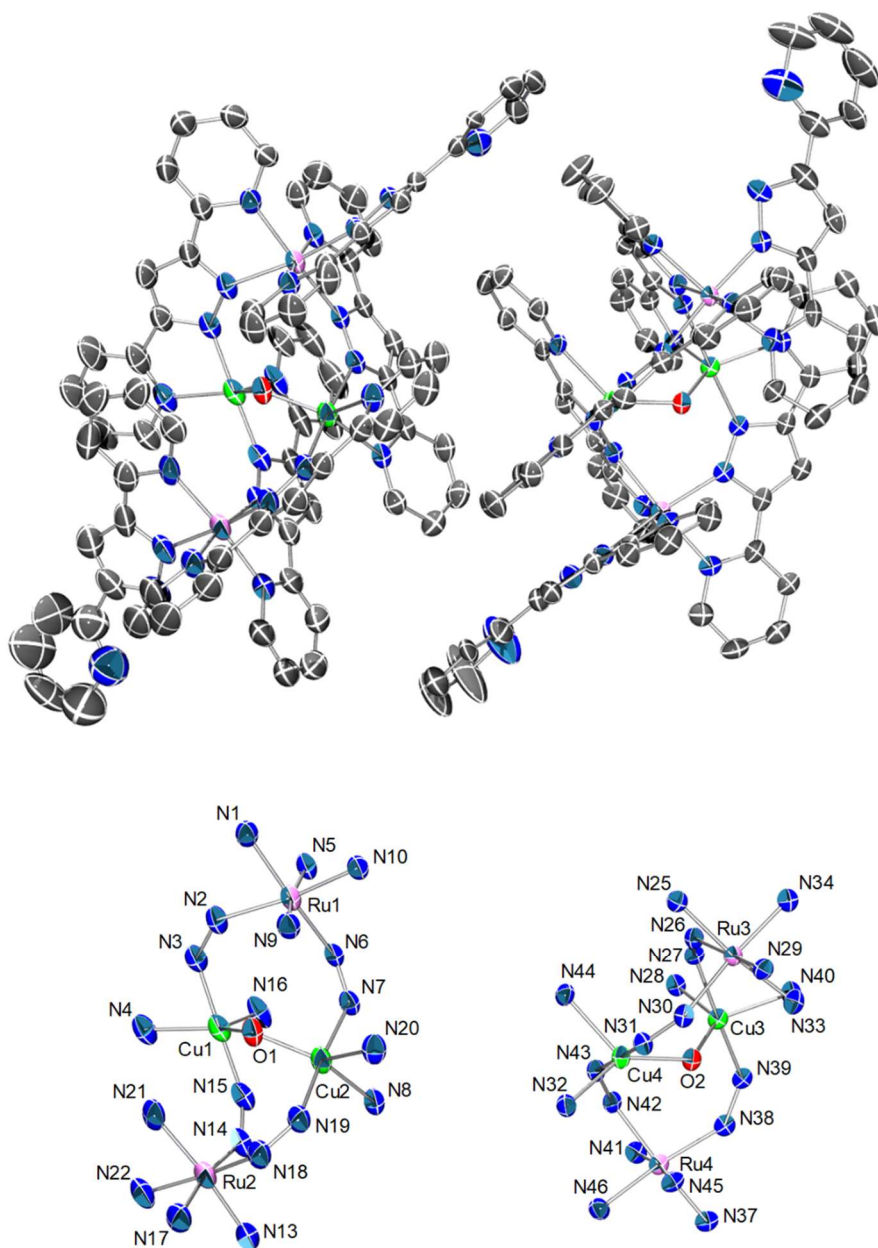


Figure 3-12 | The ORTEP drawing of cationic moiety (top) and core structure (bottom) of $[\text{Ru}_2\text{Cu}_2(\text{OH})(\text{bpp})_6](\text{TFSI})$ (50% probability ellipsoids). Hydrogen atoms are omitted for clarity. O = red, C = gray, N = blue, Cu = green and Ru = orchid.

Table 3-3 | Summary of the crystallographic data for [Ru₂Cu₂(OH)(bpp)₆](TFSI) and [Ru₂Co₂(OH)(bpp)₆](TFSI).

	Ru₂Cu₂	Ru₂Co₂
formula	C ₁₆₀ H ₁₁₀ Cu ₄ F ₁₂ N ₅₀ O ₁₀ Ru ₄ S ₄	C ₈₀ H ₅₅ Co ₂ F ₆ N ₂₅ O ₅ Ru ₂ S ₂
fw	3907.65	1944.61
color, habit	clear dark red, block	clear dark red, plate
crystal size, mm ³	2.04 x 0.20 x 0.14	0.318 x 0.146 x 0.027
crystal system	triclinic	triclinic
space group	<i>P</i> -1	<i>P</i> -1
<i>a</i> / Å	18.5608(3)	15.8400(3)
<i>b</i> / Å	19.3655(3)	18.3256(4)
<i>c</i> / Å	26.9117(3)	19.7236(2)
<i>α</i> / °	98.4250(10)	107.5710(10)
<i>β</i> / °	91.5240(10)	110.6960(10)
<i>γ</i> / °	100.3340(10)	104.105(2)
<i>V</i> / Å ³	9399.6(2)	4695.37(15)
<i>Z</i>	2	2
<i>F</i> (000)	3928	1956
<i>d</i> _{calc} , g/cm ³	1.381	1.375
<i>μ</i> (MoK α), mm ⁻¹	0.877	0.779
<i>T</i> , K	123(2)	123(2)
uniq reflns	36895	18449
<i>R</i> _{int}	0.0387	0.0417
<i>R</i> ₁	0.0632	0.0588
<i>wR</i> ₂	0.1886	0.1888
GOF	1.076	1.062

Table 3-4 | Selected bond lengths ($M_{\text{api}}\text{-N}$) of a series of tetranuclear metal complexes.

complex	Ru_2Zn_2		Ru_2Cu_2		Ru_2Co_2	
	bond	length / Å	bond	length / Å	bond	length / Å
$M_{\text{api}}\text{-N}$	Ru1-N1	2.067(3)	Ru1-N1	2.066(4)	Ru1-N1	2.060(5)
	Ru1-N2	2.080(3)	Ru1-N2	2.070(4)	Ru1-N2	2.073(5)
	Ru1-N5	2.060(3)	Ru1-N5	2.055(4)	Ru1-N5	2.073(4)
	Ru1-N6	2.064(3)	Ru1-N6	2.070(4)	Ru1-N6	2.053(4)
	Ru1-N9	2.087(4)	Ru1-N9	2.101(4)	Ru1-N9	2.079(5)
	Ru1-N10	2.026(3)	Ru1-N10	2.032(4)	Ru1-N10	2.024(4)
	Ru2-N13	2.069(4)	Ru2-N13	2.054(5)	Ru2-N13	2.059(4)
	Ru2-N14	2.057(3)	Ru2-N14	2.045(5)	Ru2-N14	2.051(4)
	Ru2-N17	2.069(3)	Ru2-N17	2.048(7)	Ru2-N17	2.064(4)
	Ru2-N18	2.069(3)	Ru2-N18	2.044(6)	Ru2-N18	2.066(5)
	Ru2-N21	2.084(3)	Ru2-N21	2.080(5)	Ru2-N21	2.078(4)
	Ru2-N22	2.028(3)	Ru2-N22	2.033(6)	Ru2-N22	2.030(4)
			Ru3-N25	2.057(4)		
			Ru3-N26	2.062(4)		
			Ru3-N29	2.067(4)		
			Ru3-N30	2.054(4)		
			Ru3-N33	2.084(4)		
			Ru3-N34	2.032(4)		
			Ru4-N37	2.058(4)		
			Ru4-N38	2.053(4)		
			Ru4-N41	2.065(4)		
			Ru4-N42	2.062(4)		
			Ru4-N45	2.091(4)		
			Ru4-N46	2.018(4)		
average		2.063(3)		2.058(4)		2.059(4)

Table 3-5 | Selected bond lengths ($M_{\text{core}}\text{-N}$) of a series of tetranuclear metal complexes.

complex	Ru_2Zn_2		Ru_2Cu_2		Ru_2Co_2	
	bond	length / Å	bond	length / Å	bond	length / Å
$M_{\text{core}}\text{-N}$	Zn1-N3	2.132(3)	Cu1-N3	1.960(6)	Co1-N3	2.113(4)
	Zn1-N4	2.102(3)	Cu1-N4	2.126(6)	Co1-N4	2.076(5)
	Zn1-N15	2.108(3)	Cu1-N15	1.958(5)	Co1-N15	2.071(4)
	Zn1-N16	2.105(3)	Cu1-N16	2.172(5)	Co1-N16	2.092(4)
	Zn2-N7	2.123(2)	Cu2-N7	1.968(4)	Co2-N7	2.087(4)
	Zn2-N8	2.094(3)	Cu2-N8	2.107(3)	Co2-N8	2.086(4)
	Zn2-N19	2.115(2)	Cu2-N19	1.970(5)	Co2-N19	2.085(4)
	Zn2-N20	2.103(4)	Cu2-N20	2.190(4)	Co2-N20	2.086(5)
			Cu3-N27	1.966(4)		
			Cu3-N28	2.171(4)		
			Cu3-N39	1.961(4)		
			Cu3-N40	2.135(4)		
			Cu4-N31	1.959(4)		
			Cu4-N32	2.139(4)		
			Cu4-N43	1.964(4)		
			Cu4-N44	2.173(4)		
average		2.110(3)		2.057(4)		2.087(4)

Table 3-6 | Selected bond lengths ($M_{\text{core}}\text{-O}$) of a series of tetranuclear metal complexes.

complex	Ru_2Zn_2		Ru_2Cu_2		Ru_2Co_2	
	bond	length / Å	bond	length / Å	bond	length / Å
$M_{\text{core}}\text{-O}$	Zn1-O1	1.940(3)	Cu1-O1	1.943(4)	Co1-O1	1.933(4)
	Zn2-O1	1.943(3)	Cu2-O1	1.935(4)	Co2-O1	1.932(5)
			Cu3-O2	1.930(3)		
			Cu4-O2	1.943(3)		
average		1.942(3)		1.938(4)		1.933(5)

Based on aforementioned success in the development of a series of tetranuclear complexes and the relevant study on a series of pentanuclear complexes, the effect of geometrical isomerism of the precursor on the structural features of the resulting multinuclear complexes is discussed. The reaction of *fac*-[Ru(Hbpp)₃]²⁺, which has three Hbpp ligands directing the same side, with first-row transition metal ions afforded a series of pentanuclear complexes. On the contrary, the use of *mer*-[Ru(Hbpp)₃]²⁺, which has two out of three Hbpp ligands directing the same side, as a precursor gave a series of tetranuclear metal complexes. In the both of two series of multinuclear metal complexes, ruthenium ions at their apical position are in hexacoordinated octahedral geometry, and first-row transition metal ions bridged by an oxygen atom are in pentacoordinated distorted trigonal bipyramidal geometry. In addition, the numbers of bpp ligands contained in the structures are identical between tetranuclear and pentanuclear metal complexes.

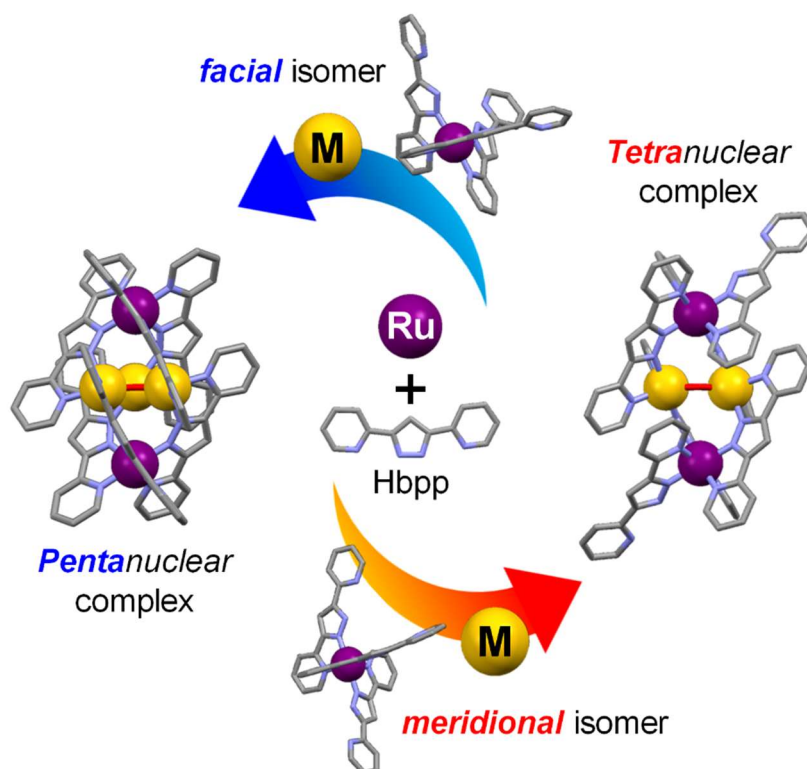
On the other hand, there exist several structural differences between the two series of multinuclear metal complexes. First, the tetranuclear metal complexes have two bpp ligands with vacant coordination sites, whereas the coordination sites of bpp ligand in the pentanuclear complexes are fully occupied by metal ions. Second, the steric hindrance around the hydroxo-bridged metal centers are largely different; although the M₃(μ₃-OH) moiety in the pentanuclear complexes is surrounded by bpp ligands, the M₂(μ₂-OH) moiety of the tetranuclear complexes is less sterically hindered. As a result, for the tetranuclear complexes, large substrates can be accessible to the hydroxo-bridged metal centers.

These two structural features, vacant coordination sites and large substrate-accessible sites, should differentiate the properties of tetranuclear complexes from those of pentanuclear complexes.

Conclusion

The author succeeded in the selective formation of a series of heterometallic tetranuclear complexes. The synthesis was achieved by the stepwise synthetic strategy composed of two step complexations. In this synthetic strategy, a ruthenium mononuclear complex, *mer*-[Ru(Hbpp)₃](TFSI)₂, was used as a precursor. The complex is a geometrical isomer of *fac*-[Ru(Hbpp)₃](ClO₄)₂ described in chapter 1. The complexation using facial isomer afforded the selective formation of heterometallic pentanuclear complexes, on the other hands, the complexation using meridional isomer afforded the selective formation of heterometallic tetranuclear complexes. Each hetero multinuclear complex has the structural features reflecting the structure of their precursor.

By the development of the stepwise synthetic strategy using ruthenium mononuclear complex as a precursor, two different series of heterometallic multinuclear complexes can rationally and selectively be synthesized.



References

1. B.-H. Zhu, Y. Shibata, S. Muratsugu, Y. Yamanoi, H. Nishihara, *Angew. Chem. Int. Ed.* **2009**, *48*, 3858–3861.
2. R. H. Ismayilov, W.-Z. Wang, G.-H. Lee, C.-Y. Yeh, S.-A. Hua, Y. Song, M.-M. Rohmer, M. Bénard, S.-M. Peng, *Angew. Chem. Int. Ed.* **2011**, *50*, 2045–2048.
3. S. Muratsugu, K. Sodeyama, F. Kitamura, S. Tsukada, M. Tada, S. Tsuneyuki, H. Nishihara, *Chem. Sci.* **2011**, *2*, 1960–1968.
4. T. Murahashi, K. Shirato, A. Fukushima, K. Takase, T. Suenobu, S. Fukuzumi, S. Ogoshi, H. Kurosawa, *Nat. Chem.* **2012**, *4*, 52–58.
5. E. Y. Tsui, R. Tran, J. Yano, T. Agapie, *Nat. Chem.* **2013**, *5*, 293–299.
6. B. Rausch, M. D. Symes, G. Chisholm, L. Cronin, *Science* **2014**, *345*, 1326–1330.
7. V. W.-W. Yam, K.-M. A. Vonika, S. Y.-L. Leung, *Chem. Rev.* **2015**, *115*, 7589–7728.
8. J. Rohacova, O. Ishitani, *Chem. Sci.* **2016**, *7*, 6728–6739.
9. K. Yoneda, K. Adachi, K. Nishio, M. Yamazaki, A. Fuyushiro, M. Katada, S. Kaizaki, S. Kawata, *Angew. Chem. Int. Ed.* **2006**, *45*, 5459–5461.
10. R. Sessoli, H.-L. Tsai, A. R. Schake, S. Wang, J. B. Vincent, K. Foiling, D. Gatteschi, G. Christou, D. N. Hendrickson, *J. Am. Chem. Soc.* **1993**, *115*, 1804–1816.
11. R. Sessoll, D. Gatteschi, A. Caneschi, M. A. Novak, *Nature* **1993**, *365*, 141–143.
12. T. Matsumoto, G. N. Newton, T. Shiga, S. Hayami, Y. Matsui, H. Okamoto, R. Kumai, Y. Murakami, H. Oshio, *Nat. Commun.* **2014**, *5*, 3865.
13. P. Buchwalter, J. Rosé, P. Braunstein, *Chem. Rev.* **2015**, *115*, 28–126.
14. P. L. Arnold, D. Patel, C. Wilson, J. B. Love, *Nature* **2008**, *451*, 315–317.
15. P. L. Arnold, G. M. Jones, S. O. Odoh, G. Schreckenbach, N. Magnani, J. B. Love, *Nat. Chem.* **2012**, *4*, 221–227.
16. S. Ogo, K. Ichikawa, T. Kishima, T. Matsumoto, H. Nakai, K. Kusaka, T. Ohhara, *Science* **2013**, *339*, 682–684.
17. M. Okamura, M. Kondo, R. Kuga, Y. Kurashige, T. Yanai, S. Hayami, V. K. K. Praneeth, M. Yoshida, K. Yoneda, S. Kawata, S. Masaoka, *Nature* **2016**, *530*, 465–468.
18. X. Jiang, J. Li, B. Yang, X.-Z. Wei, B.-W. Dong, Y. Kao, M.-Y. Huang, C.-H. Tung, L.-Z. Wu, *Angew. Chem. Int. Ed.* **2018**, *57*, 7850–7854.
19. T. Shiga, G. N. Newton, H. Oshio, *Dalton Trans.* **2018**, *47*, 7384–7394.
20. R. Chakrabarty, P. S. Mukherjee, P. J. Stang, *Chem. Rev.* **2011**, *111*, 6810–6918.
21. L.-J. Chen, H.-B. Yang, M. Shionoya, *Chem. Soc. Rev.* **2017**, *46*, 2555–2576.
22. J. S. Kanady, E. Y. Tsui, M. W. Day, T. Agapie, *Science* **2011**, *333*, 733–736.

23. S. Horiuchi, Y. Tachibana, M. Yamashita, K. Yamamoto, K. Masai, K. Takase, T. Matsutani, S. Kawamata, Y. Kurashige, T. Yanai, T. Murahashi, *Nat. Commun.* **2015**, *6*, 7742.
24. D. Fujita, Y. Ueda, S. Sato, N. Mizuno, T. Kumasaka, M. Fujita, *Nature* **2016**, *540*, 563–566.
25. K. M. Lancaster, M. Roemelt, P. Ettenhuber, Y. Hu, M. W. Ribbe, F. Neese, U. Bergmann, S. DeBeer, *Science* **2011**, *334*, 974–977.
26. Y. Umena, K. Kawakami, J.-R. Shen, N. Kamiya, *Nature* **2011**, *473*, 55–60.
27. M. Suga, F. Akita, K. Hirata, G. Ueno, H. Murakami, Y. Nakajima, T. Shimizu, K. Yamashita, M. Yamamoto, H. Ago, J.-R. Shen, *Nature* **2015**, *517*, 99–103.
28. K. Brown, M. Tegoni, M. Prudêncio, A. S. Pereira, S. Besson, J. J. Moura, I. Moura, C. Cambillau, *Nat. Struct. Biol.* **2000**, *7*, 191–195.
29. H. Ube, K. Endo, H. Sato, M. Shionoya, *J. Am. Chem. Soc.* **2019**, *141*, 10384–10389.
30. A. Altomare, G. Casciarano, C. Giacovazzo, A. Guagliardi, *J. Appl. Cryst.*, **1993**, *26*, 343.
31. G. M. Sheldrick, *Acta Cryst.*, **2015**, *C71*, 3.
32. A. L. Spek, *Acta Cryst.*, **2009**, *D65*, 148.
33. D. P. Rillema, D. S. Jones, C. Woods and H. A. Levy, *Inorg. Chem.* **1992**, *31*, 2935.

General Conclusion

The on-demand control over the distribution of the oxidation states in multinuclear metal complex is a promising way to obtain the materials with target functionality. However, the electron transfer reactions in multinuclear metal complex are quite complicated due to the strong electronic interaction between composed metal ions. Therefore, the establishment of the comprehensive guideline for controlling the electron transfer reactions in multinuclear metal complex is of great significance. To address such issue, in this thesis, the author focused on the development of the rational synthetic strategy for obtaining the series of heterometallic multinuclear complexes and the systematic investigation of redox behaviors in the obtained complexes.

The rational procedure to enable the on-demand installation of metal ions into the multinuclear metal complex was successfully developed by utilizing the stepwise synthetic method. The synthetic strategy is constructed by two step complexations, (1) the preparation of the ruthenium mononuclear complex as a precursor and (2) the reaction between the ruthenium mononuclear complex and first-row transition metal ion. As a result, the syntheses of two series of heterometallic multinuclear complexes which have different arrangement of metal ions with keeping the same molecular framework were achieved. The key to success is to use two kinds of geometrical isomers of the ruthenium mononuclear complex. The complexation using the facial isomer leads to the selective formation of heterometallic pentanuclear complexes. On the other hands, the complexation using the meridional isomer leads to the selective formation of heterometallic tetranuclear complexes. By changing the precursor, two kinds of heterometallic multinuclear complexes reflecting the structure of the precursor were successfully synthesized.

The distribution of oxidation states in all complexes, which alters during the electron transfer reactions, were clarified based on the results of electrochemical measurement, UV-vis absorption spectroscopy and UV-SEC measurement. As a result, a general picture of the electron transfer reactions in the system was unveiled, and unique electron transfer reaction, in which a metal center is reduced during oxidation of the complex, was discovered. Furthermore, the two factors that impact the redox behavior of the complexes were determined.

Collectively, the development of the stepwise synthetic strategies using the geometrical isomers of the ruthenium mononuclear complex, two kinds of a series of heterometallic multinuclear complexes can rationally and selectively be generated. These results offer a powerful and rational strategy to enable the precise arrangement of metal

ions in multinuclear metal complex. Furthermore, the systematic investigation of a series of pentanuclear complexes demonstrated that the flexible transfer of electrons in clustered redox-active sites can be programmed by the precise arrangement of the metal ions.

Acknowledgements

This thesis summarizes my Ph. D. research from April 2014 to March 2020 at the Department of Structural Molecular Science, School of Physical Science, The graduate University for Advanced Studies (SOKENDAI) under the supervision of professor Shigeyuki Masaoka.

First of all, I would like to show my greatest appreciation to my supervisor professor Shigeyuki Masaoka for his patience, guidance and continuous support of my research. I am deeply grateful to Professor Mio Kondo for her warm-hearted encouragement, instructive direction and invaluable discussion. I would like to thank Professor Yutaka Saga for beneficial advices. I really look up to them and I have decided to be a researcher because I could meet them and study under them.

I would like to show my appreciation to Professor Hiroshi Yamamoto, professor Genki Kobayashi, professor Osami Shoji, professor Tetsuro Kusamoto and professor Norie Momiyama for teaching me the important things to be a nice researcher.

I gratefully acknowledge to professor Yoshihito Watanabe for giving me important sentences and many encouragements. I would like to be a great person like him in future.

I express my appreciation to current members and alumni of Masaoka group, professor Vijayendran K. K. Praneeth, professor Masaki Yoshida, Dr. Go Nakamura, professor Masaya Okamura, Dr. Yuki Okabe, Dr. Takahiro Itoh, Dr. Pondchanok Chinapang, Dr. Arisa Fukatsu, Ms. Yukino Fukahori, Dr. Takafumi Enomoto, Dr, Lee Sze Koon, Mr. Riku Ushijima, Mr. Hikaru Iwami, Ms. Chihiro Matsui, Mr. Kento Kosugi, Mr. Masahiro Tasaki, Ms. Mami Kachi, Mr. Takuya Akai, Mr. Soshi Kato, Ms. Mei Ishihara, Ms. Misa Tomoda, Ms. Mayu Fujisawa, Mr. Hayato Tatewaki, Mr. Ryo Tomiyasu, Mr. Yusuke Nakayama, Mr. Hirotaka Hamaguchi and Mr. Shinki Fujisawa for their friendship and discussion. I hope all of them can catch own happy in their life.

I appreciate the kind help of technician staffs, Ms. Miho Matsuda, Ms. Mari Kanaike, Ms. Reiko Kuga, Ms. Akane Shibata that regulate the laboratory operation. I appreciate the assistance from secretaries, Ms. Kyoko Kawashima, Ms. Mayuko Taniwake and Ms. Kyoko Nogawa for administration works.

Special thanks dedicated to professor Masaya Okamura, professor Vijayendran K. K. Praneeh, Dr. Lee Sze Koon, Mr. Hikaru Iwami, Mr. Takuya Akai and Ms. Misa Tomoda for their valuable advices and helping hand in my research. I could proceed and summarize my research because of their many helps.

I would like to thank professor Theodor Agapie and his group members in Caltech for invaluable experiences through the internship. I could learn various things which are important for my life.

Last but not least, I would like to thank for the care, support and encouragement from my family and all of my friends.

List of Publications

Chapter 1 & 2

Hitoshi Izu, Mio Kondo, Masaya Okamura, Sze Koon Lee, Misa Tomoda, Takuya Akai, Vijayendran K. K. Praneeth, Mari Kanaike, Satoshi Kawata and Shigeyuki Masaoka
“Juggling of Electrons: Precise Manipulation of Electron Transfers in Clustered Five Redox Sites”
Submitted.

Chapter 3

Hitoshi Izu, Mio Kondo, Yutaka Saga, Hikaru Iwami and Shigeyuki Masaoka
“Rational Synthetic Strategy for Heterometallic Multinuclear Complexes”
Chemistry Letters accepted.

Other Publications

Takuya Akai, Mio Kondo, Sze Koon Lee, **Hitoshi Izu**, Takafumi Enomoto, Masaya Okamura, Yutaka Saga and Shigeyuki Masaoka

“Effect of Metal Ion Substitution on the Catalytic Activity of a Pentanuclear Metal Complex”

Dalton Transactions accepted.

Vijayendran K. K. Praneeth, Mio Kondo, Masaya Okamura, Takuya Akai, **Hitoshi Izu** and Shigeyuki Masaoka

“Pentanuclear Iron Catalysts for Water Oxidation: Substituents Provide Two Routes to Control Onset Potentials”

Chem. Sci., **2019**, *10*, 4628-4639.